Naval Research Laboratory
Washington, DC 20375-5000

NRL Memorandum Report 6400

Co-Aligning the RAIDS Instruments

DIANNE K. PRINZ

Upper Atmospheric Physics Branch
E.O. Hulburt Center for Space Research
Space Science Division

February 9, 1989

SECURITY CLASSIFICATION OF THIS PAGE

REPORT DOCUMENTATION PAGE

Form Approved
OMB No. 0704-0188

1a. REPORT SECURITY CLASSIFICATION UNCLASSIFIED	1b. RESTRICTIVE MARKINGS
2a. SECURITY CLASSIFICATION AUTHORITY	3. DISTRIBUTION/AVAILABILITY OF REPORT Approved for public release; distribution unlimited.
2b. DECLASSIFICATION/DOWNGRADING SCHEDULE	
4. PERFORMING ORGANIZATION REPORT NUMBER(S) NRL Memorandum Report 6400	5. MONITORING ORGANIZATION REPORT NUMBER(S)
6a. NAME OF PERFORMING ORGANIZATION Naval Research Laboratory 6b. OFFICE SYMBOL (If applicable) Code 4142	7a. NAME OF MONITORING ORGANIZATION
6c. ADDRESS (City, State, and ZIP Code) Washington, DC 20375-5000	7b. ADDRESS (City, State, and ZIP Code)
8a. NAME OF FUNDING/SPONSORING ORGANIZATION 8b. OFFICE SYMBOL (If applicable)	9. PROCUREMENT INSTRUMENT IDENTIFICATION NUMBER
8c. ADDRESS (City, State, and ZIP Code)	10. SOURCE OF FUNDING NUMBERS PROGRAM ELEMENT NO. 61153N33 / PROJECT NO. / TASK NO. RR033-02-46 / WORK UNIT ACCESSION NO.
11. TITLE (Include Security Classification) Co-Aligning the RAIDS Instruments	
12. PERSONAL AUTHOR(S) Prinz, Dianne K.	
13a. TYPE OF REPORT Interim 13b. TIME COVERED FROM 4/87 TO 9/88	14. DATE OF REPORT (Year, Month, Day) 1989 February 9 15 PAGE COUNT 106
16. SUPPLEMENTARY NOTATION	

17. COSATI CODES		
FIELD	GROUP	SUB-GROUP

18. SUBJECT TERMS (Continue on reverse if necessary and identify by block number)
Ultraviolet instrumentation, Optical alignment, Ebert-Fastie spectrograph, techniques, Field of view,

19. ABSTRACT (Continue on reverse if necessary and identify by block number)

The RAIDS (Remote Atmospheric and Ionospheric Detection System) experiment consists of eight optical instruments that are to make multi-spectral measurements of emissions from neutral and ionized constituents of the earth's atmosphere from an orbiting satellite in the 1990 time frame. The primary goal of RAIDS is to verify theoretical concepts, developed under an Accelerated Research Initiative, which indicate that optical remote-sensing techniques can be used to obtain ionospheric parameters on a global scale.

Seven of the instruments are to be attached to a scan platform, mounted in the satellite so as to scan tangent-ray heights between 675 km and 720 km. Six of these instruments have generically similar telescopes and

(Continues)

20. DISTRIBUTION/AVAILABILITY OF ABSTRACT ☒ UNCLASSIFIED/UNLIMITED ☐ SAME AS RPT ☐ DTIC USERS	21. ABSTRACT SECURITY CLASSIFICATION UNCLASSIFIED
22a. NAME OF RESPONSIBLE INDIVIDUAL Dianne K. Prinz	22b. TELEPHONE (Include Area Code) (202) 767-2481 22c. OFFICE SYMBOL Code 4142

DD Form 1473, JUN 86 *Previous editions are obsolete.* SECURITY CLASSIFICATION OF THIS PAGE

S/N 0102-LF-014-6603

19. ABSTRACTS (Continued)

viewing orientations, the basic telescope components of each being a spherical off-axis collecting mirror and a field-selecting slit, oriented in flight so that the direction corresponding to altitude is parallel to the width of the slit. Three of these instruments use interference filters for wavelength selection, and three use a modified 1/8th meter Ebert-Fastie scanning spectrometer.

Fundamental parameters needed in interpreting the data will be the altitude regime observed by each instrument and the imaging characteristics of each instrument within that field of view. Since simultaneous measurments of the same altitude regime in a multiplicity of wavelengths will enchance the scientific returns, the goal in co-aligning the instruments to the scan platform is to have the centers of the fields of view project onto the same altitude regime to within about 1 km. The subject of this report is how to achieve that goal for the six generically similar instruments.

Toward that end, the predicted imaging characteristics were analyzed under a variety of conditions of illumination, and with considerations of misalignment of the telescopes, primarily using a raytracing code developed by the author. Included were assessments of the applicability of traditional telescope alignment techniques to the RAIDS telescopes, assessments of laboratory sources for determining the fields of view, and predictions of the instrument response functions within the field of view.

The report presents the results, and proposes specific procedures to accomplish co-alignment under the mechanical constraints imposed by the payload design. It is intended to provide guidance to the RAIDS investigators during two phases of the RAIDS project: preparation of the instruments for flight, and analyses of the flight data.

CONTENTS

CO-ALIGNING THE RAIDS INSTRUMENTS

I. INTRODUCTION.

Within the basic research programs of the Upper Atmospheric Physics Branch of the Space Science Division is a project identified by the acronym RAIDS (Remote Atmospheric and Ionospheric Detection System). The RAIDS experiment is to be aboard a satellite that is to be launched into a nearly polar, circular (~830 km) orbit in the 1990 time frame. RAIDS includes eight optical instruments that are to make multi-spectral measurements of emissions from neutral and ionized atmospheric constituents, observing toward the limb. The primary goal of RAIDS is to verify theoretical concepts which indicate that optical remote-sensing of particular naturally-occurring emissions can be used to obtain ionospheric parameters on a global scale.

Development of the instrumentation, a joint venture with RAIDS co-investigators from the Aerospace Corporation, has progressed through manufacture of the eight instruments. Optical alignment is underway. This report is intended to support that work and the future work of installing the instruments in the payload. Although primarily intended as a working document for the RAIDS experimenters during the development phase of the project, it contains information about the response functions of the instruments that should prove useful during the data-analyses phase.

Seven of the RAIDS instruments are to be mounted on a scan platform, designed to permit viewing tangent-ray heights, denoted herein as impact altitudes, from ~75 km to ~720 km (corresponding to depression angles of ~26.5° and ~10° from the anti-velocity direction of the satellite) when the satellite orbital altitude is ~830 km. Six of these instruments have generically similar telescopes and viewing orientations. The telescope of each is designed to have its field-selecting slit at the tangential focus of a spherical, off-axis collecting mirror, and each instrument is to be oriented within the satellite so that the direction corresponding to impact altitude is across the width of the slit. These are the six instruments with which this report is concerned.

The telescopes of these instruments can be grouped into two categories, distinguished by the approximate focal lengths: 1/8th meter and 1/4 meter. Within a category, the telescopes are identical except for the size of the slit and the angle of the slit plane to the central ray.

Three of the instruments use interference filters for wavelength selection and three use an asymmetric 1/8th-meter, wavelength-scanning, Ebert-Fastie spectrograph. The detecting system of each of these instruments is non-imaging, i.e. a photometer or a photomultiplier.

The instruments are to make simultaneous measurements in orbit. Interpretation of the data will require knowledge of the field of view of each instrument relative to an earth-based coordinate system. Neglecting flexion effects, this is obtained from knowledge of: (1) the field of view of an instrument relative to an optical reference cube on the RAIDS payload as each instrument is installed in the payload; (2) the alignment errors of

Manuscript approved October 12, 1988.

the optical cube relative to the satellite axes as the payload is installed in the satellite; (3) the satellite attitude relative to the earth-based coordinate system at the time of the measurement. Data interpretation may also require knowledge of the instrument response within the field of view.

This report is aimed at providing guidelines for acquiring that comprehensive set of parameters. It presents predictions of the field-of-view response of the instruments and provides guidelines for verifying the predictions in the laboratory. From those measurements, it proposes a parameter to be used to align the flat reference mirror on each instrument which, in turn, will be used to align the instrument to the payload optical reference cube. Finally, it proposes procedures to accomplish the alignment to the payload reference surface.

With emphasis on two instruments representing each of the two categories of telescopes, the report examines the response function of the telescope alone, and the response function of the combined telescope and spectrograph. Since the response functions depend on both the optical configuration and the illumination, a variety of probable conditions were considered. For the optical configuration, these included the instruments as shown in the design drawings from which the instruments were manufactured, angular and translational misalignments of the telescope mirror, and translation between the spectrograph and telescope. Conditions of illumination included sources of various angular size at infinity, and sources at finite distances, as might be considered for determination of the field of view in the laboratory.

Most of the optical analyses were based on results obtained using a raytracing code developed by the author. The detailed raytracing results are presented in the Appendices. All of the results that concern the field of view of an instrument can be understood by keeping in mind: (1) the character of the image at the plane of the telescope slit from a point source of light, and (2) and the position of that image relative to the slit aperture. That is, the image of a point source of light produced by the spherical telescope mirror at the plane of the slit, sometimes called the point-spread function, is almost the same for all directions of the source within the field of view of the slit for the RAIDS instruments. Thus, knowing the point-spread function for one point in the field of view, i.e. for one direction of the source relative to center of the mirror, the signal for all points in the field of view (neglecting diffraction effects) can be understood by translating the point-spread function to the slit-plane coordinates corresponding to the reflected direction of the source and examining that part of the function not vignetted by the boundary of the slit aperture.

The report will show that the optical design goals of an individual instrument (spatial or spectral resolution, signal strength, etc.) can be maintained under considerable angular misalignment of the telescope mirror from the design. However, this property makes it difficult to ensure co-alignment among the fields of view when the instruments are attached to the scan platform. The report also will show that calculations of anticipated

signals and analyses of the flight data should keep in mind that the altitude contributions within the field of view can be quite asymmetric, particularly within a spectral line of the spectrometers. For example, if a source emitting specific wavelengths is spatially confined in altitude to a region narrower than the angular size of the slit-width, and is passed through the field of view by moving the scan platform while a spectrometer is at a fixed wavelength setting, the results predict that the shape and peak of the intensity versus altitude will depend on the precise wavelength setting within the bandpass of an emission feature.

The report will show that the instruments have several other peculiarities. The spectrometers, modified from the standard symmetric Ebert-Fastie design to accommodate the detector, are not optimized with regard to spectral resolution. The 1/8th meter telescopes are not optimized with regard to the tangential focus for the full field of view, although the inclusion of a filter in front of the slit could alter this conclusion. The telescope causes the illuminated area on components after the telescope slit to change in an unusual way with increasing altitude across the field of view, as the illumination becomes increasingly depleted from the center outward. However, none of these peculiarities significantly affects the original design goals.

II. NOMENCLATURE.

Certain nomenclature has evolved among the experimenters to simplify identification of components of the RAIDS payload. The six generically similar instruments are identified by the detection system used and the wavength(s) obsevered. That is, three of the instruments are called photometers and three are called spectrometers. In each photometer instrument, an interference filter is used for wavelength selection and a photometer for detection. These are further identified by the principal emission feature each observes: 5890Å (ionized sodium), 6300Å (atomic oxygen), or 7774Å (atomic oxygen). In each spectrometer instrument, the telescope slit is the entrance slit of a modified 1/8th meter, wavelength-scanning, Ebert-Fastie spectrograph, and a photomultiplier behind the exit slit is the detector. These are further identified by the spectral region each observes: NIR (Near Infrared: 7250-8700 Å), NUV (Near Ultraviolet: 2950-4000 Å), or MUV (Mid Ultraviolet: 1900-3200 Å).

The parts of the scan-platform structure to which these instruments are attached are called fins. The plane of a fin is perpendicular to the rotational axis of the scan platform and holds two instruments.

For the instruments, the front rectangular cone which attaches to the telescope body and acts as a sun-shade is called the snout. The structure that holds a mirror or grating is called a cell. The term "mask" is used to indicate the open area within a plane on the front surface of a cell.

The term "absolute field of view" means the field of view detected by

an instrument relative to the earth, e.g. in the slit width direction, it indicates the impact altitudes observable by an instrument at one position of the scan platform. The term "co-alignment" is used in discussing the absolute fields of view between or among instruments. The term "full field of view" means the magnitude of the field of view between the extreme directions detectable by an instrument, neglecting scattering and diffraction effects.

The full width at half of the maximum of a curve is denoted by the acronym FWHM. FOV is used as an acronym for "field of view".

The angular direction of the component of the FOV along the impact altitude is referred to either as the altitude direction or as the slit-width direction. The angular direction of the component of the FOV perpendicular to the impact altitude is referred to either as the longitude direction or as the slit-length direction.

The central ray of the telescope is that ray which strikes the center of the exposed part of the telescope mirror and is reflected to the center of the slit.

"RSI" references Research Support Instruments, Inc., the company which provided the mechanical drawings and manufactured the RAIDS instruments.

III. CO-ALIGNMENT GOALS.

Figure 1 illustrates the optical layout of two instruments representing the two generic categories of 1/8th meter (NUV) and 1/4 meter (MUV) telescopes. Figures 2 and 3 illustrate the orientation of the instruments relative to the satellite axes, and are intended to show that the length of the telescope slit of these instruments is to be parallel to the Z-axis of the satellite. Since the satellite orbit is to be nearly polar, with the RAIDS instruments observing in the anti-velocity direction, the length of the slit determines the longitude regime observed, while the width of the slit determines the altitude regime observed. Thus, misalignments corresponding rotations about each of the axes of the satellite will affect the observations as follows. Rotation about the satellite X-axis will shift the longitude regime of the observations. Rotation about the satellite Z-axis will shift the altitude regime observed for each angle of the scan-platform (by about 1 km per arc-minute at the lower altitudes). Rotation about the satellite Y-axis will result in the FOV spanning a larger altitude regime over the length of the slit (by about 2.3 km per degree at the lower altitudes observed).

The goal for co-aligning the instruments is to have the observed impact altitudes be the same to within about 1 km over the fields of view of common magnitude, with misalignments solely in the direction perpendicular to altitude being less than about one-tenth of the FOV in that direction. Under the expected orbital viewing conditions (impact altitudes between 75 km and 720 km from an 830 km orbit), 1 km subtends an angle of about 1 arc-minute from the satellite when the impact altitude is 75 km, and about

2.7 arc-minutes when the impact altitude is 720 km.

The most restrictive interpretation of this goal is to require that misalignments in the altitude directions be less than 1 arc minute over the entire, full fields of view that are common among the instruments.

Considerations of anticipated signals have resulted in slit sizes that produce unequal fields of view among the instruments. The slit subtenses can be determined from Table 1, which lists the relevant design parameters. "Mirror angle" is the angle of incidence of the central ray. "Focal distance" is the distance between the center of the mirror and the center of the slit. "Slit angle" is the angle between the normal to the slit plane and the reflected central ray from the mirror. (See Figure 1.) The "limiting apertures" for a telescope are the primary apertures that limit rays prior to the slit. These are equal in size and two in number: (1) a baffle that functions as a Lyot-stop, and (2) the mirror mask, i.e. the front opening of the cell that holds the mirror.

TABLE 1. Telescope design parameters.

	MIRROR		FOCAL	SLIT			LIMITING APERTURES		
	RADIUS	ANGLE	DISTANCE	WIDTH	LENGTH	ANGLE	WIDTH	LENGTH	SEPARATION
	(cm)	(deg)	(cm)	(cm)	(cm)	(deg)	(cm)	(cm)	(cm)
NIR	25	10.145	12.3063	0.025	0.45	1.8328	2.1	2.5	15.0
NUV	25	10.145	12.3063	0.025	0.45	1.8328	2.1	2.5	15.0
5890A	25	10.145	12.3063	*0.025	*0.45	0.0	2.1	2.5	15.0
MUV	50	8.0	24.7026	0.050	0.90	1.8328	4.2	5.0	35.0
6300A	50	8.0	24.7026	0.100	0.90	0.0	4.2	5.0	35.0
7774A	50	8.0	24.7026	0.100	0.90	0.0	4.2	5.0	35.0

*: The slit dimensions for the 5890Å photometer are not yet final.

As will be shown in a later section, the magnitude of the full FOV passed by a slit is larger than the slit subtense, particularly in the altitude direction, both because the spherical mirror is used off-axis in this direction, and because of the size of the two limiting apertures within a telescope. The resulting images of distant point sources are not the "lines" shown in textbook illustrations of the tangential focus, but instead, are curved, elongated, arrowhead-like entities. (See Figure 4(a).) As a result, the FOV is increased, particularly in the altitude direction containing the "tails" of the arrowhead, which corresponds to increasing impact altitudes. Table 2 lists both the slit-subtenses and the approximate magnitude of the full FOV passed by a telescope slit.

TABLE 2. Slit-subtense and full geometric field of view of the telescopes.

TELESCOPE	SLIT-SUBTENSE		~ FULL FOV	
	WIDTH (deg)	LENGTH (deg)	WIDTH (deg)	LENGTH (deg)
NIR	0.115	2.09	0.207	2.5
NUV	0.115	2.09	0.207	2.5
5890Å	*0.115	*2.09	*0.207	*2.5
MUV	0.115	2.09	0.184	2.5
6300Å	0.232	2.09	0.288	2.5
7774Å	0.232	2.09	0.288	2.5

*: The slit dimensions used were 0.0250 cm X 0.45 cm.

The above considerations can be used obtain the permissible rotations among the common fields of view. We assume that the FOV of each instrument is a rectangle, and let the smallest of these rectangles have width W and length L. We also let the components of the permissible misalignment among the group of smallest rectangles be: $\pm$ A in the width (altitude) direction, and $\pm$ P in the length direction. Since A < P, and A < W < L, elementary plane geometry can be used to show that the permissible rotation is approximately equal to $\pm$arcsin(2*A/L). Using A = 0.00833 degrees (0.5 arc-minute) and L = 2.5 degrees, the permissible rotation is about $\pm$0.4 degrees.

In summary, the permissible misalignments among the common fields of view are approximately:

(1) $\pm$ 0.5 arc-minute in the slit-width direction,
(2) $\pm$ 7.0 arc-minutes in the slit-length direction,
(3) $\pm$ 0.4 degrees rotation.

IV. CO-ALIGNMENT: THE RELEVANT AXES.

For an accessible optical reference, each instrument has a flat mirror, known as a boresight mirror, that attaches to fixture which, in turn, can be attached to the front of the snout. (See Figure 3.) The fixture utilizes diagonal pins and a 3-pad contact to enable reproducibility of the angles between attachments. In theory, the last step in the co-alignment process is accomplished by aligning the boresight mirror of each instrument relative to some reference surface on the payload, to within the permissible misalignments, as the instruments are attached to the fins. However, whether this results in actual co-alignment of the fields of view depends on the relative alignment of boresight mirror and telescope mirror

for each instrument. Also, there is a mechanical constraint in the amount by which an individual instrument can be rotated to align it in the direction corresponding to altitude as it is attached to the fin. And, in addition to mutual alignment of the instruments, consideration of alignment of the RAIDS payload to the satellite must be given. Discussion of these topics requires that we first define the following six axes.

1. The PAYLOAD REFERENCE AXIS is defined as the normal at the center of that side of an optical cube attached to the RAIDS payload baseplate facing the hemisphere of light incident on the instruments. Two perpendicular sides of the cube will be used to align the RAIDS payload within the satellite. In Figures 2 and 3, the cube is shown as being perfectly aligned with the satellite axes, the side defining the payload reference axis being perpendicula- to the +Y-axis of the satellite.

2. The BORESIGHT AXIS is defined as the normal at the center of the flat boresight mirror when it is attached to an instrument.

3. The MECHANICAL AXIS of a telescope is defined here as the incident centerline in the mechanical design drawing, i.e. the line in the drawing that passes through the centers of the apertures and the center of the mirror. This also could be called the ATTACHMENT AXIS, since it was the reference line used by RSI to locate the feet of an instrument, and by Aerospace to locate the holes for those feet in a fin.

Since the attachment holes have limited tolerance in the direction corresponding to altitude ($\pm$ 0.2°), the mechanical axis (or some other reference to the feet) of an individual instrument must be established before beginning the optical alignment of a telescope. That this can be done accurately enough remains to be proven, because no special requirements were imposed on the manufacturing of an individual instrument to ensure that the separable parts between the front of the instrument and the feet were maintained with special precision relative to this axis.

4. The OPTICAL AXIS of a RAIDS telescope is defined here as a line along the direction of incidence of the central ray, i.e. a line along the incident ray that strikes the center of the exposed part of the telescope mirror and, afterward, is reflected to the center of the slit. If aligned exactly as designed, the optical axis would be coincident with the mechanical axis.

For most telescopes this axis usually defines a unique direction of incidence, fixed relative to the surface of at least one optical element in that only that angle of incidence will produce an image of the required quality, the "required quality" usually being that the size be a minimum in some dimension, such as width, length, or diameter. In other words, the axis is independent of the telescope housing and can be determined experimentally by visually examining the image quality from a beam of

nearly parallel light and changing the direction of the beam relative to the element until the image has the required quality. Aligning the telescope then consists of positioning and orienting the element within the instrument so that the image with this quality is correctly located therein.

But a spherical mirror has unique imaging properties only when the normal at its center is coincident with the central ray. When the mirror is used in a configuration other than this, as it is in a RAIDS telescope, the image quality is not a sensitive measure of the angle of incidence, which defines the optical axis. Specifically, if we require determination of the component of the optical axis in the altitude direction to an accuracy of $\pm$0.5 arc-minute, to do so from the image quality requires that the image quality change by a measurable amount as the angle of incidence is changed by $\pm$0.5 arc-minute in that direction. But, as will be shown in this report, the image quality at the slit is insensitive to changes of mirror-angle and source direction that are equivalent to changes of at least $\pm$12 arc-minutes in the optical axis in the altitude direction.

Compounding the problem is the fact that it is impossible to view the image at the plane of the slit when it is attached to the telescope body. That is, the flight slit is a part of the structure subsequent to the telescope. RSI has provided an alignment fixture that attaches to the decoupled telescope body, duplicating the slit-plane distance and angle. The fixture has a small hole at what should be the center of the slit. However, the precision required in duplicating the slit-center in the altitude (slit-width) direction is very high, since the FOV is shifted 0.5 arc-minute by about a 0.0007 inch shift in an 1/8 m focal length telescope, and by about a 0.0014 inch shift in a 1/4 m focal length telescope.

If instead of a visual determination, one attempts to locate the optical axis from the signal through an instrument, this report will show that there is no identifying attribute of the signal that allows determination of the component of the optical axis in the altitude direction.

In short, the optical axis of a RAIDS telescope, defined in the traditional manner from the central ray, can not be precisely determined. It is not fixed to the mirror; its component in the altitude direction has no meaning without the slit. (The optical axis appearing in the design drawings, however, is useful as a reference direction in discussing the raytracing results. In those discussions it is referred to as the design optical axis.)

5. Rather than the traditional optical axis, we propose to define a FIELD-OF-VIEW AXIS for an instrument in a manner that uses the signal from an instrument when it is in its flight configuration. Then, if the relation of this axis to the boresight axis is determined, as the instruments are installed on the fins, the boresight axes can be mutually

aligned in a manner that will result in co-alignment of the flight fields of view.

The procedure used to determine this axis in the laboratory must result in correct identification of the axis for the flight fields of view, must have the accuracy required, and must enable determination of the relation of this axis to the boresight axis. The general procedure, in effect, is to move a source across the FOV along each of the two component directions. However, the shape of the signal and, consequently, the identifying feature and the accuracy of determining the components of the axis, are dependent on the size of the image of the source at the plane of slit in the direction of motion, the effective source distance, and the extent to which the telescope mirror is illuminated. The signal from a spectrometer has an additional FOV dependency on the precise wavelength setting within a spectral line. In a later section of this report, the constraints upon the laboratory source and other setup requirements will be discussed.

The conclusion drawn from the raytracing results is that, under the proper setup conditions, the feature of the signal that could be used to identify the field-of-view axis for all of the instruments is the center of the FWHM.

6. The SCAN AXIS is defined as the normal to the plane of motion of a point on a fin. When the payload is installed in the satellite, this axis should be parallel to the satellite Z-axis for all three fins to which the six instruments are attached. (See Figure 2.)

V. RAYTRACING: OVERVIEW AND ASSUMPTIONS.

The mechanical drawings from which the instruments were manufactured were used to obtain the location and orientation of all relevant elements in the optical systems. Appendix A lists the values used for raytracing each instrument, referenced to a coordinate system whose origin is centered in the telescope aperture called the Lyot-stop. The Lyot-stop is located at the backward image of the grating, the intended limiting aperture in the comparable spectrometer, and is sized to prevent the telescope mirror from directly viewing the edges of the first baffle in the snout.

The +Z axis of this reference coordinate system points outward, toward the incident light, along the line that is both the optical axis and the mechanical axis in the design. (See Figure 1.) Relative to the detecting part of the instrument, the +X axes of the reference coordinate systems used for the NUV and 5890Å instruments point in the opposite direction of +X reference axes for the MUV, 6300Å and 7774Å instruments. This resulted from the different orientation of the instruments in the top-view mechanical drawings (on which Figure 1 is based) and the convention of the author (to have the +Y-axis of the reference system pointing into the page of a top-view mechanical drawing). In the payload, the detecting system of

each of the six instruments is oriented toward the payload baseplate.

The local coordinate system on the surface of each element has its +Z axis pointing along the normal labeled $\hat{N}$ in Figure 1, with its +Y axis into the plane of the figure.

Whenever an optical system was raytraced using relative positions and orientations as given in Appendix A, the results are labeled "as designed". All of the raytracing which included a spectrometer assumed that the entrance slit, Ebert mirror (denoted as SPEC MIRROR in Figure 1), and grating were aligned relative to each other and sized as designed.

Although most of the raytracing was done for the NUV and MUV instruments, the results at or behind the entrance slit of the spectrometer (which also is the telescope slit) are quite applicable to results that would be obtained at or behind the telescope slit of a photometer having a similar telescope mirror and the same slit size, because everything but the plane of the slit is the same in the two telescopes; the 1.8328° difference in the angle of the telescope slit planes between a spectrometer and a photometer has little effect on the results.

All raytracing begins by starting rays from points within a plane called the entrance aperture, and sending each ray away from this plane, toward the hemisphere containing the first element of the optical system. In the authors raytracing code, although the boundary of the entrance aperture may be elliptical or rectangular, the points within the boundary form a grid-like pattern, with equal spacing between rows and equal spacing between columns. (Uniform illumination or a uniform source is simulated when the spacing between the rows is equal to the spacing between columns.) Similarly, the angular span of the cone of rays leaving each point is equally divided in each of the two component directions, X and Y. (Isotropic illumination or an isotropically emitting source is approximately simulated when the angular spacings in the two directions are equal.) The center of the cone can be offset in either or both of these directions. The reference direction for zero offsets in all of the raytracing was the design optical axis.

An infinitely distant point source is simulated by setting the cone subtenses to zero, the direction of source being specified by the offset angles. Parallel rays at the specified direction from the grid pattern of points within the boundary of the entrance aperture then complete the simulation of such a source.

To simulate a thin emitting layer at some impact altitude within the FOV, the most commonly used source was an infinitely distant line of point sources parallel to the Y-axis (longitude) direction, the line subtending an angle comparable to the FOV in the longitude direction, i.e. about 2.1°. Such a source is defined to the code by setting the X-angle subtense of the cone of rays to zero and the Y-angle subtense to a value at least equal to the magnitude of the FOV in the longitude direction, e.g. 2.1°. The division of the Y-angle cone then determines the spacing of points along the line, and the offset angle in the X direction (denoted as OFFSETX

in the Appendices) then determines the impact altitude.

Any surface that affects rays reaching the detector is considered an element, e.g. baffles are elements when they can affect subsequent illumination by terminating some rays. Although the finite size of an optical element can limit rays, if the boundary is symmetric about the local origin used for the element, a separate baffle or mask element is not inserted because the code is written to terminate rays beyond an input width and length symmetric about the center. The effect of a baffle or mask was, simply, termination of rays; that is, scattering and diffraction from the edges of such surfaces or from the illuminated surfaces of mechanical components of the optic-cells was neglected.

The fidelity of the raytracing results depends on several inputs to the code and several assumptions. The spacing of initial rays, with regard to both position and angle, is important because a false sense of illumination can occur if care is not taken. For example, in the RAIDS instruments the Lyot-stop and the opening in the telescope mirror cell have the same dimensions, but the plane of the front of the mirror cell is not parallel to the plane of the Lyot-stop. Thus, if the entrance aperture is at the Lyot-stop and rays are sent parallel to the design optical axis from a grid-like pattern within the full dimensions of the Lyot-stop, rays from at least one column on either side of the entrance aperture will not strike the mirror. In effect, the mirror is being illuminated by a beam that is narrower than the width of the Lyot-stop, by at least two column spacings. To maintain illumination of the full width of the mirror, the column spacing can be made small by increasing the number of columns across the width of the entrance aperture. However, this increases the total number of rays through the system, thereby increasing the execution time for the code.

An alternative approach is to slightly decrease the size of the entrance aperture. The latter was the method used for this report when raytracing was done using the Lyot-stop as the entrance aperture from which rays emanated. This can affect the results when contributions from the edges of the mirror are significant, as they are toward the limits of the full FOV.

The fidelity of the raytracing results also is dependent on the assumption that all points of a surface have the same sensitivity, i.e. that there is not a spatial dependence on such parameters as the reflectivity of a mirror or the efficiency of a grating or detector to the same wavelength of incident light. Since the position and shape of the illuminated area on optical components and the detector change with the direction of the incident parallel beam, predicted features of the signal, such as the direction corresponding to the peak, could be affected by departures from this assumption.

Another assumption affecting the fidelity of the raytracing results for the spectrometers is that diffraction by the telescope slit does not change the directional information in rays from the telescope mirror. That is,

raytracing for the spectrometers, as done for most of this report, used the telescope slit as a baffle to limit rays, rather than as a source of rays. Since exact calculations of the intensity distribution in the diffraction pattern exiting the slit are too complex to consider here, we take the simplistic view that the net effect of diffraction, as it affects subsequent illumination, is to broaden the beam about the incident direction of each ray by an angle equal to $2\lambda/d$, where d is the slit width and λ is the wavelength of the incident light. If λ is the longest observable wavelength for each instrument, the broadening would be: ~0.4° in the NIR, ~0.18° in the NUV, and ~0.07° in the MUV. Since the undiffracted geometric beam width exiting the slit for the ~f/5 telescope systems of these instruments is ~9.7°, the raytracing results presented in this report should be most accurate for the MUV instrument.

Because diffraction from the slit was neglected, the initial spacings of rays in angle and position have added importance when raytracing a spectrometer since they determine the distribution of rays that will pass through the telescope slit (the entrance slit of the spectrometer) and become the "signal".

VI. RAYTRACING OUTPUTS

The output of the author's raytracing code gives six pieces of information for each element: (1) the number of rays that struck the element; (2) the four extreme intersections of those rays, i.e. the maximum and minimum X and Y intersections in the local coordinate system of the element; (3) position and angle identifiers to determine which initial ray caused the extreme intersections of (2); (4) the number of rays that made it to the last element, i.e. that were not stopped by a baffle or mask after the element; (5) the extreme intersections for the subset of rays that made it to the last element; (6) position and angle identifiers to determine which initial ray caused the extreme intersections of (4).

For the last element, all of the X,Y intersection pairs are stored. Although there are many ways to display this information, e.g. spot-diagram, contour lines or surfaces, etc., the author has found an "array diagram" to be the most useful because of the amount of quantitative, rather than qualitative, information it contains. (Figures 4 and 5 are examples of such an output.) In an array diagram, the surface of the last element is divided into a mesh network, the size of the mesh in width and length being determined either by direct inputs at the time of execution or by the resulting extreme intersections. Each section of the mesh is one element of an array. The code then calculates the number of rays that fall within each section of the mesh, and outputs these numbers to form the array diagram. The rows and columns of the array correspond, respectively, to the local X and Y coordinates of the last element, with X increasing across the page and Y increasing down the page. Printout of the X and Y

coordinates for the first element of the array (the element in the upper left corner of the page) provide the necessary information to locate the position of the array relative to the origin of the local coordinate system of the last element.

The format of the array diagram is extremely useful for predicting signals in both photographic and electronic detecting systems because the mesh can be adjusted to correspond to the minimum sampling size, e.g. the typical grain size of a photographic emulsion, the pore size of a microchannel plate, or the pixel size of a readout device.

The code also outputs the sum of each row of the array, the sum of each column, and a running sum whose column width is determined by the width of the entrance aperture. These quantities are useful if the detecting system provides one dimensional information or if the entrance aperture is a slit.

Since the detecting systems of the six RAIDS instruments are of zero dimension, i.e. they only provide information on the total radiation reaching a detector, the most frequently used outputs were the total number of rays passing the elements. However, the array diagrams were very useful in evaluating alignment techniques and in determining the instrument response function to the field of view.

VII. TELESCOPE ALIGNMENT CAUTIONS.

Since the telescopes are to be aligned individually and at two different places (NRL and Aerospace), it must be mentioned that several techniques traditionally used to align telescopes can lead to considerable misalignment among the absolute fields of view. Detailed analyses of this subject are presented in Appendix B, summarized as follows.

1. As mentioned earlier in defining the optical axis, the quality (size and shape) of the image at the telescope slit can not be used to determine an absolute angular reference in the altitude direction because it is insensitive to changes of the mirror angle that change the center of the absolute FOV by more than the angular magnitude of the slit width. Furthermore, if aligned to the design specifications, although the central ray of a parallel beam whose direction is along the optical axis passes thru the center of the slit, the image of this beam is not centered at the slit in the width (altitude) direction. (See Figures 4 (A) and 5 (A).)

2. The quality of the image at the telescope slit depends on the size, shape, and position of the illuminated area of the mirror, as well as the angles of incidence. In other words, different alignment techniques can lead to different alignments of the telescope mirror. (See Figure 6.)

VIII. INSTRUMENT PECULIARITIES.

A. TELESCOPE FOCAL DISTANCES

1. AVAILABLE ADJUSTMENTS

Optimum alignment of a telescope usually includes adjustment of the distance between the mirror and the slit, as well as adjustment of the mirror angle. But, there is no provision in the design of the RAIDS telescopes for adjusting the focal distance except at the mirror. This adjustment is within the cell of the mirror, being a change in thickness of the Kel-F pads that prevent the mirror surface from touching the cell. Although the 1/4 m telescopes have a thin (about 0.018 inch) shim between the cell and the telescope body, changing the thickness of the shim would change the footprint of the instrument because one foot is part of the mirror-cell structure.

2. DESIGNED FOCAL DISTANCES

In raytracing the MUV and NUV telescopes using the specifications in the design drawings, it was discovered that the slit plane for the 1/8th meter NUV was not at the minimum image width for either of the two conditions one might consider: (1) rays parallel to the design optical axis that fill the entrance aperture, or more appropriately, (2) rays from a FOV comparable to the slit subtenses, say 0.1° by 2.1°, that fill the entrance aperture. If the slit center is moved along the central ray, keeping the plane of the slit at the design angle, these two focii are at mirror-center to slit-center distances of 12.2811 cm and 12.2783 cm, respectively, while the designed slit distance is 12.3063 cm, about 280 microns (0.011 inch) farther from the mirror than the tangential focus for the larger FOV. (For the 1/4 m MUV, the two focii are nearly coincident, at 24.7016 cm and 24.7013 cm, respectively, and the designed mirror-to-slit distance is nearly equal, being 24.7026 cm.)

As stated in Appendix B, the tangential focal distance is a function of the size of the illumination on the mirror. The simple formula given in textbooks for the tangential focus of parallel light from a spherical mirror ($R\cos(\phi)/2$, where ϕ is the angle of incidence at the center of the mirror) is obtained only when the beam has a very small diameter. However, it appears that this was the distance chosen for the NUV, since the designed focal distance differs from the simple formula results by less than 0.001 inch. (For the 1/4 m MUV, the simple formula would have placed the slit 0.022 inches farther from the mirror than the tangential focus for the larger FOV with a fully filled entrance aperture - far enough to have broadened the image of an altitude line source by 10% to 15%.)

One reason for the designed focal distance for the NUV could have been a late design change for the spectrometers: the displacement of the exit slit behind the plane of the entrance slit. Rationale that could have led

to a longer telescope mirror-to-slit distance is the following. Assume that the initial source for the Ebert mirror is at the tangential focus of the telescope, not at the entrance slit, and that the light reflected from the Ebert mirror travels to a plane mirror, which then provides the second source for the Ebert mirror. Suppose that the Ebert mirror images this light into the narrowest size at a distance approximately equal to the inital source distance. If this image is to be maintained narrowest at the exit slit as the exit slit is moved further from the Ebert mirror, the initial source distance also should be increased. However, this argument, which neglects the entrance slit, is not supported by raytracing (discussed below). Furthermore, raytracing for a condition which increased the distance between the telescope mirror and the subsequent parts of the instrument by 2 mm from the design, did not show any significant change in the location within the spectrometer of the minimum image width for the full FOV, although the minimum image width did increase by about 35% because of the translation. (See Figures 35 and 36.)

A second possible reason for the designed mirror-to-slit distance could have been consideration of the effect on the focal distance of the filter to be placed in front of the slit. From Snell's law of refraction, a plane parallel filter having thickness "t" and index of refraction "n" placed in a converging beam of f-number "f" increases the focal distance by an amount "d", given by:

$$d = t\left[1 - \frac{2f}{A}\right] , \quad \text{where}$$

$$A = \sqrt{n^2(1 + 4f^2) - 1} \quad .$$

For the telescopes, f = ~5. If, for example, n = 1.5, then d/t = 0.335. Then, such a filter could increase the focal distance by the required 280 microns if it were about 0.835 mm thick.

B. SPECTROMETERS

1. BACKGROUND

The design of the standard 1/8th meter Ebert-Fastie spectrometer was modified in several ways for the RAIDS instruments. The entrance and exit slits were made straight-sided, rather than curved. In order to fit the detectors to the instruments, the spectrometers were modified to be asymmetric in two ways. If we define the length axis of the spectrometer to be a line along that normal to the Ebert mirror which passes through the

center of the grating, and the width axis to be perpendicular to the length axis, (1) along the width axis, the exit slit is 0.447 cm farther from the grating than is the entrance slit, and (2) along the length axis, the plane of the exit slit is 0.134 cm behind the plane of the entrance slit. In addition, the telescope is coupled to the spectrometer so that the central ray from the telescope is offset, toward the center of the Ebert mirror, by 1.8328° from the direction of the length axis of the spectrometer. (See Figure 1.) This and the lateral displacement of the exit slit cause the Ebert mirror to be illuminated asymmetrically on the light passages to and from the grating.

2. DESIGNED FOCAL DISTANCE

Raytracing results show that the narrowest image of the full FOV passed by the entrance slit and the narrowest image of the entrance slit width are both located about 2 mm inside the design plane of the exit slit, i.e. at a plane that is about 0.67 mm inside the plane of the entrance slit. At this inside plane, the full width of the image from the full FOV is about 350 microns for the NUV and about 700 microns for the MUV, whereas at the designed slit plane, the full width is about 630 microns for the NUV and 985 microns for the MUV. At the inside plane, the width of the image of the entrance slit for comparable illumination of the Ebert mirror is about 375 microns, whereas at the designed slit plane, the image width is about 655 microns. (The location of the plane for the minimum image width of the entrance slit did not change when the angle of the central ray illuminating the spectrometer was changed to be parallel to the length-axis of the spectrometer, as might be the illumination condition in aligning the spectrometer.) Therefore, if the assumptions used in the raytracing are correct, the spectral resolution will be slightly less than expected, the NUV being more affected than the MUV. (See Figure 22.)

IX. TELESCOPE FIELD-OF-VIEW EFFECTS.

Appendix C discusses the contribution to the signal directly behind the telescope slit from various directions within the FOV for the NUV and MUV instruments. The FOV direction parallel to the design optical axis is the zero-degree reference in both the "X" (altitude) direction and the "Y" (longitude) direction. The results show the asymmetry of the FOV in the altitude direction relative to the design optical axis when the telescopes are aligned exactly as designed. If we define the field-of-view axis to be the direction corresponding to the center of the FWHM of the signal within the FOV, the component of the field-of-view axis in the altitude direction is about 1.0 arc-minute from the design optical axis for the MUV, and about 1.3 arc-minutes for the NUV. Both axes are shifted toward the FOV direction that makes a smaller angle of incidence at the mirror than the direction parallel to the design optical axis. This direction corresponds

to increasing altitude in both instruments.

If the MUV and NUV telescopes were aligned so that the FOV axes were parallel, the relative contribution to the signal from comparable absolute FOV directions would be very similar. Furthermore, as shown in Appendix C, as the telescope mirror angle is changed from that in the design, the signal behind the telescope slit shifts relative to the zero-degree reference of the design optical axis (at twice the angle by which the mirror normal is changed), but the shape changes very little (until vignetting by the baffles becomes significant). Thus, even if the telescope mirrors were misaligned, co-alignment between the instruments still could be achieved by off-setting the boresight axis of each instrument by appropriate amounts during installation so that the FOV axes were parallel.

But, detecting the signal directly behind the flight slit of a telescope is not possible in the spectrometer instruments. And, the FOV distribution in the signal directly behind the telescope slit is not necessarily carried through to the exit slit of the spectrometer. Thus, we need to establish: (1) the criterion to be used to determine the field-of-view axis of the spectrometer instruments, and (2) the relation of the field-of-view axis for the spectrometer instruments relative to the field-of-view axis for photometer instruments.

X. SPECTROMETER FIELD-OF-VIEW EFFECTS.

Appendix C also discusses the signal at the exit slit of the NUV and MUV instruments for monochromatic sources of equal intensity that form lines perpendicular to the altitude direction. The results show that the contribution to the signal from any one altitude depends on the wavelength setting (grating angle) of the spectrometer, but that, like the signal behind the telescope slit, the shape for a particular wavelength setting does not significantly change with similar angular misalignments of the telescope mirror.

The results also show that when the grating angle is set to the center of the FWHM of the line shape from a nearly monochromatic source that fills the <u>full</u> FOV, the signal has a distribution with altitude that is reasonably centered within the full FOV of the instrument. Within a given instrument, this attribute is independent of the wavelength of the incident light. If we use the center of the FWHM of this signal to define the altitude component of the field-of-view axis for the NUV and MUV instruments, and if the two instruments are installed in the payload with the FOV axes parallel, the two instruments will have nearly equal relative contributions from the same altitude over the lower half of the altitude regime both observe. Over the upper half, the NUV signal will have, first lower, then higher relative contributions, the cross-over occurring ~3 arc-minutes from the nearly coincident centers of the FWHM.

XI. THE EFFECT OF TRANSLATIONS OF THE TELESCOPE MIRROR ON CO-ALIGNMENT.

The preceding discussion has concentrated on the FOV effects for the instruments when aligned as designed, with minor excursions to consider purely angular misalignments of the telescope mirror. But there are two translational misalignments, both due to the position of the telescope mirror within its cell, that also can affect co-alignment and the magnitude of the FOV.

The first concerns the thickness of the Kel-F pads which prevent the mirror from touching the front of the cell. Raytracing shows that changing the thickness of the pads from that required to position the mirror at the designed location, shifts the absolute FOV by 0.125 arc-minutes per 0.001 inch change in pad thickness in the 1/8th meter instruments and by 0.05 arc-minute per 0.001 inch in the 1/4 meter instruments, but that the effect on the spatial and spectral resolution is insignificant since the pad thickness can not be changed by large amounts.

These results can be predicted from the following simple geometric considerations of: (a) the reflected central ray (defined, as before, as the ray from the center of the mirror that passes through the center of the slit), and (b) the change in focal distance caused by a change in pad thickness. (See Figure ***.) Although the reflected central ray does not correspond to the center of the FOV, it can be used to estimate shifts in the the FOV. If we assume that:

(1) the slit is fixed at the design location, which was a distance "L" from the designed location of the mirror center;
(2) the mirror sides are maintained parallel to the walls of the cell, which keeps the normal at the mirror center at an angle "α" relative to the direction of the design optical axis;
(3) the pads are changed in thickness by an amount "d" from that required to place the mirror in the designed position, where "d" is positive if an increase in thickness and negative if a decrease,

then the angle "θ" between the normal of the mirror at its center and the reflected ray that passes through the center of the slit is given by:

$$\tan(\theta) = \frac{\tan(\alpha)}{1 + d/(L\cos(\alpha))} ,$$

and the angle $(\alpha-\theta)$, which measures the shift in the FOV, and is given by:

$$\tan(\alpha-\theta) = \frac{(d/L)\sin(\alpha)}{1 + (d/L)\cos(\alpha)} \simeq (d/L)\sin(\alpha) .$$

Values of "L" and "α" are respectively 12.3063 cm and 10.145 deg for the 1/8th meter telescopes, and 24.7026 cm and 8.0 deg for the 1/4 meter

telescopes. From these, the aforementioned results can be obtained.

The distance L' between the center of the mirror and the center of the slit after the pad thickness is changed is given by:

$$L' = L\sqrt{1 + 2(d/L)\cos(\alpha) + (d/L)^2} \ .$$

Using the fact that $(d/L)<<1$, the change in distance is given approximately by:

$$L' - L \simeq d\cos(\alpha) \ .$$

If the tangential focus truly is at the design distance, changing the pad thickness would increase the size of the illumination at the slit from an inifintely distant point source by an amount approximately equal to the absolute value of $W(L'-L)/L$, where W is the illuminated width of the telescope mirror. For the 1/8 m and 1/4 m telescopes, W is 2.1 and 4.2, respectively. The wider illumination at the slit increases the FOV in the altitude direction because the sides of the defocused beam from larger offset angles can then enter the slit. The magnitude of the increase is about the same for the 1/8th m and 1/4 m telescopes: about 4 microns per 0.001 inch change in pad thickness. Since the same width at the slit represents twice the angular FOV in the altitude direction in the 1/8th m telescopes as in the 1/4 m telescopes, the increase in the altitude component of the FOV for the 1/8 m telescopes is twice that for the 1/4 m telescopes: about 0.12 arc-min per 0.001 inch change in pad thickness for the 1/8th meter instruments and about 0.06 arc-min per 0.001 inch for the 1/4 meter instruments. Since the pad thickness can not be changed by many thousandths of an inch, the effect should be small.

The second effect to the FOV caused by translating the mirror within its cell concerns its lateral displacement from the design, i.e. translation perpendicular to that considered above. Again, simple geometric considerations can be used to predict the raytracing results. If we again assume that sides of the mirror remains parallel to the walls of the cell, and use the definitions given above, where "d" now is a lateral displacement from the design, positive in a direction away from the slit, the angle "θ" of the reflected central ray relative to the normal at the mirror center is given by:

$$\tan(\theta) = \tan(\alpha) + d/(L\cos(\alpha)) \ ,$$

and the shift in the FOV $(\alpha-\theta)$ is given by:

$$\tan(\alpha-\theta) = \frac{-(d/L)\cos(\alpha)}{1 + (d/L)\sin(\alpha)} \simeq -(d/L)\cos(\alpha) \ .$$

This shows that the FOV shift caused by lateral translation is significantly larger than that caused by depth translation, by the ratio of $\cos(\alpha)/\sin(\alpha)$. Since "$\alpha$" is 10.145°for the 1/8th meter instruments and 8.0° for the 1/4 meter instruments, the value of the ratio is about 5.6 for

the 1/8th meter instruments and about 7.1 for the 1/4 meter instruments. Thus, the FOV is shifted about 0.7 arc-minute per 0.001 inch displacement for the 1/8th m telescopes and 0.35 arc-minutes per 0.001 inch displacement in the 1/4 m telescopes. Therefore, careful centering of the telescope mirror within the cell is very important.

The effect of the lateral displacement on the magnitude of the FOV is less than that for the change in pad thickness, by the ratio of $\sin(\alpha)/\cos(\alpha)$. That is, the distance between the mirror and the slit after a lateral displacement of "d" is given by:

$$L' = L\sqrt{1 + 2(d/L)\sin(\alpha) + (d/L)^2} .$$

Using the fact that $(d/L)<<1$, the change in distance is given approximately by:

$$L' - L \simeq d\sin(\alpha) .$$

The increase in "image" width at the slit is, as before, approximately equal to $W(L'-L)/L$. Thus, the FOV in the altitude direction is increased by 0.02 arc-min per 0.001 inch of lateral displacement in the 1/8th meter instruments, and by 0.008 arc-min per 0.001 inch in the 1/4 meter instruments.

The table below summarizes the results.

TABLE 3. Effect on the altitude component of the FOV caused by 0.001 inch translations about the design of the telescope mirror within its cell.

TRANLATION DIRECTION	FOV EFFECT	1/8 M (ARC-MIN)	1/4 M (ARC-MIN)
Depth	Shift	0.125	0.05
Depth	Increase	0.12	0.06
Width	Shift	0.70	0.35
Width	Increase	0.02	0.008

XII. SOURCES FOR MAPPING THE FOV RESPONSE AND DETERMINING THE FOV AXIS.

Ideally, the illumination that should be used to map the FOV response is equivalent to a point source at infinity, i.e. a unidirectional parallel beam, large enough to completely fill the front aperture of the instrument at all offset angles of the instrument to the beam required by the experiment. (The largest offset angles are dictated by the anticipated in-flight presence of off-axis sources much brighter than those intended to be measured, e.g. the sun relative to the airglow.) In theory, a parallel beam of illumination is produced by placing a point source at the focus of

a mirror whose surface is a paraboloid of revolution.

In practice, the effective source usually is a small, but finite-sized aperture placed at the focus of the mirror and illuminated by an emitting source of light, positioned so that the beam illuminating the instrument comes from an off-axis section of the mirror unobstructed by the source of light or the aperture holder. Thus, in practice, the illumination is not a perfectly parallel beam, even if the figure of the mirror for the section used is perfect. Inherent in it are aberrations caused by the finite size of the effective source. That is, the beam reflected from the mirror from points within the effective source that are off the axis of revolution of the surface is not parallel. The angle of reflection has terms that depend, either individually or in product form, on the ratio of the off-axis distance of the source point to the focal length, and on the ratio of the off-axis mirror distance to the focal length. The first of these determines the angular FOV, which should be small in the direction of the component of the FOV to be measured. The second is largely responsible for the non-parallelsim; thus, the instrument and mirror should be oriented so that the off-axis direction of the section of the mirror used is perpendicular to the direction of the component of the FOV to be measured.

Less stringent requirements on the source are needed to determine the components of the field-of-view axis of an instrument because the source size then can be increased in the direction perpendicular to the component being measured. That is, the source can effectively be a "line" at infinity, rather than a "point", because of the symmetry of the optical systems in the direction corresponding to the slit-length. However, the line must be accurately oriented, else the effective source size is increased in the direction of the component to be measured.

Since a "line" source at infinity is difficult to reproduce in the laboratory, raytracing was used to examine the shape of the signals behind the telescope and exit slits of the MUV and NUV instruments as sources of finite angular size or at finite distances were passed across the FOV. Appendix D shows the results. As anticipated, the most critical parameter is the full size (including aberrations) of the image of the source at the plane of the telescope slit in the direction of the component of the field-of-view axis to be measured. For determining the component in the altitude direction, this should be no larger than the slit-width. The equations developed from simple geometric optical considerations and given in Appendix D can be used to estimate the required source distance to achieve this. However, if the response of one or more of the optical components or the detector is dependent on the area illuminated, the effective source distance should be infinity, since sources at finite distances do not duplicate the illumination the optical system will have in flight.

XIII. SUMMARY OF RESULTS PERTAINING TO CO-ALIGNMENT.

Because of the spherical off-axis telescope mirror, the optical axis of a RAIDS instrument, if defined in the traditional manner by the central ray, is not a useful quantity for determining the field of view. Its component in the altitude (slit-width) direction can not be accurately determined, either visually or from the signal. In lieu of it, we defined a field of view axis determined from the signal when the instrument was in its flight configuration, proposing that the components of this axis be defined by the center of the FWHM of the signal as a source satisfying specific conditions was moved across the field of view in the component direction. The source conditions for determining the component in the altitude direction were: (1) that the width of the "image" of the source at the plane of the slit (including aberrations) be no larger than the slit-width, and (2) if any optical element or detector has a response dependent on the area illuminated, the effective source distance be infinity. Since the response of a spectrometer to a particular direction of illumination was shown to depend on the wavelength setting of the grating within a spectral line, a pre-condition for a spectrometer instrument is that the grating first be set at the wavelength position corresponding to the maximum signal from an angularly broad source, i.e. a source producing illumination over the full field of view of the instrument.

The co-alignment process places more restrictions on the alignment of the telescope mirror than does attainment of the optical goals. The raytracing results have demonstrated that the optical goals for spatial or spectral resolutions can be achieved under misalignments of the telescope mirror equivalent to more than $\pm$12 arc-minute shifts in the absolute field of view. But the co-alignment process has a mechanical limitation on the amount of rotation in the direction corresponding to altitude of $\pm$12 arc-min, which requires that the altitude component of the field of view axis be aligned to the mechanical axis within this limit. A critical step determining the outcome is the lateral positioning of the telescope mirror in its cell. Lateral displacement of the center of the mirror from that in the design results in a shift of the absolute field of view of about 0.7 arc-min per 0.001 inch displacement for an 1/8th meter instrument.

XIV. PROPOSED ALIGNMENT PROCEDURE.

The initial steps in the following procedure make extensive use of several devices RSI has provided. Three of these are alignment fixtures: one attaches to the snout (hereafter called AF1), one replaces the mirror-cell (hereafter called AF2), and one replaces the flight slit (hereafter called AF3). These fixtures have accurately positioned small holes at the position corresponding to the transit of the central ray in the design drawings. The fourth device is a baseplate to which either the NUV or the MUV instruments can be attached during alignment and vibration testing. The baseplate has provision to attach a flat reference mirror (an extra boresight mirror or a witness mirror) to its top surface.

The procedure also requires extensive used of an autocollimator or similar optical device that enables determination of the relative orientation between two flat reflecting surfaces. The procedure assumes that the device used is capable of measuring the relative orientation to better than the required accuracy of $\pm$ 0.5 arc-minute. (NRL's Solar Physics Branch has two high-quality autocollimating theodolites capable of measuring to an accuracy of $\pm$0.5 arc-second, i.e. 60 times better than required for RAIDS, and capable of doing so when viewing an area as small as ~0.25 inch in diameter.)

1. Establish the mechanical axis.

Attach AF1, AF2, and AF3 to the instrument. Position a narrow beamed laser in front of the snout so that the central holes in AF1 and AF2 are symmetrically illuminated, determined from the symmetry of intensity on the front of AF1 and in the beam exiting AF2 on a fixed surface. The distance between AF2 and the fixed viewing surface should be large enough to clearly show the distribution of intensity within the exiting beam.

2. Establish a reference axis that is fixed relative to the instrument.

Although it is not necessary at this stage of alignment, it is useful to align this reference axis parallel to the mechanical axis. The following procedure uses this requirement, and subsequent steps assume that the reference mirror has been so aligned.

Position a good quality optical transfer flat between the snout and the laser. The flat should be wide enough to span the distance between the laser beam, all of the reference mirror, and all of the area that the boresight mirror later will occupy. Align the transfer flat to the laser beam, using both the reflected and transmitted beams. Align the reference mirror to the transfer flat using an autocollimator. The direction established by the reference mirror normal is used in subsequent steps to

determine if the instrument has been moved relative to the laser. boresight mirror to the optical transfer flat.

3. Perform initial alignment of the telescope mirror.

The mirror should be centered laterally within its cell as accurately as possible. Install the cell in the telescope. Check that the instrument has not been moved relative to the laser using the autocollimator to view the reference mirror and the optical flat. Adjust the telescope mirror within its cell so that the laser beam is centered in the central hole of AF3. The beam also should pass through the hole in AF1 that is located in its extension into the beam exiting AF3.

4. Align the boresight axis to the mechanical axis.

Remove AF1 and install the boresight fixture and boresight mirror, keeping the optical flat in place. Confirm that the instrument has not moved relative to the optical transfer flat using the autocollimator to view the reference mirror and the optical flat. Move the autocollimator to view the boresight mirror through the optical transfer flat, and align the boresight mirror to the optical flat.

5. Determine the reproducibilty of boresighting.

Remove and replace the boresight fixture. Use the autocollimator to view first the boresight mirror and the optical transfer flat, then the reference mirror and optical transfer flat to determine that the instrument has not been moved during the process. Repeat the step several times.

6. Determine the the field-of-view axis relative to the mechanical axis.

The boresight fixture must be removed during the FOV measurements because the aperture in it is smaller than the front aperture of the instrument and, thus, it would affect the FOV. However, ultimately, the the angle between the boresight axis and the field-of-view axis must be determined in the two component directions. Since the components of the field-of-view axis will be determined by some position of the source, the setup conditions must at some point allow determination of the source angle relative to the boresight axis.

Align the source to the instrument. If the boresight mirror is needed for this step, the instrument must be rigidly held during its removal. The autocollimator viewing the optical transfer flat and the reference mirror

can be used to determine that motion has not occurred.

By effectively rotating the instrument about the center of the telescope mirror in one of the component directions, determine the source-to-instrument angle that corresponds to that component of the field-of-view axis. Then, change the instrument-to-source orientation by 90 degrees, align the instrument to the source and determine the other component of the field-of-view axis.

Determine the angle between the field-of-view axis and the boresight axis. If the components of this angle are greater than about ± 6 arc minutes in the direction corresponding to altitude or ± 3 arc minutes in the longitude direction, the telescope mirror must be realigned. The value of the misalignment tolerance in the altitude direction assumes that the coalignment process during installation will purposely offset the instrument angularly (using the boresight mirror) so that the field-of-view axis ends up pointing properly to within the required accuracy of $\pm$ 0.5 arc-minute in the altitude direction. The value is about 1/2 of the maximum that could be tolerated, so that installation on a fin has some adjustment available. The misalignment tolerance in the longitude direction, likewise is about 1/2 of the maximum, in this case, it being assumed that the lack of flatness of a fin could add to the offset.

7. (Optional) Realign the boresight mirror to be parallel to the field-of-view axis.

Since purposely off-setting one mirror to achieve alignment of a second optical system is fraught with the possibility of a sign error in the transfer process, an alternative procedure would be to re-align the boresight axis to the field-of-view axis for each instrument at this step of the procedure. The source used to determine the field-of-view axis then could be used to check the result.

XV. PROPOSED CO-ALIGNMENT PROCEDURE

The goals of this procedure are to install the instruments so that: (1) the FOV axes are parallel to each other, and (2) during motion of the scan platform, the field-of-view axis for each instrument moves in a plane perpendicular to what will be the Z-axis of the satellite. Thus, co-alignment involves not only mutual alignment of the instruments, but also alignment of the instruments relative to RAIDS payload structure and alignment of the payload structure relative to the satellite.

The procedure assumes that the optical cube shown in Figure 2 establishes the set of three orthogonal axes that will be used for reference both during installation of the payload into the satellite and

during installation of the instruments onto the fins. That is, it assumes that, although the exact location of the optical cube has yet to be determined, it's surfaces will be aligned to be perpendicular to the satellite axes wherever it is located, to within the tolerances of the baseplate mounting holes that will be used to attach the RAIDS payload to the satellite. It further assumes that the relation between the field-of-view axis and the boresight axis is known for each instrument.

The procedure is based on the availability of an autocollimating theodolite and two high-quality transfer flats. The flats should be as large as possible. These requirements are driven by the following three geometric conditions of the RAIDS payload. The first is the distance among the optical alignment surfaces (boresight mirrors and optical cube). The second is the angle between the payload reference axis and the boresight axis of any one instrument. The third is that three different mounting surfaces (fins) are used to mount the six instruments.

Regarding the first, at the front of the payload, the optical alignment surfaces (boresight mirrors and optical cube) span large distances: about 28 inches along the Z-axis of the satellite and, depending on the location of the optical cube, about 18 inches along the X-axis of the satellite. (See Figure 3.) Regarding the second, the design limits of the scan platform angle relative to the surface of the baseplate are 26.5° and 10°. The lower limit of 10° means that the scan platform can not be rotated to move the boresight axis of an instrument to (or through) a direction parallel to the payload reference axis. The third geometric condition compounds the difficulty caused by the first two conditions because it means that the scan axis must be determined three times.

The procedure is detailed in the following steps.

1. Perform preliminary installation of the instruments onto the fins.

   (The boresight fixtures should be attached beforehand.) Adjust the attachment of each instrument to center it within the "play" available.

2. Establish a transfer surface whose normal is parallel to the payload reference axis in the vicinity of the projected area of the boresight mirror of one instrument.

   (Although the instrument selected may be dictated by the sizes of the available transfer flats, it would be best if the instrument first aligned is the one whose boresight axis is most closely aligned with its field-of-view axis.) Move the scan platform to the small-angle limit. Position a good quality optical transfer flat as close to the payload as will still allow access to adjust the instruments on the fins. The position of the flat in the satellite X-Z plane should be so that the surface of the

optical cube defining the payload reference axis can be viewed through the flat, and so that the maximum dimension of the flat extends toward the boresight mirror of the first instrument to be co-aligned. Using an autocollimating theodolite to view the surface of the optical cube through the transfer flat, align the flat to be parallel to to the surface of the optical cube.

Since it is unlikely that the surface of the transfer flat will extend far enough, position a second good quality optical transfer flat so that it: (a) allows access to adjust the instrument attachment; (b) has at least an inch overlap with the surface of the first transfer flat; and (c) extends well beyond the projected area of the boresight mirror for the instrument to be co-aligned.

Move the autocollimating theodolite to view the overlap region of the two transfer flats, and align the surface of the second transfer flat to be parallel to the surface of the first.

3. Align the field-of-view axis of the first instrument relative to the satellite X-Y plane, and establish the scan-angle reference.

The angle of the field-of-view axis of this instrument relative to the baseplate will be used as the scan-angle reference for all of the other instruments. If installation of the other instrument uncovers some abnormality in its attachment, readjustment may be required.

Change the angle of the theodolite about the axis corresponding to a rotation about the satellite Z-axis by an amount that anticipates viewing the boresight axis (10°) and reposition the theodolite to view the boresight mirror. Turning off the room lights to observe the illumination from the autocollimating theodolite should assist in determining the position. If the theodolite can not be aligned to the boresight axis at any position for the current angle settings, change the angle settings (and position, if required) until it can. Record the theodolite angles.

Align the theodolite to the transfer surface, changing only the angles. Record the theodolite angles.

Knowing the offsets required between the boresight axis and the field-of-view axis, determine if the field-of-view axis of this instrument is in the X-Y plane of the satellite. If it is not, shim the feet as required.

4. Determine the scan axis for the fin of the instrument aligned above.

Re-align the theodolite to the boresight axis. Move the scan platform through an angle that still permits aligning the theodolite to both transfer flat and boresight mirror. (A third transfer flat may be required to accomplish this. It should be overlapped and aligned with the second,

as done in Step 2 above for the first and second transfer flats.) Reposition the theodolite and align it to the boresight axis at the new scan-angle. Record the theodolite angles.

Changing only the angles, align the theodolite to the transfer flat. Record the theodolite angles.

Repeat the process at several scan-angles. Using the recorded angles, determine the relation between the scan axis for this fin and the payload reference axis.

NOTE: At this point, there are two alternative ways to proceed.

(A) Continue using transfer surfaces parallel to the payload reference axis.

(B) Establish a transfer surface parallel to the boresight axis of the first instrument aligned at one position of the scan platform.

Although it is usually a good practice to co-align to a primary reference, i.e. to the payload reference axis, the considerable off-set distances of the boresight axes to the primary reference in this case make the process so complex that it probably is wise to chose (B), since this would be more likely to ensure that the instruments end up looking in the same direction.

---

5. Establish a transfer surface parallel to the boresight axis of the first instrument aligned.

At a fixed position of the scan platform, use the autocollimating theodolite to align the second transfer flat to the boresight axis of the first instrument aligned. The transfer flat should be positioned so as to: (a) overlap the projected boresight mirror area of as many instruments as possible, and (b) allow access to adjust the instrument's attachment.

6. Co-align the other instruments to the first instrument aligned.

Alternately align the theodolite to the boresight axis of one instrument, then (changing only the theodolite angles) align the theodolite to the transfer flat. Adjust the instrument alignment as required. At the optimum co-alignment, record the two sets of theodolite angles.

Reposition the theodolite, and repeat the process for the next instrument, etc. Re-establish the transfer surface across the payload as required.

7. Determine the scan axis of the other fins.

If the scan-platform angles can easily be reproduced and if the transfer flat has sufficient extension in the appropriate direction, the

scan axis of a fin can be checked or determined at the co-alignment of each instrument done in Step 6, returning the scan platform to the angle that exactly duplicates the position it had in aligning the transfer flat to the boresight axis of the first instrument. Otherwise, a procedure similar to Step 4 should be done for at least one instrument on each fin.

8. Using the measurements of the theodolite angles, determine the relation of the field-of-view axis of each instrument to the payload reference axis and to the scan axis.

9. Check that the transfer process has been done correctly.

Chosing some instrument other than the first aligned, begin the transfer process from the optical cube to the boresight mirror, keeping the transfer surfaces parallel to the surface of the optical cube that defined the payload reference axis. At a position of the scan platform previously used in the co-alignment process, realign the theodolite alternately to the boresight axis of the instrument and to the normal to the transfer flat, changing only the angles of the theodolite. After recording the two sets of angles, determine that the relation between the field-of-view axis of the instrument and the payload reference axis is the same as was previously obtained.

Repeat the process for at least one other angle of the scan platform.

XVI. SUMMARY.

Co-aligning the six generically similar RAIDS instruments begins with alignment of the telescopes, requiring that the component of the field of view axis in the direction corresponding to altitude be less than $\pm$12 arc-minutes from the mechanical (or attachment) axis. Determining the field-of-view axis requires careful consideration of the source: the size of the illumination it produces at the telescope slit, and the illuminated area it produces on the optical components and detector.

Since co-alignment refers to the absolute pointing of the instruments relative to the earth, the co-alignment process requires more than mutual alignment of the common fields of view; it requires determining the orientation of the field of view of each instrument relative to what will be the axes of the satellite. That determination is accomplished via an intermediate optical reference - an optical cube which will be attached to the RAIDS stucture and used to align the payload within the satellite. The surface of the cube in the anti-velocity direction of the satellite

establishes the payload reference axis to which individual field-of-view axes are referenced. The co-alignment procedure is made complex by three geometric factors of the payload: the 10° minimum angle of the scan platform relative to the surface of the baseplate to which the optical cube is aligned, the large distances between apertures, and the fact the instruments are attached to the scan platform via three separate fins. These factors will require numerous sequential transfers of at least two optical flats in order to accomplish the co-alignment. The proposed procedure attempts to reduce some of the complexity by carefully aligning one instrument to the optical cube, and using its boresight axis as a reference for: (a) the scan platform angle, and (b) the co-alignment of the other instruments.

ACKNOWLEDGEMENTS

Partial support for the development of RAIDS has been provided by the Defense Meteorological Satellite Program and by the Space and Naval Warfare Systems Command. Spaceflight sponsorship is provided by the Space Test Program.

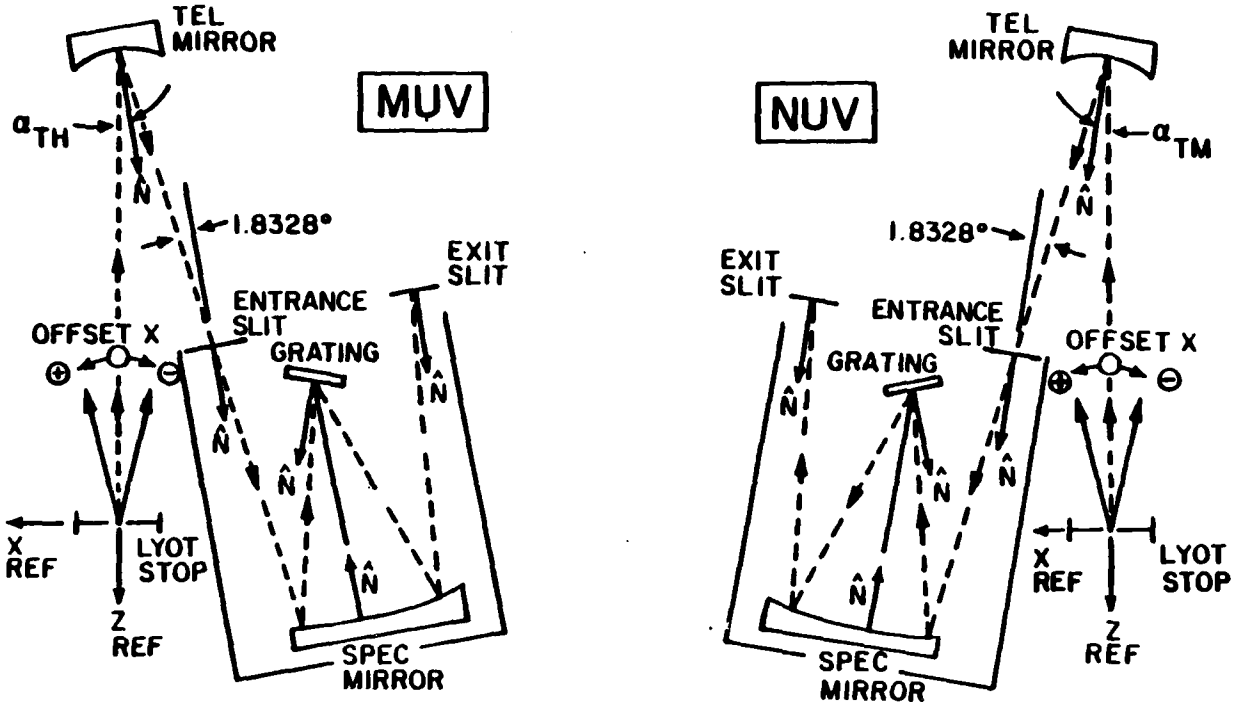

FIGURE 1. "Top" view of the optical layout of the MUV and NUV instruments (not to scale). $\hat{N}$ is the direction of the normal to each surface at the origin of the local coordinate system used to specify the surface and defines +Z of that system. The angle between Z_{REF} and $\hat{N}$ is α in Table A2 of Appendix A. The features that have been exaggerated are the angle between N for the plane of the entrance slit and the central ray (dotted line) , the asymmetry of the illumination on the spectrometer mirror on passages of light to and from the grating, and the asymmetries of the centers of the slits relative to the center of the grating across the width and along the length of the spectrometer. OFFSET X is a raytracing parameter that determines the angular offset of an incident parallel beam relative to the design optical axis in the direction corresponding to altitude, with the sign convention that higher altitudes are from the - direction for the MUV and from the + direction for the NUV.

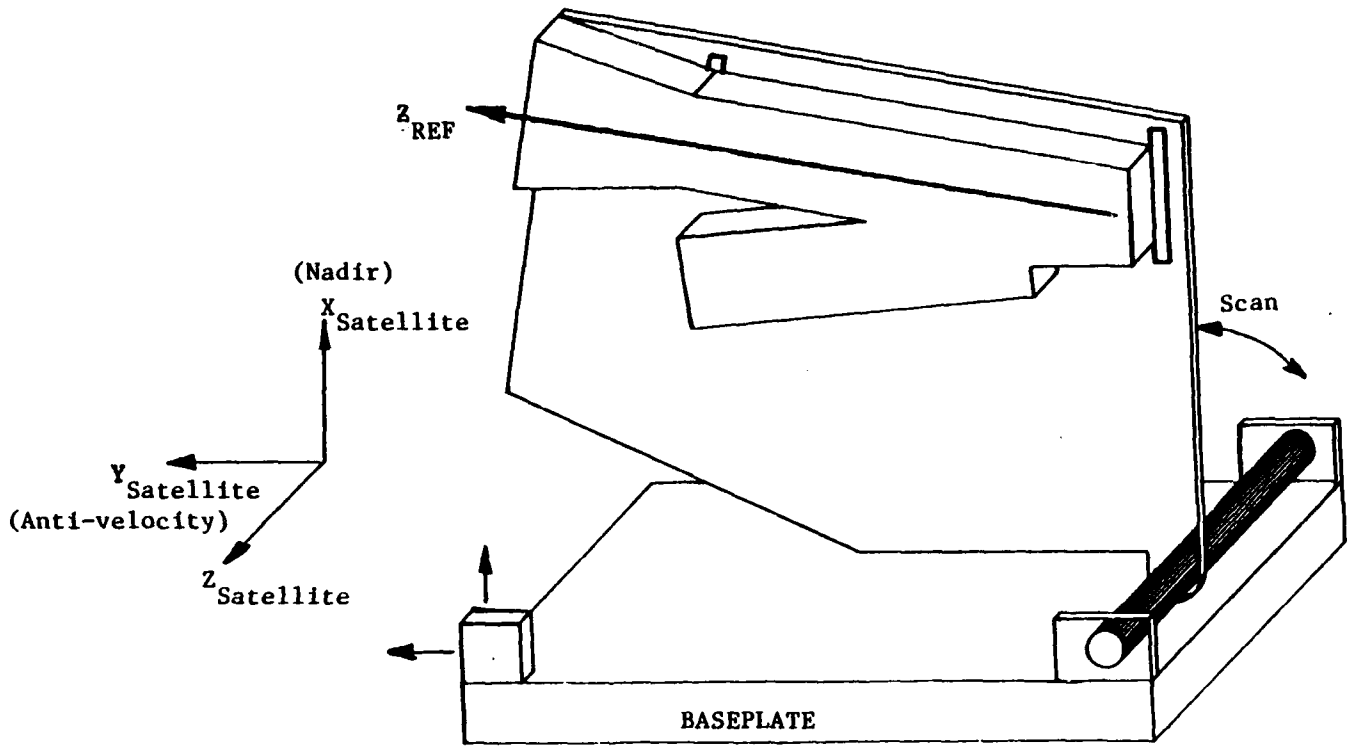

FIGURE 2. A sketch illustrating the orientation of one of the six instruments within the satellite to show the relation among the satellite axes, the two surfaces of the optical cube used to align the RAIDS payload within the satellite, the Z_{REF} axis of the coordinate system used in the raytracing code, and the scan axis of the fin to which the instrument is attached. The mechanical limits of the angle between Z_{REF} and the plane of the baseplate are 10° and 26.5°.

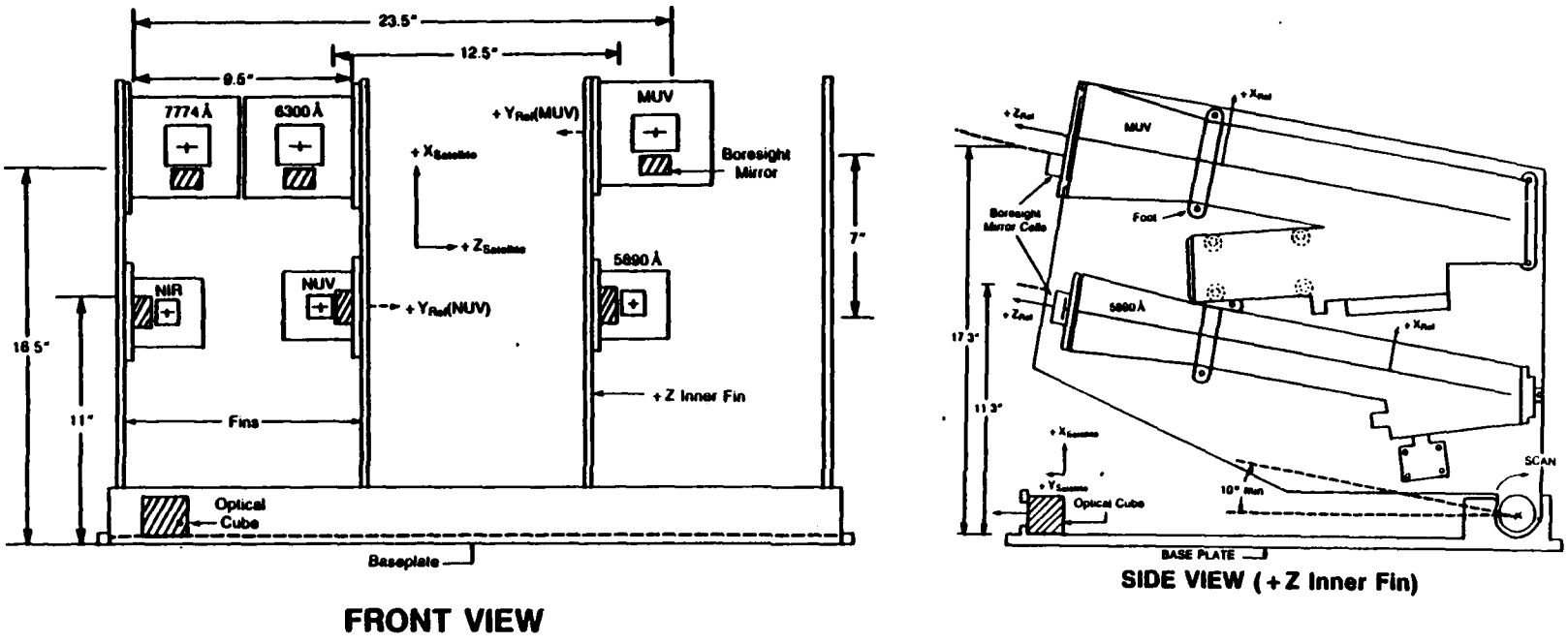

FIGURE 3. Front view (left) of the six instruments installed in the payload with the removable boresight fixtures attached (mirrors are the shaded rectangles), and side view (right) of one fin, showing the approximate relative distances among the optical surfaces used during co-alignment to illustrate the logistical requirements of the process. The exact location of the optical cube on the surface of the baseplate has not been finalized. The longer arm of the cross centered in each aperture is along the slit-length or longitude direction.

FIGURE 4 (A). Array diagram of the image at the telescope slit plane from a parallel beam incident along the design optical axis of the MUV telescope, aligned as designed (mirror angle = -8.0°). The beam originated from a grid of 51 X 51 points within a 4.1 cm X 4.9 cm entrance aperture centered in the Lyot-stop. The mirror was masked to 4.2 cm X 5.0 cm. Each element of the array is the number of rays falling within a 25 micron (X) by 50 micron (Y) area of the slit plane, with the upper left element being the number of rays falling between $-300 \leq X < -275$ micron, and $-700 \leq Y < -650$ micron. In this plane, the slit center is at (X,Y) = (0,0); the sides are at X = -250 micron and X = +250 micron. The maximum image size in the X and Y directions and the X or Y coordinates determining these (in parentheses) are:

XDIAM= 264.78 (-262.01, +2.77) micron;
YDIAM= 1242.10 (-621.05, +621.05) micron.

```
                                        +X--->
      <------------------ S L I T    W I D T H ------------------>
 0  0  0  0  0  0  0  0  0  0  0  0  0  0  0  0  0  0  0  0  0  0
 0  1  2  2  0  0  0  0  0  0  0  0  0  0  0  0  0  0  0  0  0  0
 0  2  5  5  7  5  5  2  0  0  0  0  0  0  0  0  0  0  0  0  0  0
 0  0  5  4  5  7  7 11 14  0  0  0  0  0  0  0  0  0  0  0  0  0
 0  0  2  6  5  5  7  8 29 16  0  0  0  0  0  0  0  0  0  0  0  0
 0  0  2  4  4  5  8 14 21 40  0  0  0  0  0  0  0  0  0  0  0  0
 0  0  2  5 10 11 11 16 17 29 21  0  0  0  0  0  0  0  0  0  0  0
 0  2  5 11  9 10 12 12 18 20 41  0  0  0  0  0  0  0  0  0  0  0
 0  0  1 10  8 12 10 13 14 19 33 14  0  0  0  0  0  0  0  0  0  0
 0  0  0  3 10 11 12 10 13 15 28 29  0  0  0  0  0  0  0  0  0  0
 0  0  0  2  6  9 12 13 12 16 20 40  0  0  0  0  0  0  0  0  0  0
 0  0  0  2  4 11  9 11 13 13 21 42  0  0  0  0  0  0  0  0  0  0
 0  0  0  2  4  7 10 10 12 15 18 37  8  0  0  0  0  0  0  0  0  0
 0  0  0  1  2  5  9 10 12 12 15 27 11  0  0  0  0  0  0  0  0  0
 0  0  0  2  4  8 13 14 17 17 23 39 18  0  0  0  0  0  0  0  0  0   +Y
 0  0  0  2  4  7 10 10 12 15 18 37  8  0  0  0  0  0  0  0  0  0    ↓
 0  0  0  2  4 11  9 11 13 13 21 42  0  0  0  0  0  0  0  0  0  0
 0  0  0  2  6  9 12 13 12 16 20 40  0  0  0  0  0  0  0  0  0  0
 0  0  0  3 10 11 12 10 13 15 28 29  0  0  0  0  0  0  0  0  0  0
 0  0  1 10  8 12 10 13 14 19 33 14  0  0  0  0  0  0  0  0  0  0
 0  2  5 11  9 10 12 12 18 20 41  0  0  0  0  0  0  0  0  0  0  0
 0  0  2  5 10 11 11 16 17 29 21  0  0  0  0  0  0  0  0  0  0  0
 0  0  2  4  4  5  8 14 21 40  0  0  0  0  0  0  0  0  0  0  0  0
 0  0  2  6  5  5  7  8 29 16  0  0  0  0  0  0  0  0  0  0  0  0
 0  0  5  4  5  7  7 11 14  0  0  0  0  0  0  0  0  0  0  0  0  0
 0  2  5  5  7  5  5  2  0  0  0  0  0  0  0  0  0  0  0  0  0  0
 0  1  2  2  0  0  0  0  0  0  0  0  0  0  0  0  0  0  0  0  0  0
```

FIGURE 4 (B). Array diagram of the image near the center of the telescope slit from a parallel beam incident at a 12 arc-min angle with respect to the design optical axis of the MUV telescope, with the mirror misaligned 6 arc-min in a direction toward the beam (mirror angle = -8.1°). The beam originated from a grid of 51 X 51 points within a 4.1 cm X 4.9 cm entrance aperture centered in the Lyot-stop. The mirror was masked to 4.2 X 5.0 cm. Each element of the array is the number of rays falling within a 25 micron (X) by 50 micron (Y) area of the slit plane, with the upper left element being the number of rays falling between $-300 \leq X < -275$ micron and $-700 \leq Y < -650$ micron. In this plane, the slit center is at (X,Y) = (0,0); the sides are at X = -250 micron and X = +250 micron. The maximum image size in the X and Y directions and the X or Y coordinates determining these (in parentheses) are:

XDIAM= 249.10 (-245.64, +3.46) micron;
YDIAM= 1214.70 (-607.35, +607.35) micron.

												+X--->										
		<----------							S	L	I	T		W	I	D	T	H	----------			>
0	0	0	0	0	0	0	0	0	0	0	0	0	0	0	0	0	0	0	0	0	0	
0	0	2	0	0	0	0	0	0	0	0	0	0	0	0	0	0	0	0	0	0	0	
0	0	3	6	6	5	4	0	0	0	0	0	0	0	0	0	0	0	0	0	0	0	
0	0	2	4	6	5	9	12	9	0	0	0	0	0	0	0	0	0	0	0	0	0	
0	0	0	4	5	7	6	9	28	15	0	0	0	0	0	0	0	0	0	0	0	0	
0	0	0	4	4	4	8	12	23	38	0	0	0	0	0	0	0	0	0	0	0	0	
0	0	0	5	7	10	12	18	16	28	24	0	0	0	0	0	0	0	0	0	0	0	
0	0	4	8	9	11	11	14	18	19	40	0	0	0	0	0	0	0	0	0	0	0	
0	0	0	3	12	9	11	11	16	19	34	16	0	0	0	0	0	0	0	0	0	0	
0	0	0	0	7	11	11	13	14	17	22	33	0	0	0	0	0	0	0	0	0	0	
0	0	0	0	4	8	11	12	12	16	24	39	0	0	0	0	0	0	0	0	0	0	
0	0	0	0	4	7	11	10	14	13	20	44	1	0	0	0	0	0	0	0	0	0	
0	0	0	0	3	5	10	10	12	15	18	36	10	0	0	0	0	0	0	0	0	0	
0	0	0	0	1	2	12	10	12	13	14	25	14	0	0	0	0	0	0	0	0	0	
0	0	0	0	2	4	17	14	17	18	21	38	21	0	0	0	0	0	0	0	0	0	+Y
0	0	0	0	3	5	10	10	12	15	18	36	10	0	0	0	0	0	0	0	0	0	↓
0	0	0	0	4	7	11	10	14	13	20	44	1	0	0	0	0	0	0	0	0	0	
0	0	0	0	4	8	11	12	12	16	24	39	0	0	0	0	0	0	0	0	0	0	
0	0	0	0	7	11	11	13	14	17	22	33	0	0	0	0	0	0	0	0	0	0	
0	0	0	3	12	9	11	11	16	19	34	16	0	0	0	0	0	0	0	0	0	0	
0	0	4	8	9	11	11	14	18	19	40	0	0	0	0	0	0	0	0	0	0	0	
0	0	0	5	7	10	12	18	16	28	24	0	0	0	0	0	0	0	0	0	0	0	
0	0	0	4	4	4	8	12	23	38	0	0	0	0	0	0	0	0	0	0	0	0	
0	0	0	4	5	7	6	9	28	15	0	0	0	0	0	0	0	0	0	0	0	0	
0	0	2	4	6	5	9	12	9	0	0	0	0	0	0	0	0	0	0	0	0	0	
0	0	3	6	6	5	4	0	0	0	0	0	0	0	0	0	0	0	0	0	0	0	
0	0	2	0	0	0	0	0	0	0	0	0	0	0	0	0	0	0	0	0	0	0	

FIGURE 5 (A). Array diagram of the image at the telescope slit plane from a parallel beam incident along the design optical axis of the NUV telescope, aligned as designed (mirror angle = 10.145°). The beam originated from a grid of 51 X 51 points within a 2.05 cm X 2.45 cm entrance aperture centered in the Lyot-stop. Each element of the array is the number of rays falling within a 25 micron (X) by 50 micron (Y) area of the slit plane, with the upper left element being the number of rays falling between $-125 \leq X < -100$ micron, and $-450 \leq Y < -400$ micron. In this plane, the slit center is at (X,Y) = (0,0); the sides are at X = -125 micron and X = +125 micron. The maximum image size in the X and Y directions and the X or Y coordinates determining these (in parentheses) are:

XDIAM= 181.38 (-0.03, +181.35) micron;
YDIAM= 889.66 (-444.83, +444.83) micron.

					+X--->											
<--------			S L I T			W I D T H				------->						
0	0	0	0	0	0	0	3	9	11	7	0	0	0	0	0	
0	0	0	0	0	0	17	34	15	12	3	0	0	0	0	0	
0	0	0	0	0	0	57	37	22	14	0	0	0	0	0	0	
0	0	0	0	0	6	68	33	26	21	9	8	2	0	0	0	
0	0	0	0	0	42	47	29	24	17	10	9	2	0	0	0	
0	0	0	0	0	59	39	30	22	16	12	3	0	0	0	0	
0	0	0	0	0	66	37	26	24	15	9	0	0	0	0	0	
0	0	0	0	0	71	37	26	22	14	4	0	0	0	0	0	
0	0	0	0	0	71	22	22	18	10	4	0	0	0	0	0	
0	0	0	0	1	94	31	30	24	13	5	0	0	0	0	0	+Y
0	0	0	0	0	71	37	26	22	14	4	0	0	0	0	0	↓
0	0	0	0	0	66	37	26	24	15	9	0	0	0	0	0	
0	0	0	0	0	59	39	30	22	16	12	3	0	0	0	0	
0	0	0	0	0	42	47	29	24	17	10	9	2	0	0	0	
0	0	0	0	0	6	68	33	26	21	9	8	2	0	0	0	
0	0	0	0	0	0	57	37	22	14	0	0	0	0	0	0	
0	0	0	0	0	0	17	34	15	12	3	0	0	0	0	0	
0	0	0	0	0	0	0	3	9	11	7	0	0	0	0	0	
0	0	0	0	0	0	0	0	0	0	0	0	0	0	0	0	
0	0	0	0	0	0	0	0	0	0	0	0	0	0	0	0	

FIGURE 5 (B). Array diagram of the image near the center of the telescope slit from a parallel beam incident at a 12 arc-min angle with respect to the design optical axis of the NUV telescope, with the mirror misaligned 6 arc-min in a direction toward the beam (mirror angle = 10.245°). The beam originated from a grid of 51 X 51 points within a 2.05 cm X 2.45 cm entrance aperture centered in the Lyot-stop. The mirror was masked to 2.1 cm X 2.5 cm. Each element of the array is the number of rays falling within a 25 micron (X) by 50 micron (Y) area of the slit plane, with the upper left element being the number of rays falling between $-125 \leq X < -100$ micron, and $-450 \leq Y < -400$ micron. In this plane, the slit center is at (X,Y) = (0,0); the sides are at X = -125 micron and X = +125 micron. The maximum image size in the X and Y directions and the X or Y coordinates determining these (in parentheses) are:

XDIAM= 178.62 (-0.03, 178.59) micron;
YDIAM= 873.36 (-436.68, 436.68) micron.

					+X--->											
<--------			S	L	I	T	W	I	D	T	H	-------->				
0	0	0	0	0	0	0	2	8	9	4	0	0	0	0	0	
0	0	0	0	0	0	13	31	15	13	0	0	0	0	0	0	
0	0	0	0	0	0	57	39	18	9	0	0	0	0	0	0	
0	0	0	0	0	5	68	38	27	17	10	6	1	0	0	0	
0	0	0	0	0	40	49	29	26	15	11	6	0	0	0	0	
0	0	0	0	0	61	38	31	21	16	9	0	0	0	0	0	
0	0	0	0	0	67	38	26	24	12	4	0	0	0	0	0	
0	0	0	0	0	73	35	28	22	10	0	0	0	0	0	0	
0	0	0	0	0	70	26	22	18	8	0	0	0	0	0	0	
0	0	0	0	1	93	36	29	24	10	0	0	0	0	0	0	+Y
0	0	0	0	0	73	35	28	22	10	0	0	0	0	0	0	↓
0	0	0	0	0	67	38	26	24	12	4	0	0	0	0	0	
0	0	0	0	0	61	38	31	21	16	9	0	0	0	0	0	
0	0	0	0	0	40	49	29	26	15	11	6	0	0	0	0	
0	0	0	0	0	5	68	38	27	17	10	6	1	0	0	0	
0	0	0	0	0	0	57	39	18	9	0	0	0	0	0	0	
0	0	0	0	0	0	13	31	15	13	0	0	0	0	0	0	
0	0	0	0	0	0	0	2	8	9	4	0	0	0	0	0	
0	0	0	0	0	0	0	0	0	0	0	0	0	0	0	0	
0	0	0	0	0	0	0	0	0	0	0	0	0	0	0	0	

FIGURE 6. Image array at the slit plane of the NUV telescope, aligned as designed, illustrating that parts of the image come from specific areas of the entrance aperture. Each array element is the total number of rays striking a 25 microns (X) by 50 microns (Y) area when the entrance aperture was divided into 25 sections of equal area and 961 rays (from 31 rows and 31 columns) within each area were sent toward the mirror in a direction parallel to the design optical axis. The upper right corner is at the slit coordinates X=0.0, Y= -450 microns. Each boxed region encloses the area of the image where 80% or more of the contribution to any one element of the array comes from one of the lettered sections of the entrance aperture.

IMAGE ARRAY AT SLIT PLANE

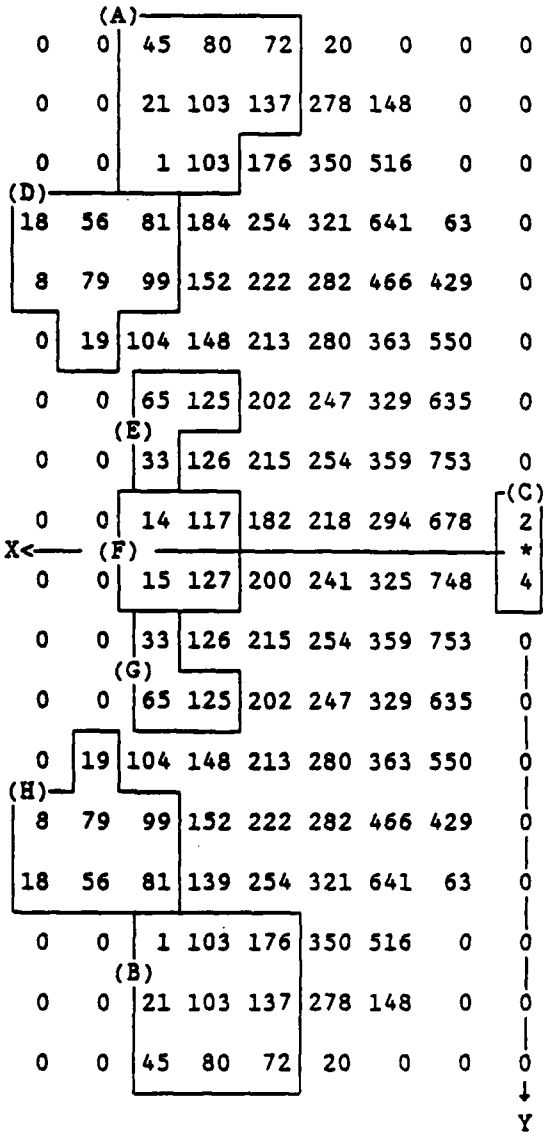

NUV
ENTRANCE APERTURE SECTIONS

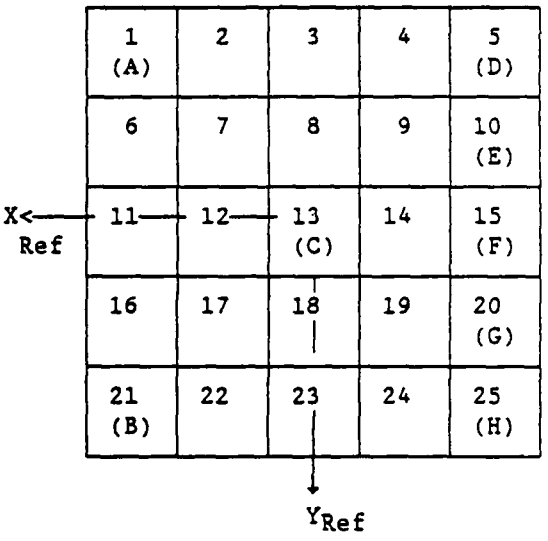

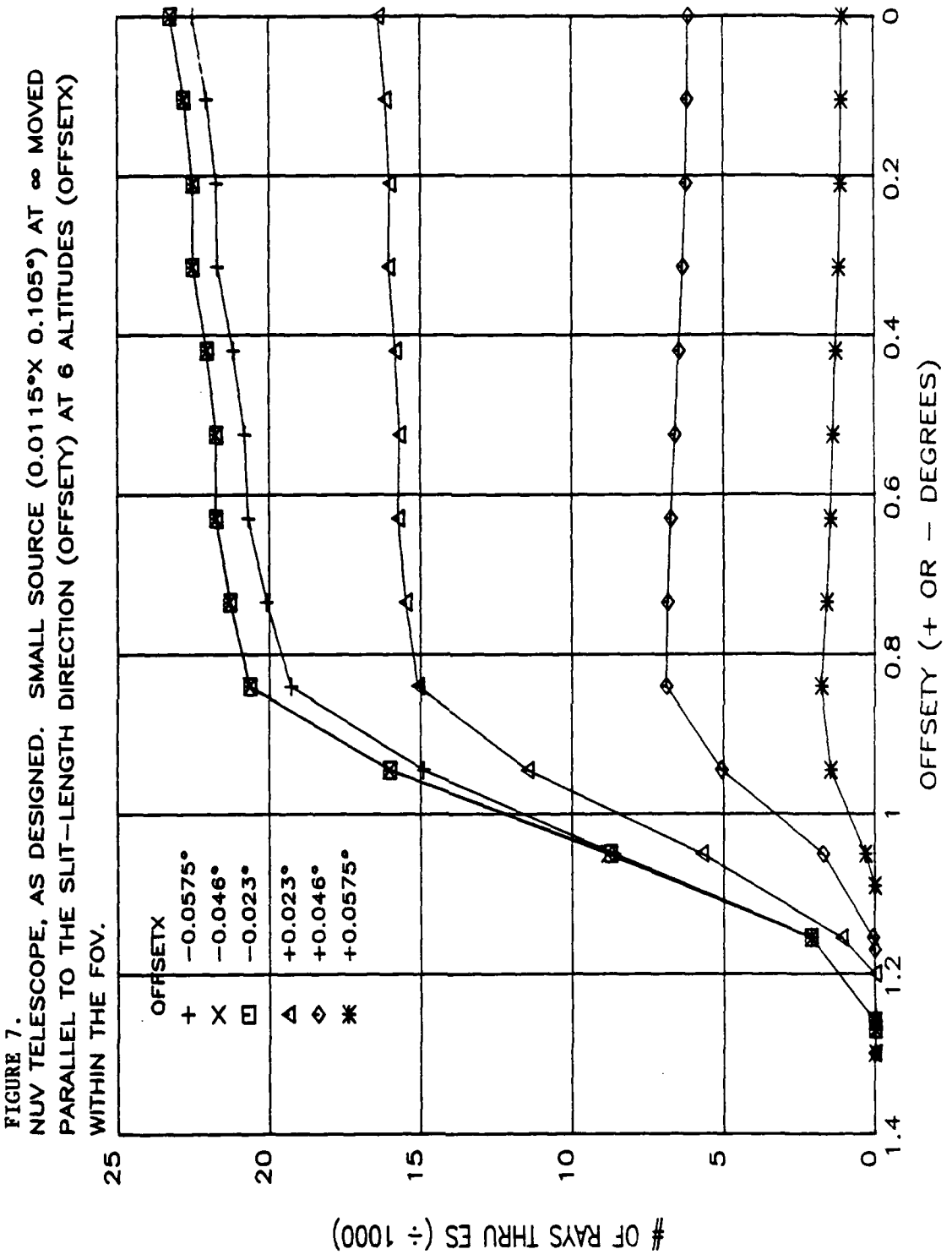

FIGURE 7.
NUV TELESCOPE, AS DESIGNED. SMALL SOURCE (0.0115°X 0.105°) AT ∞ MOVED PARALLEL TO THE SLIT-LENGTH DIRECTION (OFFSETY) AT 6 ALTITUDES (OFFSETX) WITHIN THE FOV.

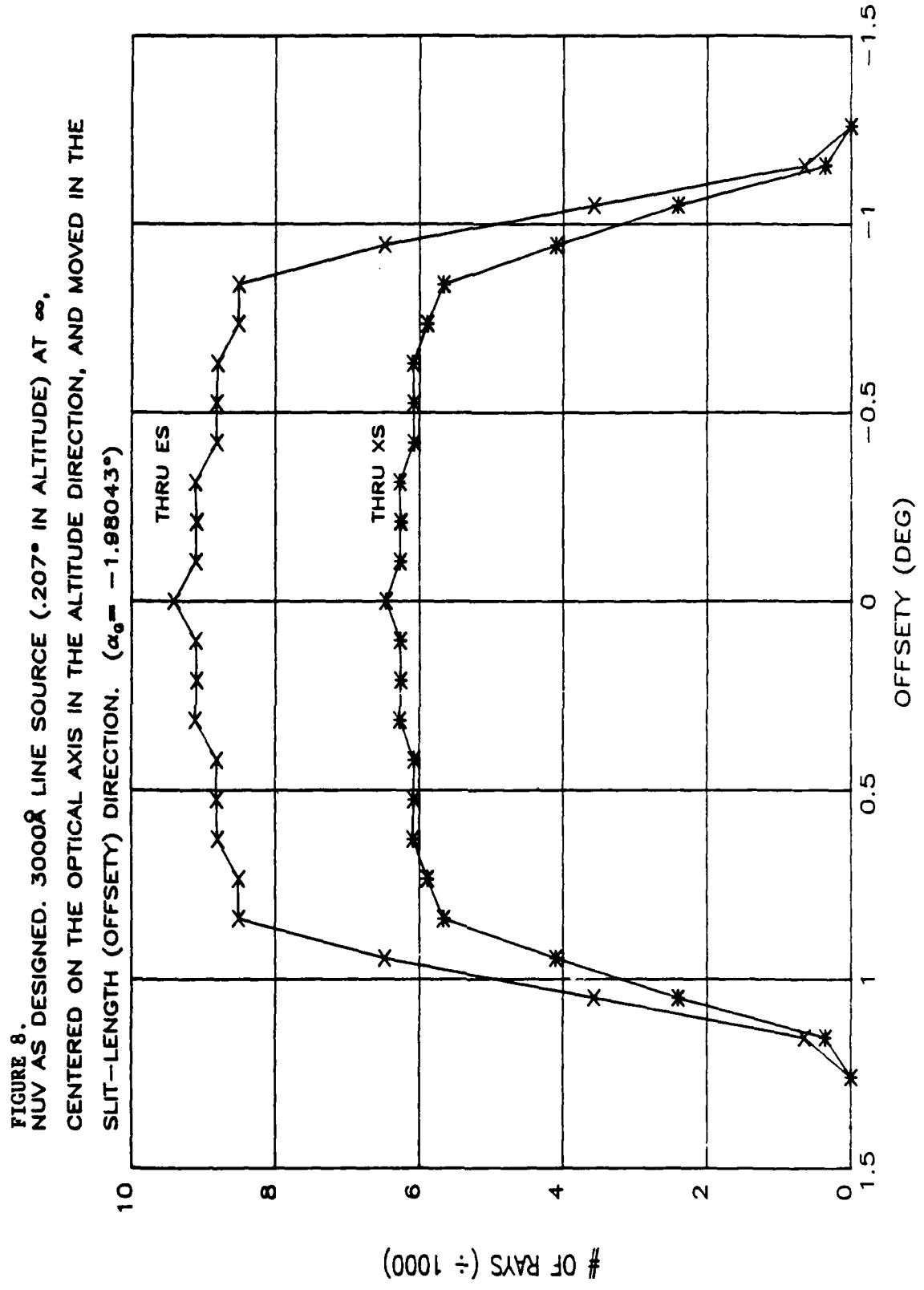

FIGURE 8.
NUV AS DESIGNED. 3000Å LINE SOURCE (.207° IN ALTITUDE) AT ∞,
CENTERED ON THE OPTICAL AXIS IN THE ALTITUDE DIRECTION, AND MOVED IN THE
SLIT−LENGTH (OFFSETY) DIRECTION. (α_0 = −1.98043°)

FIGURE 9 (A). Ray information about the extremes of illumination that pass through the entrance slit (ES), and the array diagram of the illumination at the spectrometer mirror (SM) of the NUV instrument, aligned as designed, from a longitude line source offset -0.0575° in altitude from the design optical axis. The array mesh is 0.2 cm X 0.2 cm, with the upper left element being the number of rays falling on SM between 0≤ X <0.2 cm, and -1.7≤ Y <-1.5 cm.

```
THERE WERE   20181 TOTAL RAYS FROM THE ENTRANCE APERTURE.
ELEMENT 1 (TM):         18210 RAYS PASSED.  16678 OF THESE HIT ELEMENT 4.
ELEMENT 2 (ES):         16678 RAYS PASSED.    ALL OF THESE HIT ELEMENT 4.
ELEMENT 3 (SM-MASK):    16678 RAYS PASSED.    ALL OF THESE HIT ELEMENT 4.
ELEMENT 4 (SM):         16678 RAYS PASSED,    ALL OF THESE HIT ELEMENT 4.
```

LOCAL EXTREME INTERSECTIONS FOR RAYS THAT MADE IT TO ELEMENT 4.

ELEMENT	XMIN,	Y-AT-XMIN	XMAX,	Y-AT-XMAX	YMIN,	X-AT-YMIN	YMAX,	X-AT-YMAX
1	-0.9959,	1.2250	1.0221,	-0.0034	-1.2280,	1.0168	1.2280,	1.0168
2	-0.0125,	-0.1614	0.0063,	-0.2089	-0.2250,	-0.0118	0.2250,	-0.0118
3	0.6367,	-1.1424	2.6178,	-0.1693	-1.3431,	0.6392	1.3431,	0.6392
4	0.5958,	-1.1777	2.6311,	-0.1684	-1.3764,	0.5995	1.3764,	0.5995

ILLUMINATION AT SM FOR OFFSETX = -0.0575°.

	+X--->																	
	0	0	0	0	0	0	0	0	0	0	0	0	0	0	0	0	0	0
	0	0	4	8	12	12	12	12	7	9	9	9	9	3	0	0	0	0
	0	0	11	65	75	75	75	73	58	73	77	74	72	24	0	0	0	0
	0	0	4	117	112	108	108	95	85	108	109	112	114	38	0	0	0	0
	0	0	0	139	149	153	151	104	133	141	138	138	138	46	0	0	0	0
	0	0	0	135	138	138	132	109	153	153	153	150	150	50	0	0	0	0
	0	0	0	138	138	138	114	115	136	138	142	147	147	49	0	0	0	0
	0	0	0	144	141	141	98	116	105	138	138	138	139	47	0	0	0	0
	0	0	0	153	159	159	106	123	87	153	159	159	157	51	0	0	0	0
+Y	0	0	0	144	141	141	98	116	105	138	138	138	139	47	0	0	0	0
↓	0	0	0	138	138	138	114	115	136	138	142	147	147	49	0	0	0	0
	0	0	0	135	138	138	132	109	153	153	153	150	150	50	0	0	0	0
	0	0	0	139	149	153	151	104	133	141	138	138	138	46	0	0	0	0
	0	0	4	117	112	108	108	95	85	108	109	112	114	38	0	0	0	0
	0	0	11	65	75	75	75	73	58	73	77	74	72	24	0	0	0	0
	0	0	4	8	12	12	12	12	7	9	9	9	9	3	0	0	0	0
	0	0	0	0	0	0	0	0	0	0	0	0	0	0	0	0	0	0
	0	0	0	0	0	0	0	0	0	0	0	0	0	0	0	0	0	0

FIGURE 9 (B). Ray information about the extremes of illumination and the array diagram of the illumination at the spectrometer mirror (SM) of the NUV instrument, aligned as designed, from a longitude line source offset -0.0690° in altitude from the design optical axis. The array mesh is 0.2 cm X 0.2 cm, with the upper left element being the number of rays falling on SM between 0≤ X <0.2 cm, and -1.7≤ Y <-1.5 cm.

```
THERE WERE   20181 TOTAL RAYS FROM THE ENTRANCE APERTURE.
ELEMENT 1 (TM):         18210 RAYS PASSED.  12358 OF THESE HIT ELEMENT 4.
ELEMENT 2 (ES):         12358 RAYS PASSED.     ALL OF THESE HIT ELEMENT 4.
ELEMENT 3 (SM-MASK):    12358 RAYS PASSED.     ALL OF THESE HIT ELEMENT 4.
ELEMENT 4 (SM):         12358 RAYS PASSED.     ALL OF THESE HIT ELEMENT 4.
```

LOCAL EXTREME INTERSECTIONS FOR RAYS THAT MADE IT TO ELEMENT 4.

ELEMENT	XMIN,	Y-AT-XMIN	XMAX,	Y-AT-XMAX	YMIN,	X-AT-YMIN	YMAX,	X-AT-YMAX
1	-0.9989,	1.2250	1.0190,	-0.0034	-1.2280,	1.0137	1.2280,	1.0137
2	-0.0125,	-0.1664	0.0039,	-0.2090	-0.2250,	-0.0120	0.2250,	-0.0120
3	0.6387,	-1.1425	2.6198,	-0.1693	-1.3432,	0.6411	1.3432,	0.6411
4	0.5977,	-1.1778	2.6330,	-0.1684	-1.3764,	0.6014	1.3764,	0.6014

ILLUMINATION AT SM FOR OFFSETX = -0.0690°.

	+X--->																	
	0	0	0	0	0	0	0	0	0	0	0	0	0	0	0	0	0	0
	0	0	0	12	12	12	12	12	7	9	9	9	9	3	0	0	0	0
	0	0	7	69	75	75	75	71	55	78	77	74	72	24	0	0	0	0
	0	0	1	120	112	108	108	86	94	108	109	112	114	38	0	0	0	0
	0	0	0	139	149	153	139	47	45	107	139	138	138	46	0	0	0	0
	0	0	0	135	138	138	45	0	0	16	145	150	150	50	0	0	0	0
	0	0	0	138	138	123	1	0	0	0	91	147	147	49	0	0	0	0
	0	0	0	144	141	89	0	0	0	0	60	138	139	47	0	0	0	0
+Y	0	0	0	153	159	92	0	0	0	0	53	159	157	51	0	0	0	0
↓	0	0	0	144	141	89	0	0	0	0	60	138	139	47	0	0	0	0
	0	0	0	138	138	123	1	0	0	0	91	147	147	49	0	0	0	0
	0	0	0	135	138	138	45	0	0	16	145	150	150	50	0	0	0	0
	0	0	0	139	149	153	139	47	45	107	139	138	138	46	0	0	0	0
	0	0	1	120	112	108	108	86	94	108	109	112	114	38	0	0	0	0
	0	0	7	69	75	75	75	71	55	78	77	74	72	24	0	0	0	0
	0	0	0	12	12	12	12	12	7	9	9	9	9	3	0	0	0	0
	0	0	0	0	0	0	0	0	0	0	0	0	0	0	0	0	0	0
	0	0	0	0	0	0	0	0	0	0	0	0	0	0	0	0	0	0

FIGURE 9 (C). Ray information about the extremes of illumination and the array diagram of the illumination at the spectrometer mirror (SM) of the NUV instrument, aligned as designed, from a longitude line source offset -0.0805° in altitude from the design optical axis. The array mesh is 0.2 cm X 0.2 cm, with the upper left element being the number of rays falling on SM between 0≤ X <0.2 cm, and -1.7≤ Y <-1.5 cm.

```
THERE WERE   20181 TOTAL RAYS FROM THE ENTRANCE APERTURE.
ELEMENT 1 (TM):        18210 RAYS PASSED.   8290 OF THESE HIT ELEMENT 4.
ELEMENT 2 (ES):         8290 RAYS PASSED.    ALL OF THESE HIT ELEMENT 4.
ELEMENT 3 (SM-MASK):    8290 RAYS PASSED.    ALL OF THESE HIT ELEMENT 4.
ELEMENT 4 (SM):         8290 RAYS PASSED,    ALL OF THESE HIT ELEMENT 4.
```

LOCAL EXTREME INTERSECTIONS FOR RAYS THAT MADE IT TO ELEMENT 4.

ELEMENT	XMIN,	Y-AT-XMIN	XMAX,	Y-AT-XMAX	YMIN,	X-AT-YMIN	YMAX,	X-AT-YMAX
1	-1.0019,	1.2250	1.0159,	-0.0034	-1.2280,	1.0106	1.2280,	1.0106
2	-0.0125,	-0.0594	0.0014,	-0.2090	-0.2250,	-0.0099	0.2250,	-0.0099
3	0.6406,	-1.1426	2.6217,	-0.1693	-1.3433,	0.6431	1.3433,	0.6431
4	0.5996,	-1.1779	2.6350,	-0.1684	-1.3765,	0.6033	1.3765,	0.6033

ILLUMINATION AT SM FOR OFFSETX = -0.0805°.

```
   +X--->
    0   0   0   0   0   0   0   0   0   0   0   0   0   0   0   0   0   0
    0   0   0  12  12  12  12  12   7   9   9   9   9   3   0   0   0   0
    0   0   2  74  75  75  73  49  30  62  77  74  72  24   0   0   0   0
    0   0   0 121 113 108  44   0   0   4  83 112 114  38   0   0   0   0
    0   0   0 139 148  97   0   0   0   0  21 136 138  46   0   0   0   0
    0   0   0 135 138  23   0   0   0   0   0 118 150  50   0   0   0   0
    0   0   0 138 126   0   0   0   0   0   0  81 147  49   0   0   0   0
    0   0   0 144  98   0   0   0   0   0   0  47 140  47   0   0   0   0
+Y  0   0   0 153 106   0   0   0   0   0   0  53 155  51   0   0   0   0
 ↓  0   0   0 144  98   0   0   0   0   0   0  47 140  47   0   0   0   0
    0   0   0 138 126   0   0   0   0   0   0  81 147  49   0   0   0   0
    0   0   0 135 138  23   0   0   0   0   0 118 150  50   0   0   0   0
    0   0   0 139 148  97   0   0   0   0  21 136 138  46   0   0   0   0
    0   0   0 121 113 108  44   0   0   4  83 112 114  38   0   0   0   0
    0   0   2  74  75  75  73  49  30  62  77  74  72  24   0   0   0   0
    0   0   0  12  12  12  12  12   7   9   9   9   9   3   0   0   0   0
    0   0   0   0   0   0   0   0   0   0   0   0   0   0   0   0   0   0
    0   0   0   0   0   0   0   0   0   0   0   0   0   0   0   0   0   0
```

FIGURE 9 (D). Ray information about the extremes of illumination and the array diagram of the illumination at the spectrometer mirror (SM) of the NUV instrument, aligned as designed, from a longitude line source offset -0.0920° in altitude from the design optical axis. The array mesh is 0.2 cm X 0.2 cm, with the upper left element being the number of rays falling on SM between 0≤ X <0.2 cm, and -1.7≤ Y <-1.5 cm.

```
THERE WERE   20181 TOTAL RAYS FROM THE ENTRANCE APERTURE.
ELEMENT 1 (TM):        18210 RAYS PASSED.   5030 OF THESE HIT ELEMENT 4.
ELEMENT 2 (ES):         5030 RAYS PASSED.    ALL OF THESE HIT ELEMENT 4.
ELEMENT 3 (SM-MASK):    5030 RAYS PASSED.    ALL OF THESE HIT ELEMENT 4.
ELEMENT 4 (SM):         5030 RAYS PASSED,    ALL OF THESE HIT ELEMENT 4.
```

LOCAL EXTREME INTERSECTIONS FOR RAYS THAT MADE IT TO ELEMENT 4.

ELEMENT	XMIN,	Y-AT-XMIN	XMAX,	Y-AT-XMAX	YMIN,	X-AT-YMIN	YMAX,	X-AT-YMAX
1	-1.0050,	1.2250	1.0129,	-0.0017	-1.2280,	1.0076	1.2280,	1.0076
2	-0.0125,	-0.0193	-0.0010,	-0.2091	-0.2250,	-0.0124	0.2250,	-0.0124
3	0.6426,	-1.1427	2.6237,	-0.1693	-1.3434,	0.6450	1.3434,	0.6450
4	0.6015,	-1.1780	2.6369,	-0.1684	-1.3766,	0.6053	1.3766,	0.6053

ILLUMINATION AT SM FOR OFFSETX = -0.0920°.

+X--->																	
0	0	0	0	0	0	0	0	0	0	0	0	0	0	0	0	0	0
0	0	0	12	12	12	6	0	0	0	6	9	9	3	0	0	0	0
0	0	0	76	75	63	4	0	0	0	13	73	72	24	0	0	0	0
0	0	0	121	113	30	0	0	0	0	0	59	114	38	0	0	0	0
0	0	0	139	108	0	0	0	0	0	0	21	138	46	0	0	0	0
0	0	0	135	54	0	0	0	0	0	0	0	137	50	0	0	0	0
0	0	0	138	25	0	0	0	0	0	0	0	98	49	0	0	0	0
0	0	0	144	0	0	0	0	0	0	0	0	92	47	0	0	0	0
0	0	0	153	0	0	0	0	0	0	0	0	96	51	0	0	0	0
0	0	0	144	0	0	0	0	0	0	0	0	92	47	0	0	0	0
0	0	0	138	25	0	0	0	0	0	0	0	98	49	0	0	0	0
0	0	0	135	54	0	0	0	0	0	0	0	137	50	0	0	0	0
0	0	0	139	108	0	0	0	0	0	0	21	138	46	0	0	0	0
0	0	0	121	113	30	0	0	0	0	0	59	114	38	0	0	0	0
0	0	0	76	75	63	4	0	0	0	13	73	72	24	0	0	0	0
0	0	0	12	12	12	6	0	0	0	6	9	9	3	0	0	0	0
0	0	0	0	0	0	0	0	0	0	0	0	0	0	0	0	0	0
0	0	0	0	0	0	0	0	0	0	0	0	0	0	0	0	0	0

FIGURE 10.
ALTITUDE FOV EFFECT WITHIN A SPECTRAL LINE FOR THE NUV INSTRUMENT, ALIGNED AS DESIGNED. 5 GRATING SETTINGS FOR 3000 Å INCIDENT LIGHT.

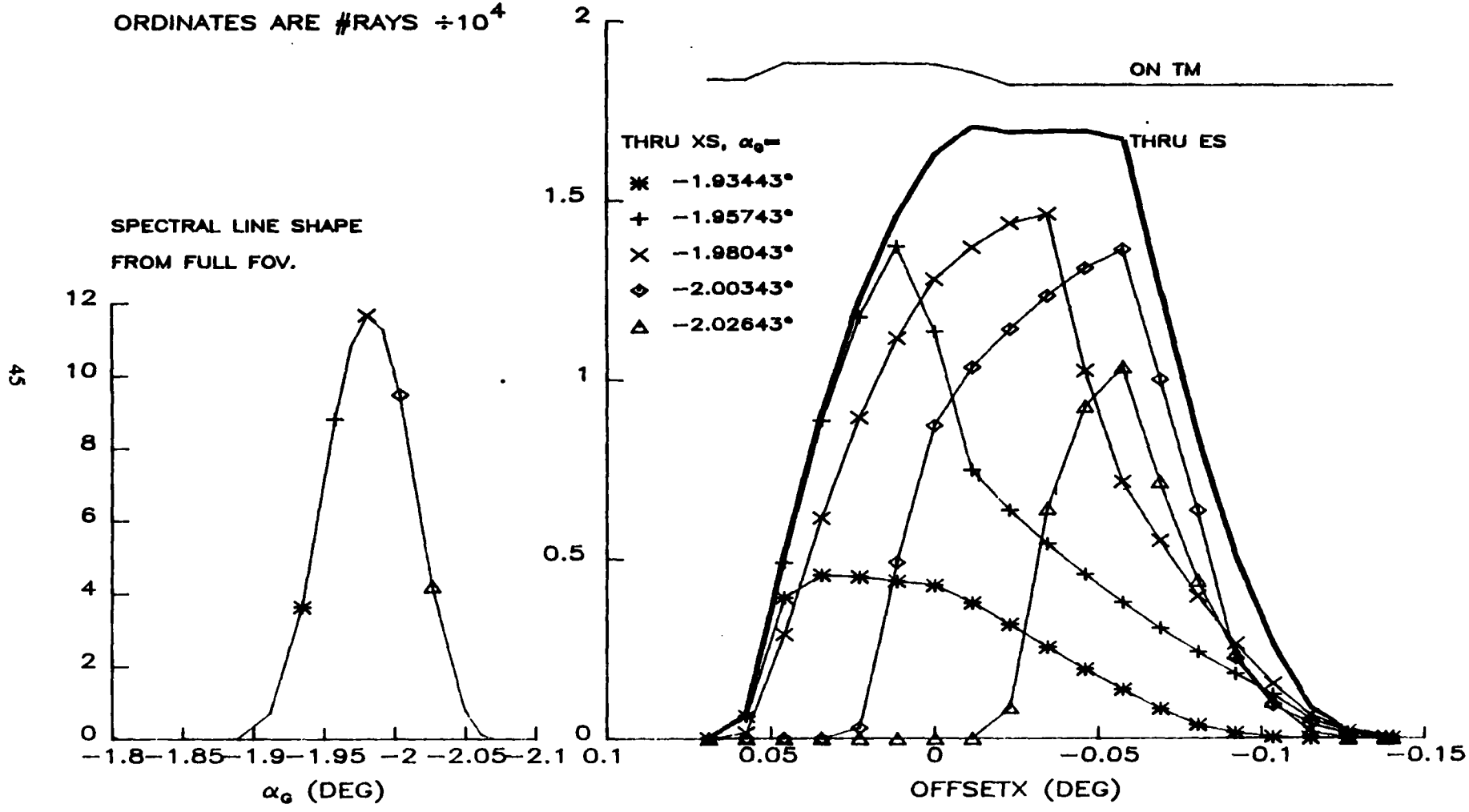

FIGURE 11.

NUV: SPECTRAL LINE SHAPES FOR LONGITUDE LINE SOURCES AT 7 ALTITUDES WITHIN THE FOV. (λ INCIDENT = 3000 Å. INSTRUMENT AS DESIGNED)

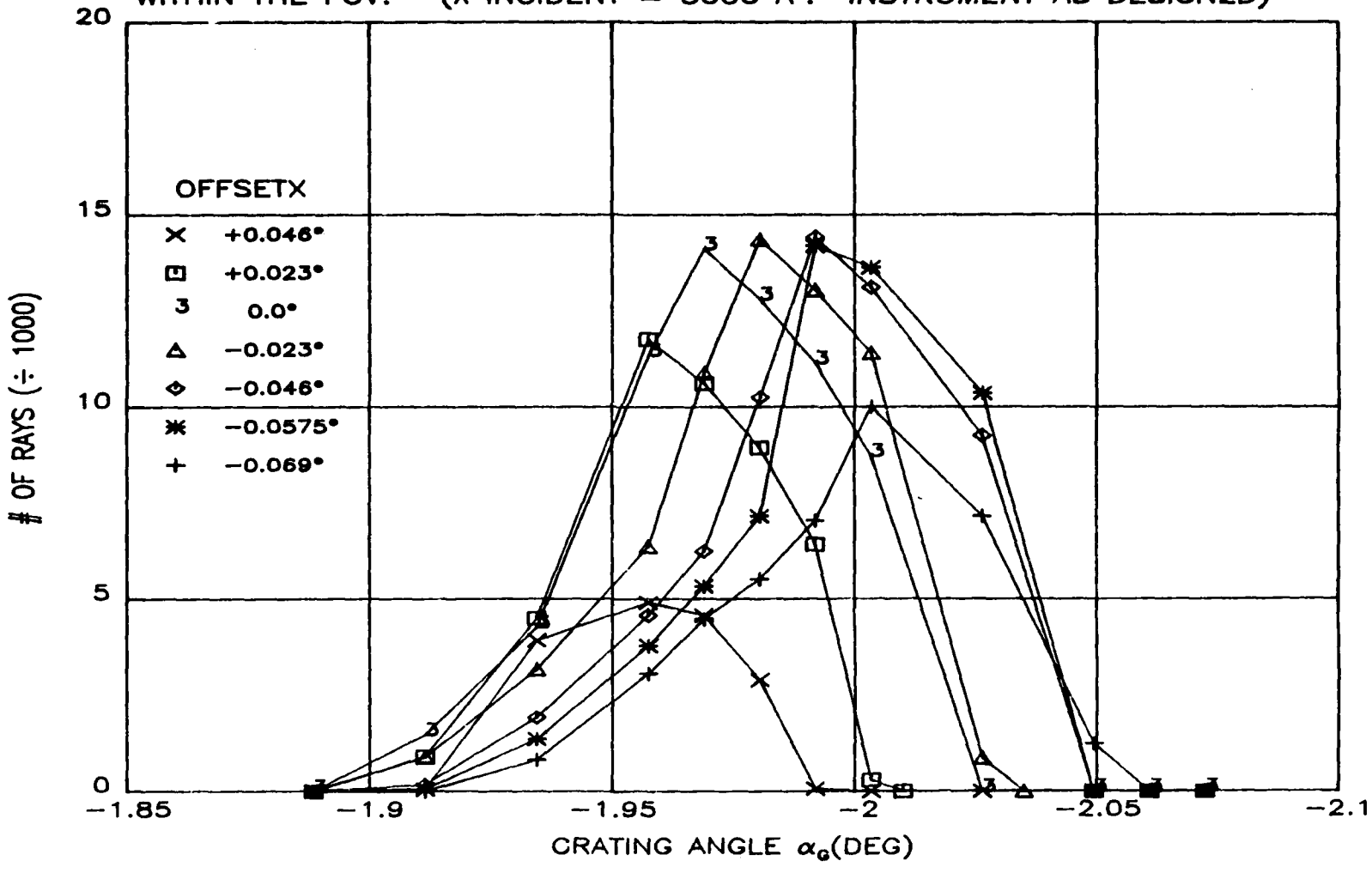

FIGURE 12.
ALTITUDE FOV EFFECT WITHIN A SPECTRAL LINE FOR THE MUV INSTRUMENT, ALIGNED AS DESIGNED. 5 GRATING SETTINGS FOR 1900 Å INCIDENT LIGHT.

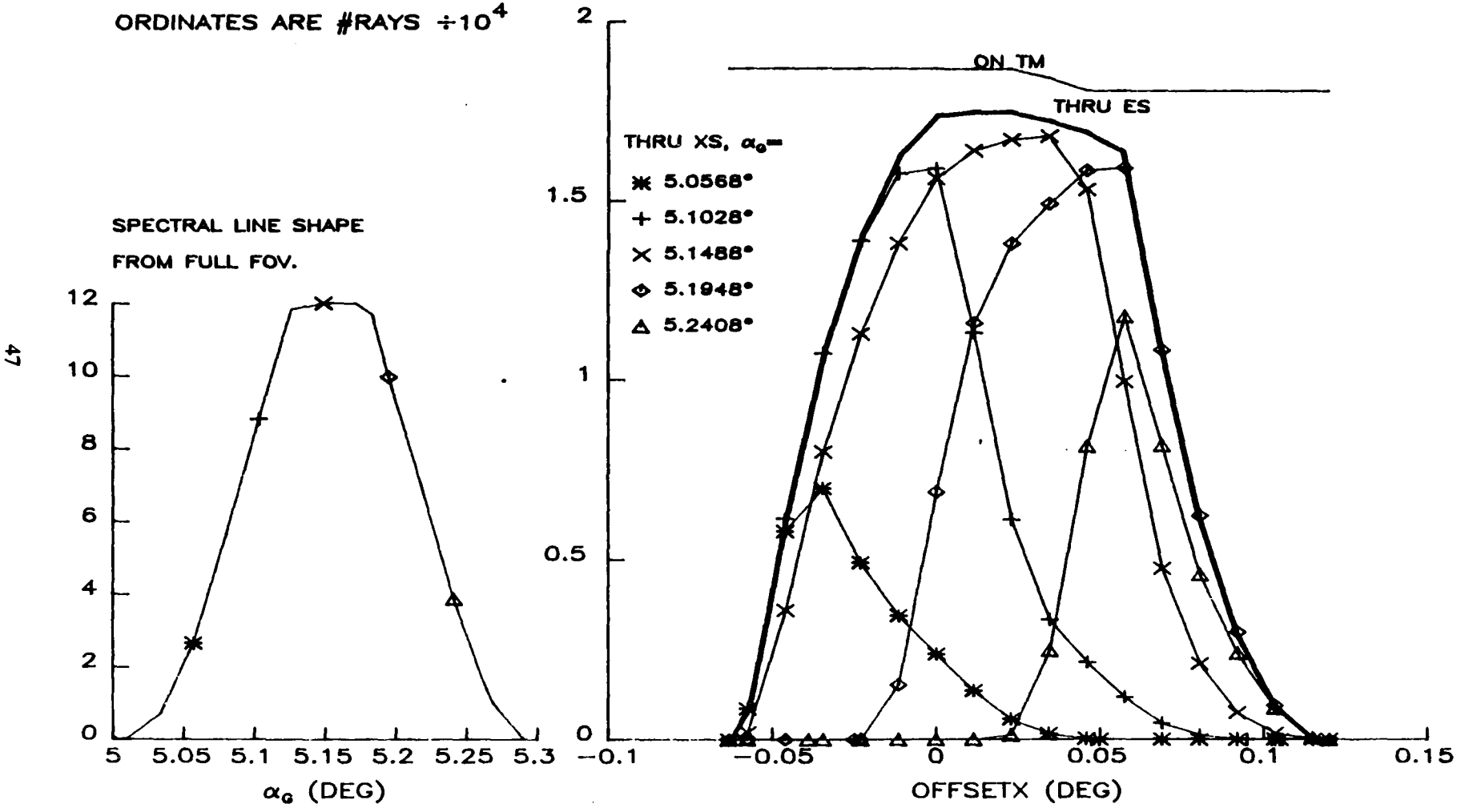

FIGURE 13.
MUV: SPECTRAL LINE SHAPES FOR LONGITUDE LINE SOURCES AT 7 ALTITUDES WITHIN THE FOV. (λ INCIDENT = 1900 Å. INSTRUMENT AS DESIGNED)

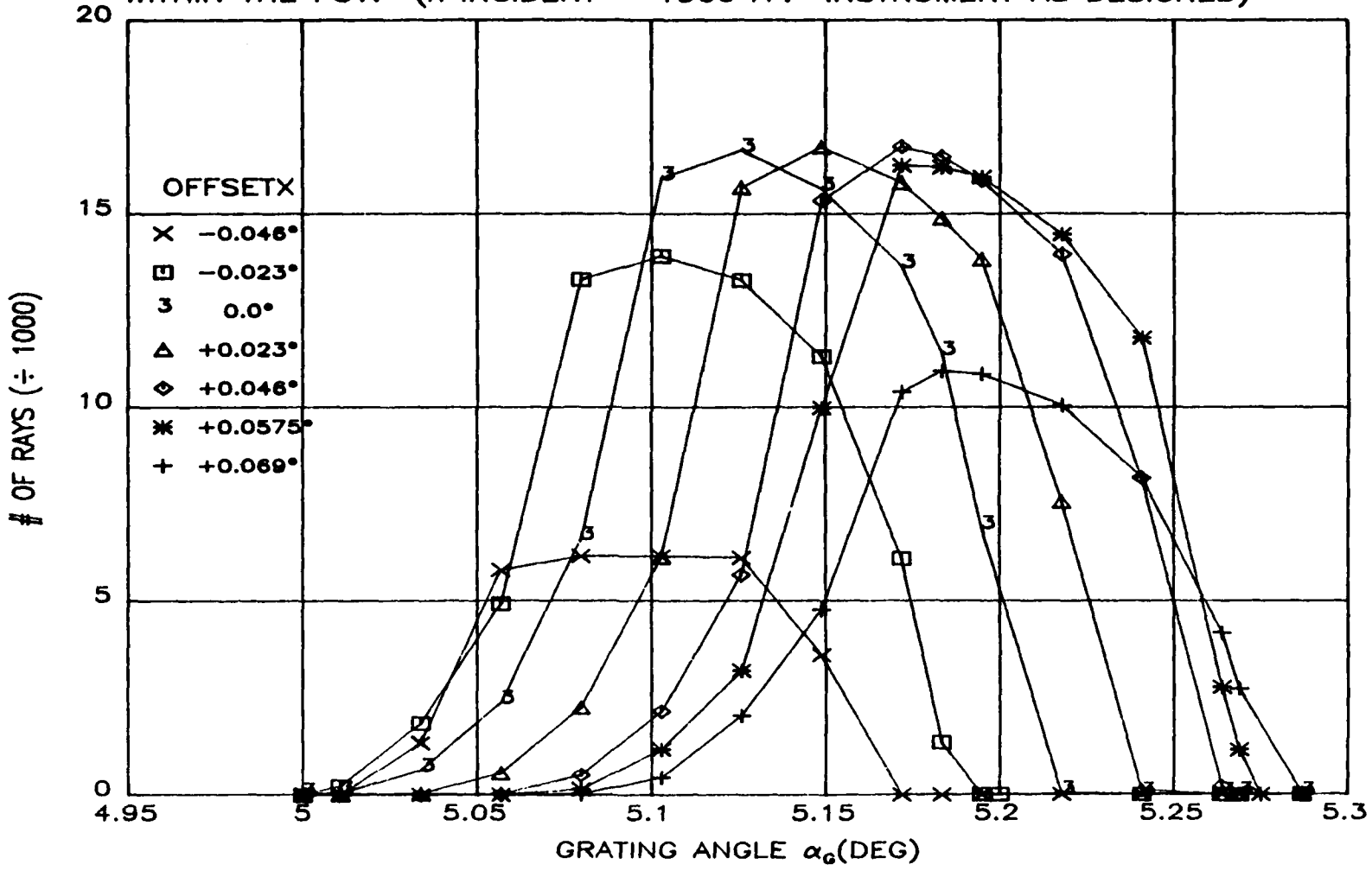

FIGURE 14.

NUV & MUV COMPARISON. NUV OUTPUT MULTIPLIED BY 1.15 AND 1.24.

MUV: 1900 Å, α_o= 5.1488° (CENTRAL RAY THRU ES & XS)

NUV: 3000 Å, α_o= −1.98043° (CENTRAL RAY THRU ES & XS)

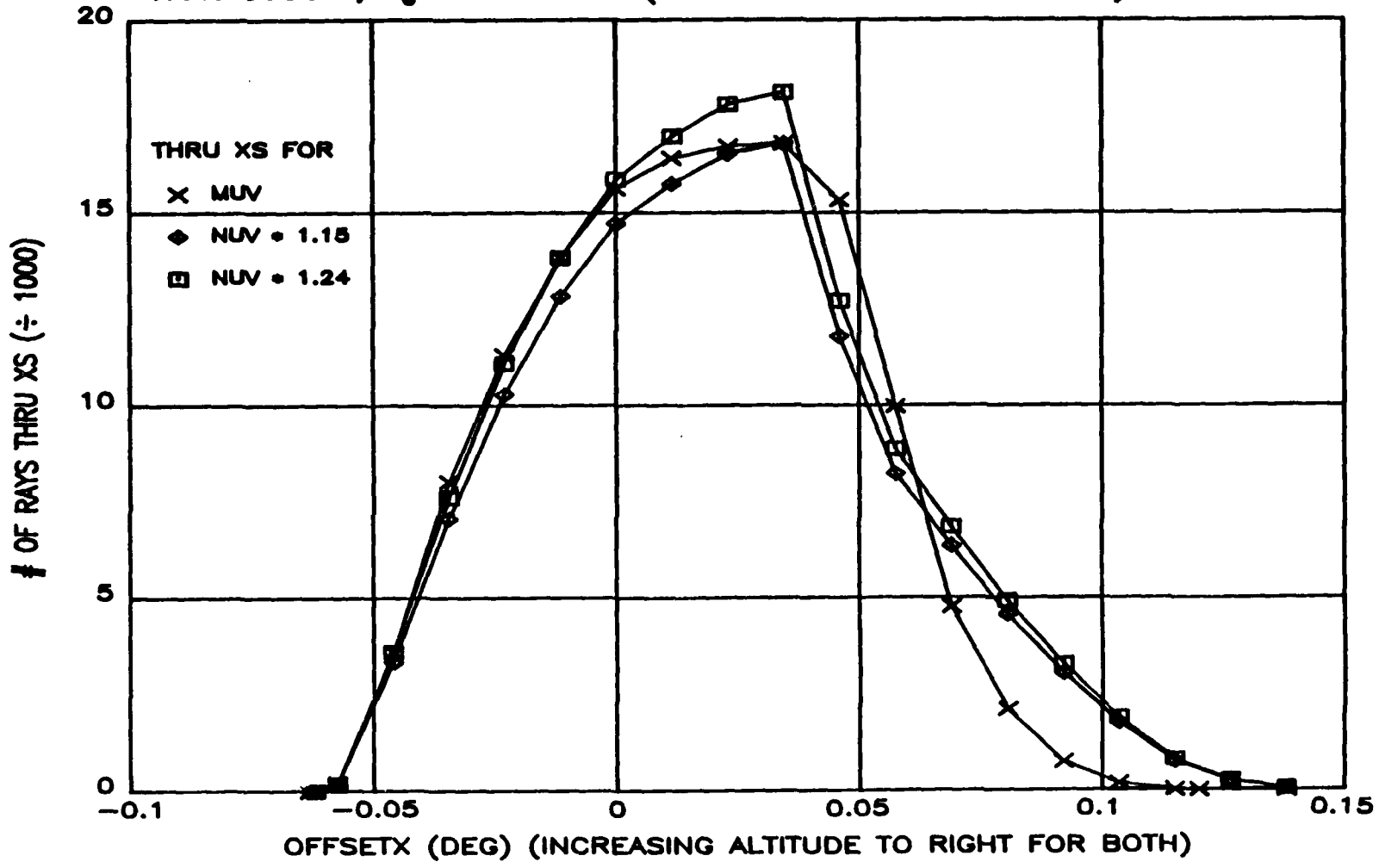

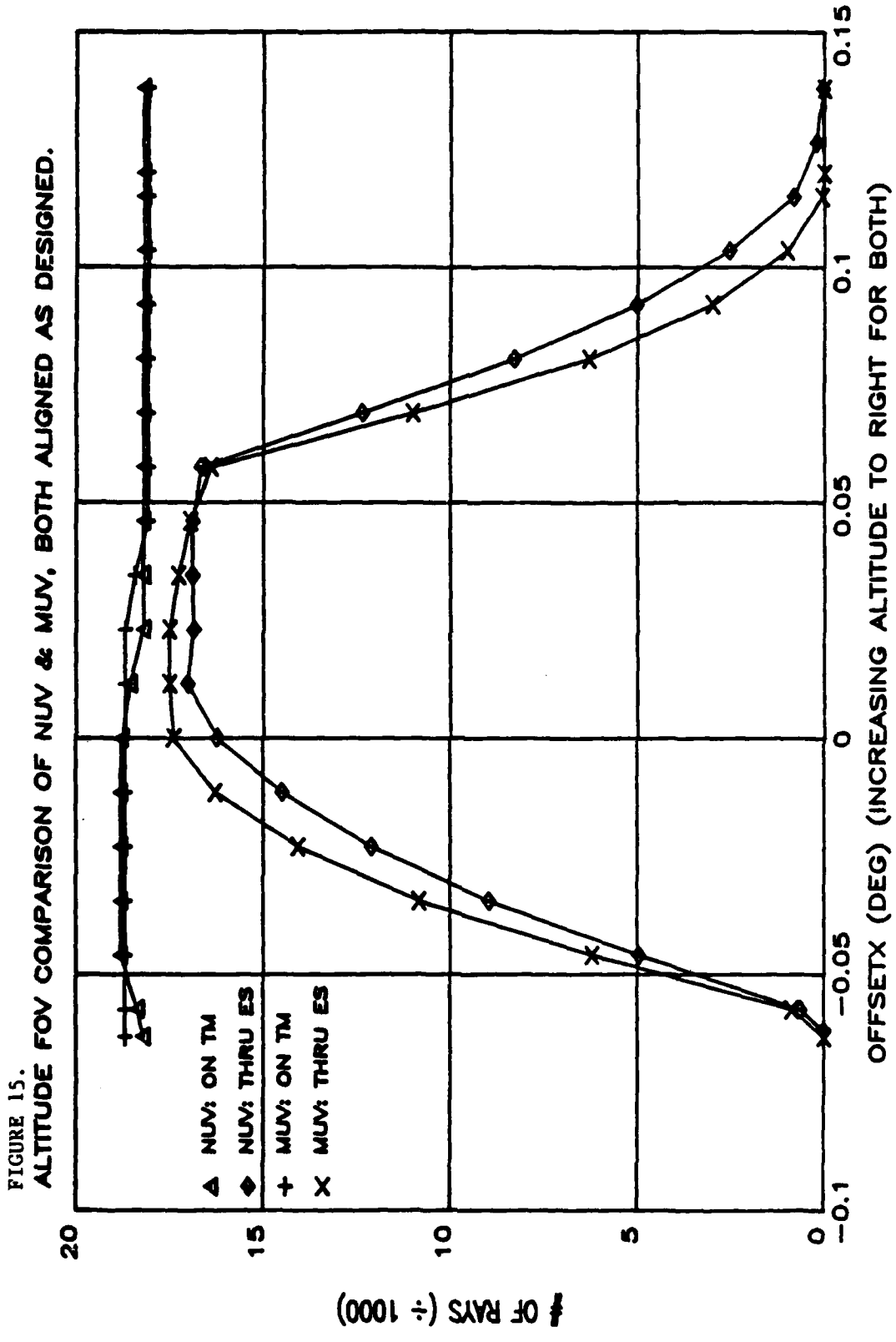
ALTITUDE FOV COMPARISON OF NUV & MUV, BOTH ALIGNED AS DESIGNED.
NUV: ON TM
NUV: THRU ES
MUV: ON TM
MUV: THRU ES
OF RAYS (÷ 1000)
OFFSETX (DEG) (INCREASING ALTITUDE TO RIGHT FOR BOTH)
20
15
10
5
0
-0.1
-0.05
0
0.05
0.1
0.15

FIGURE 15.

FIGURE 16.

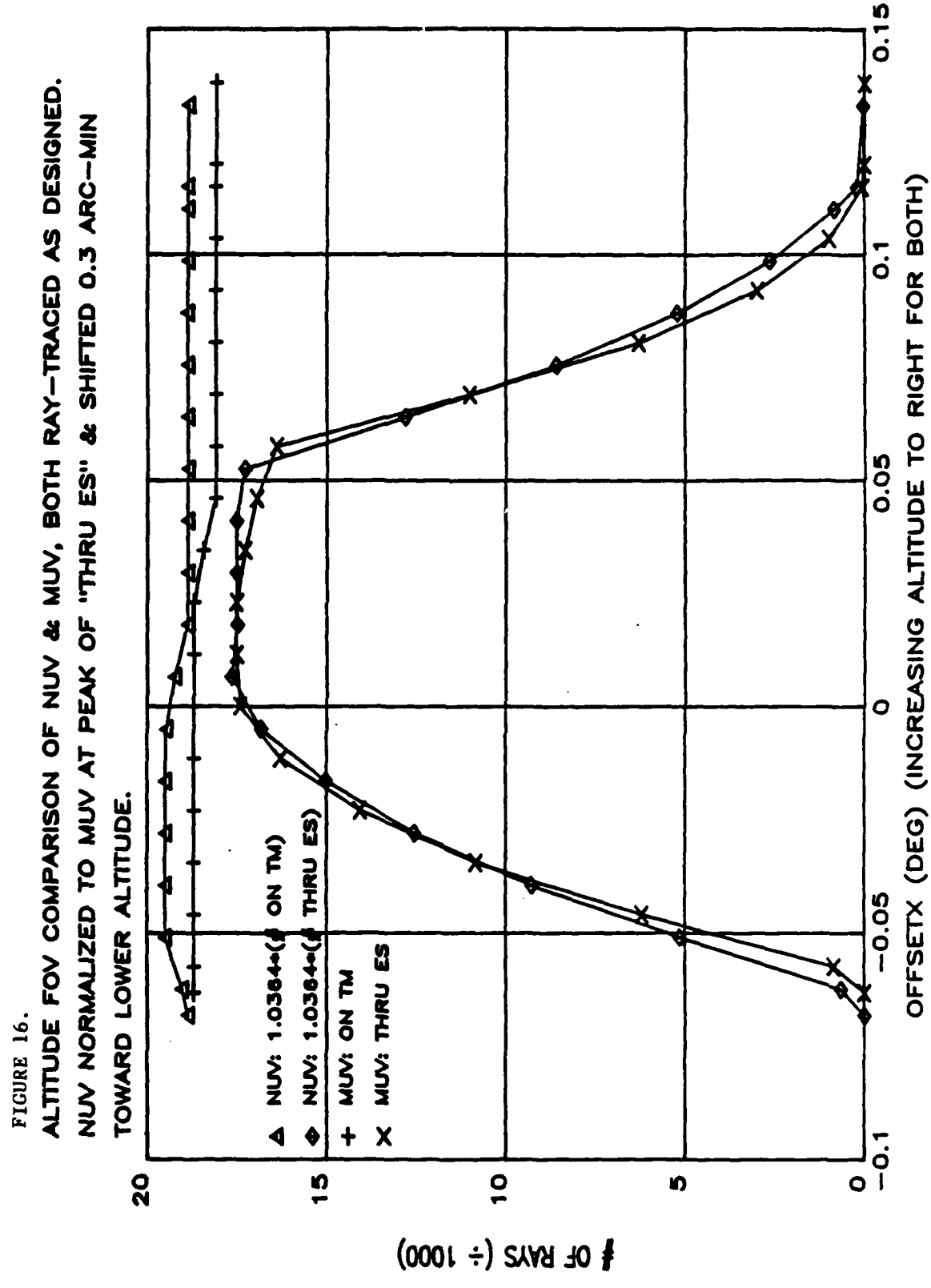
ALTITUDE FOV COMPARISON OF NUV & MUV, BOTH RAY-TRACED AS DESIGNED.
NUV NORMALIZED TO MUV AT PEAK OF "THRU ES" & SHIFTED 0.3 ARC-MIN
TOWARD LOWER ALTITUDE.
NUV: 1.0384×(# ON TM)
NUV: 1.0384×(# THRU ES)
MUV: ON TM
MUV: THRU ES
OF RAYS (÷ 1000)
OFFSETX (DEG) (INCREASING ALTITUDE TO RIGHT FOR BOTH)
20
15
10
5
0
−0.1
−0.05
0
0.05
0.1
0.15

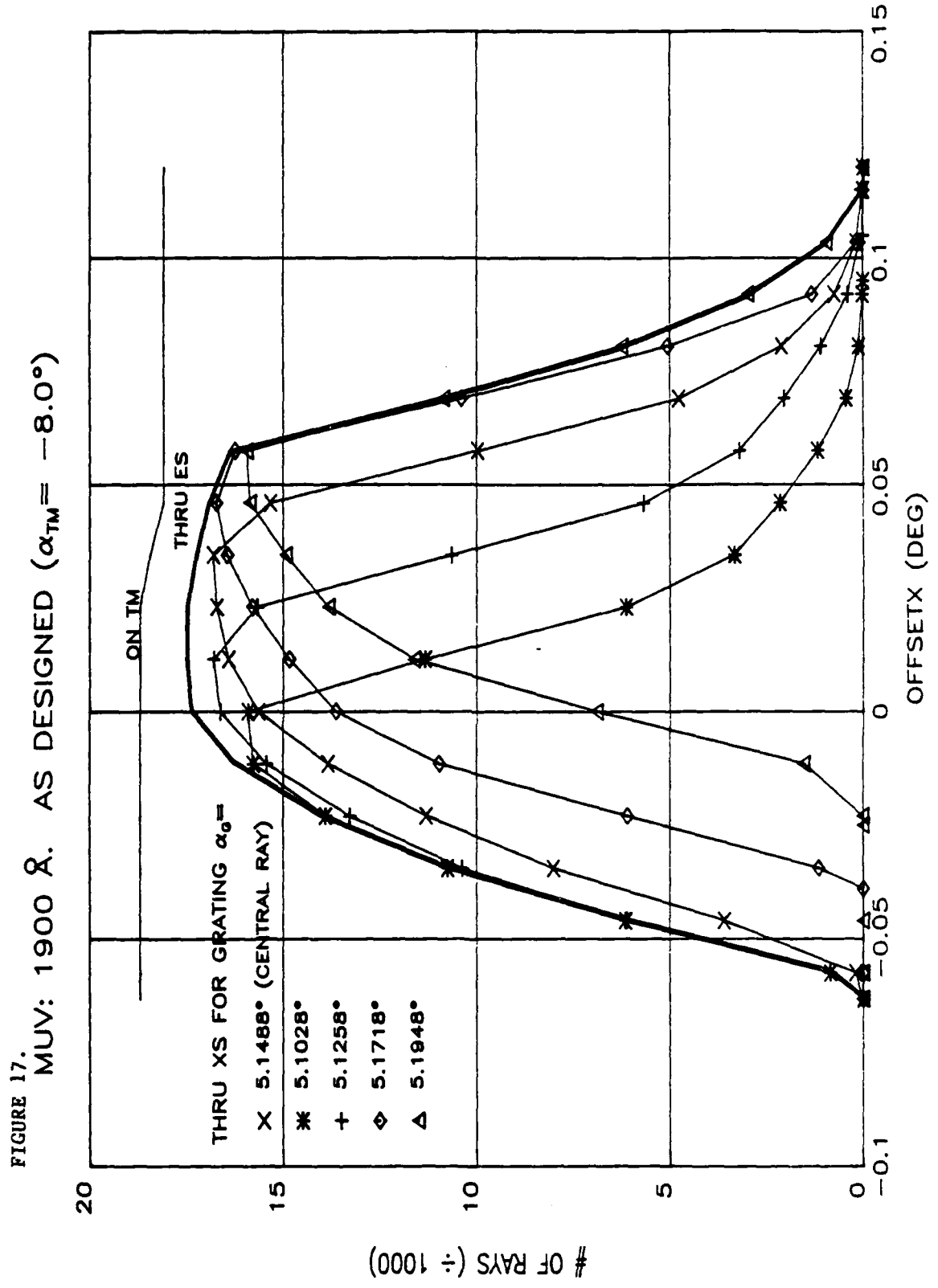
MUV: 1900 Å. AS DESIGNED (α_{TM} = −8.0°)
ON TM
THRU ES
THRU XS FOR GRATING α_G=
× 5.1488° (CENTRAL RAY)
✱ 5.1028°
+ 5.1258°
◇ 5.1718°
△ 5.1948°
OF RAYS (÷ 1000)
OFFSETX (DEG)
20
15
10
5
0
−0.1
−0.05
0
0.05
0.1
0.15

FIGURE 17.

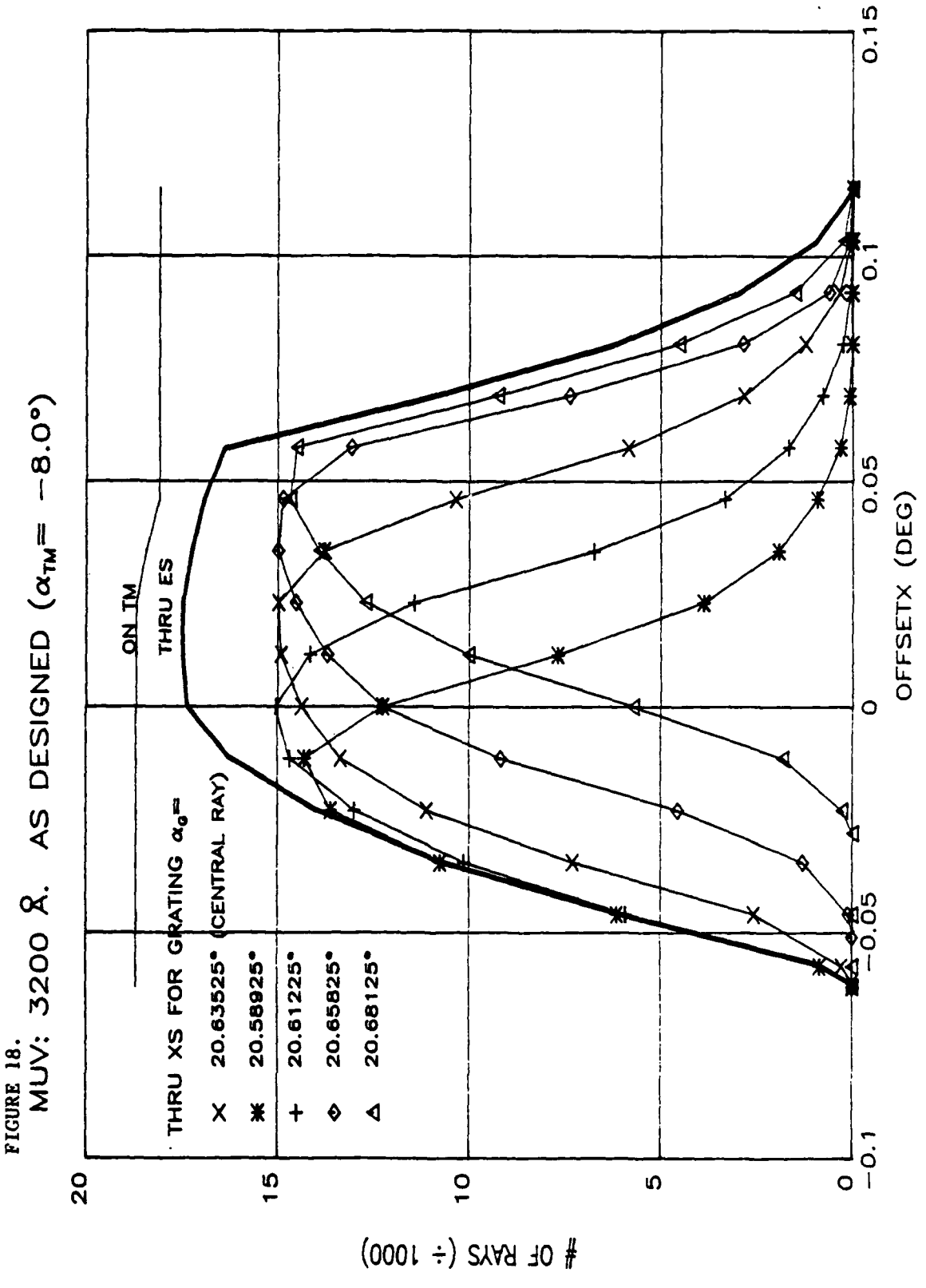
MUV: 3200 Å. AS DESIGNED (α_{TM}= −8.0°)
ON TM
THRU ES
THRU XS FOR GRATING α_G=
× 20.63525° (CENTRAL RAY)
✱ 20.58925°
+ 20.61225°
◇ 20.65825°
△ 20.68125°
OF RAYS (÷ 1000)
20
15
10
5
0
−0.1
−0.05
0
0.05
0.1
0.15
OFFSETX (DEG)

FIGURE 18.

FIGURE 19.
MUV: SPECTRAL LINE SHAPES FOR LONGITUDE LINE SOURCES AT 7 ALTITUDES WITHIN THE FOV. (λ INCIDENT = 3200 Å. INSTRUMENT AS DESIGNED)

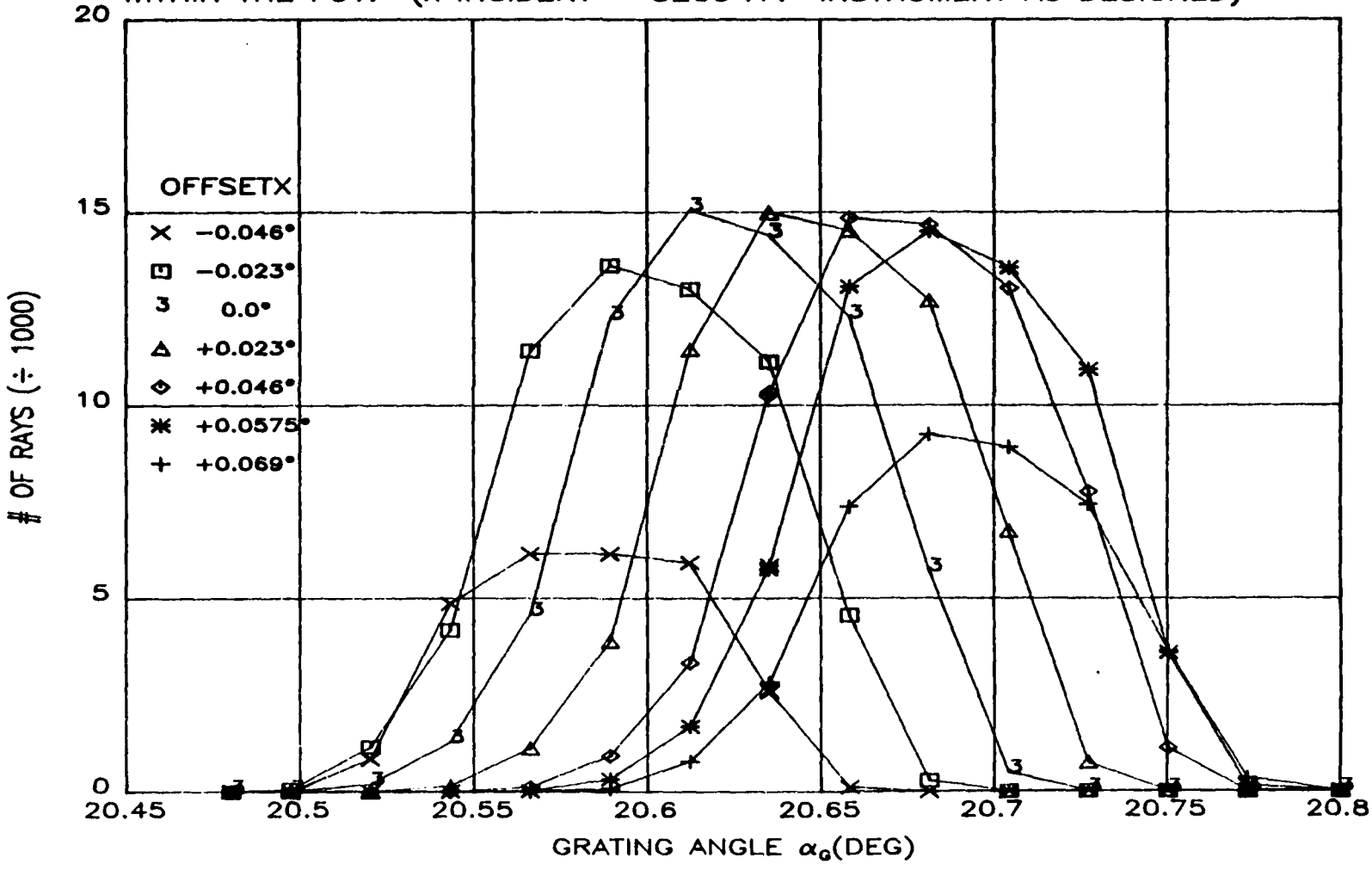

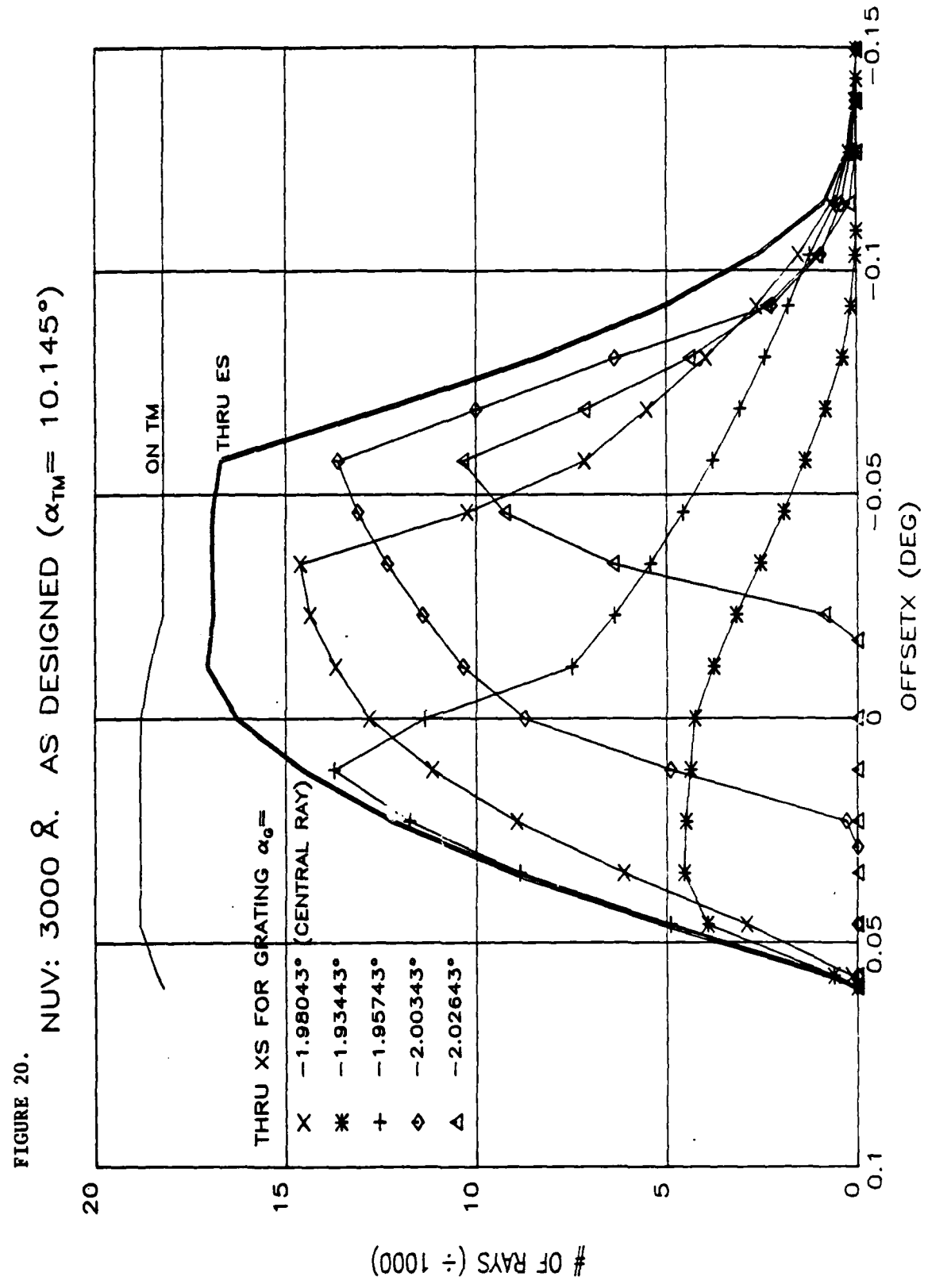
NUV: 3000 Å. AS DESIGNED (α_{TM}= 10.145°)
ON TM
THRU ES
THRU XS FOR GRATING α_0=
(CENTRAL RAY)
× −1.98043°
✱ −1.93443°
+ −1.95743°
◇ −2.00343°
△ −2.02643°
OF RAYS (÷ 1000)
20
15
10
5
0
0.1
0.05
0
−0.05
−0.1
−0.15
OFFSETX (DEG)

FIGURE 20.

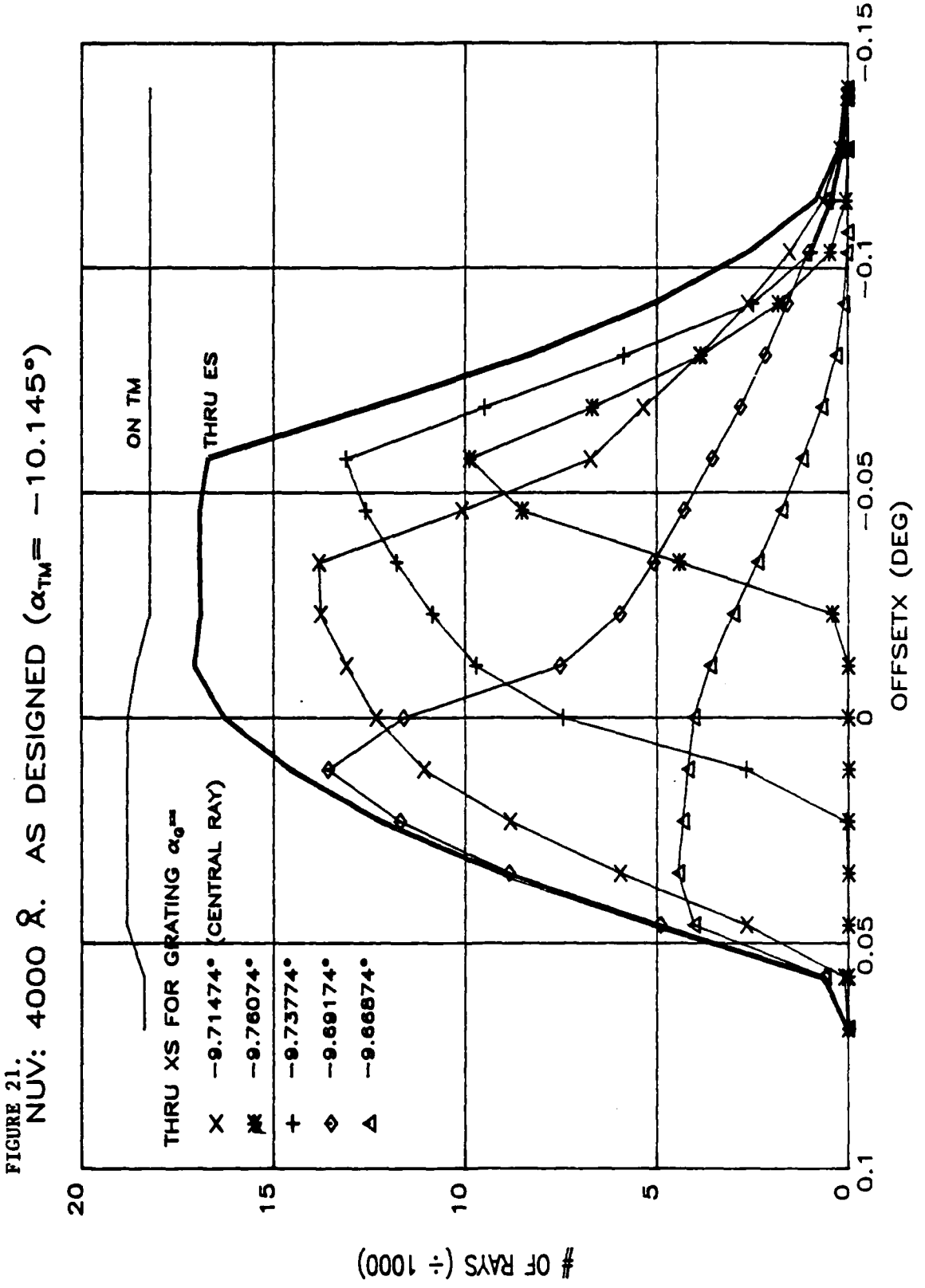
NUV: 4000 Å. AS DESIGNED (α_{TM}= −10.145°)
ON TM
THRU ES
THRU XS FOR GRATING α_o=
× −9.71474° (CENTRAL RAY)
✱ −9.76074°
+ −9.73774°
◇ −9.69174°
△ −9.66874°
OF RAYS (÷ 1000)
20
15
10
5
0
0.1
0.05
0
−0.05
−0.1
−0.15
OFFSETX (DEG)

FIGURE 21.

FIGURE 22.
NUV AND MUV AS DESIGNED: SPECTRAL LINE SHAPES FROM FULL FOV. λ INCREASES TOWARD THE RIGHT, AT THE RATE OF 129.3 (NUV) & 83.9 (MUV) Å PER DEGREE.

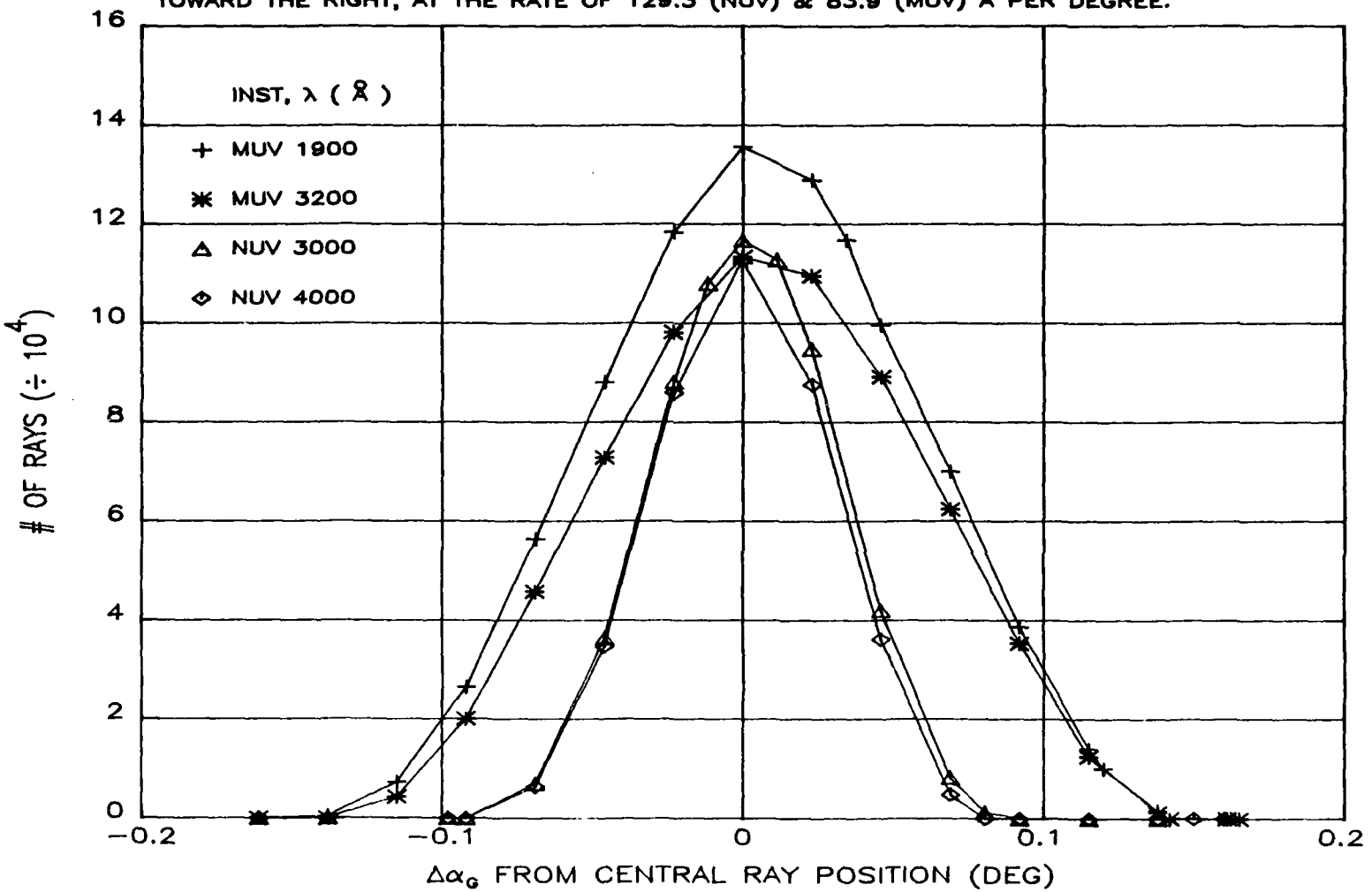

FIGURE 23.

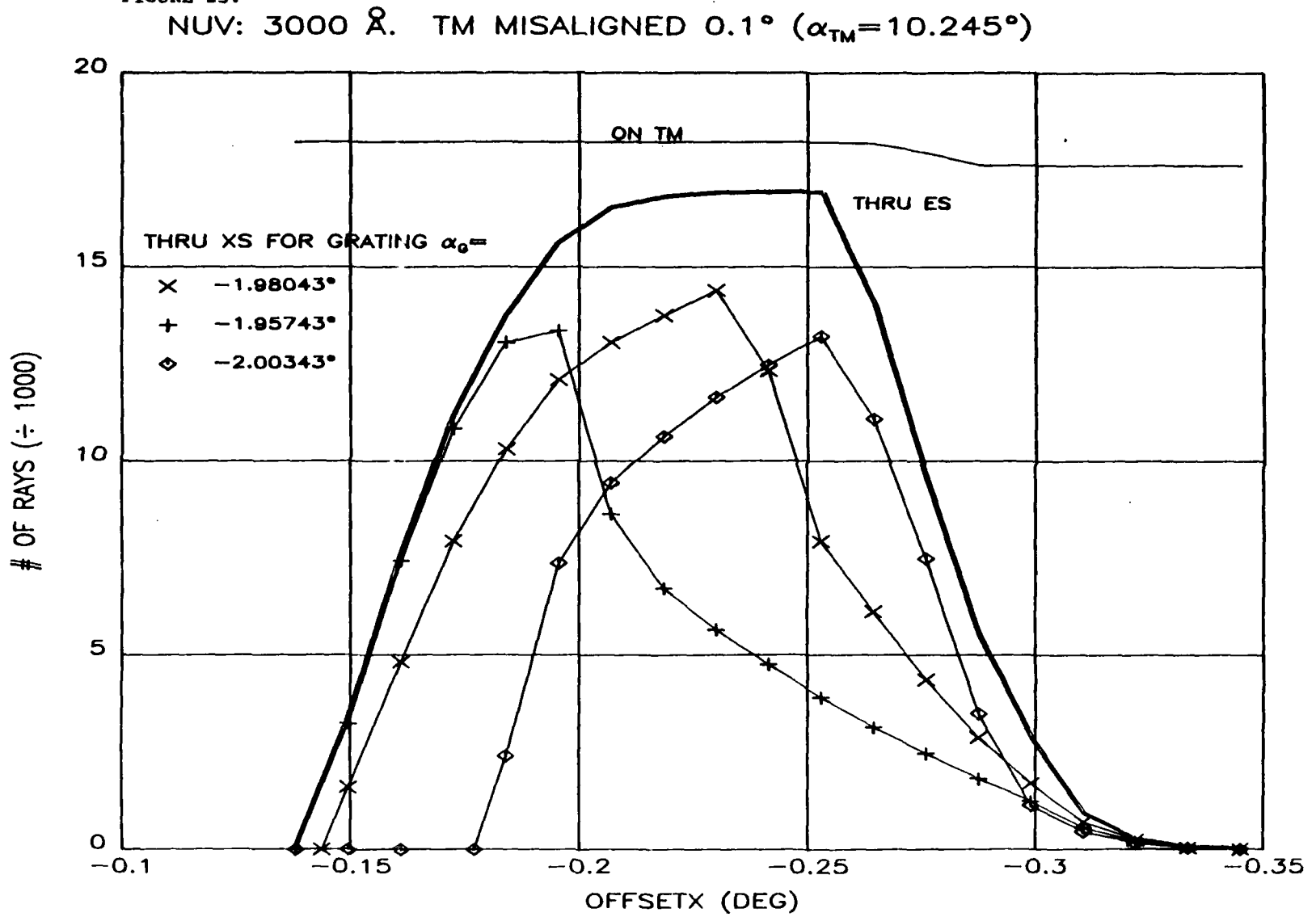
NUV: 3000 Å. TM MISALIGNED 0.1° (α_{TM}=10.245°)
ON TM
THRU ES
THRU XS FOR GRATING α_0=
−1.98043°
−1.95743°
−2.00343°
OF RAYS (÷ 1000)
OFFSETX (DEG)
20
15
10
5
0
−0.1
−0.15
−0.2
−0.25
−0.3
−0.35

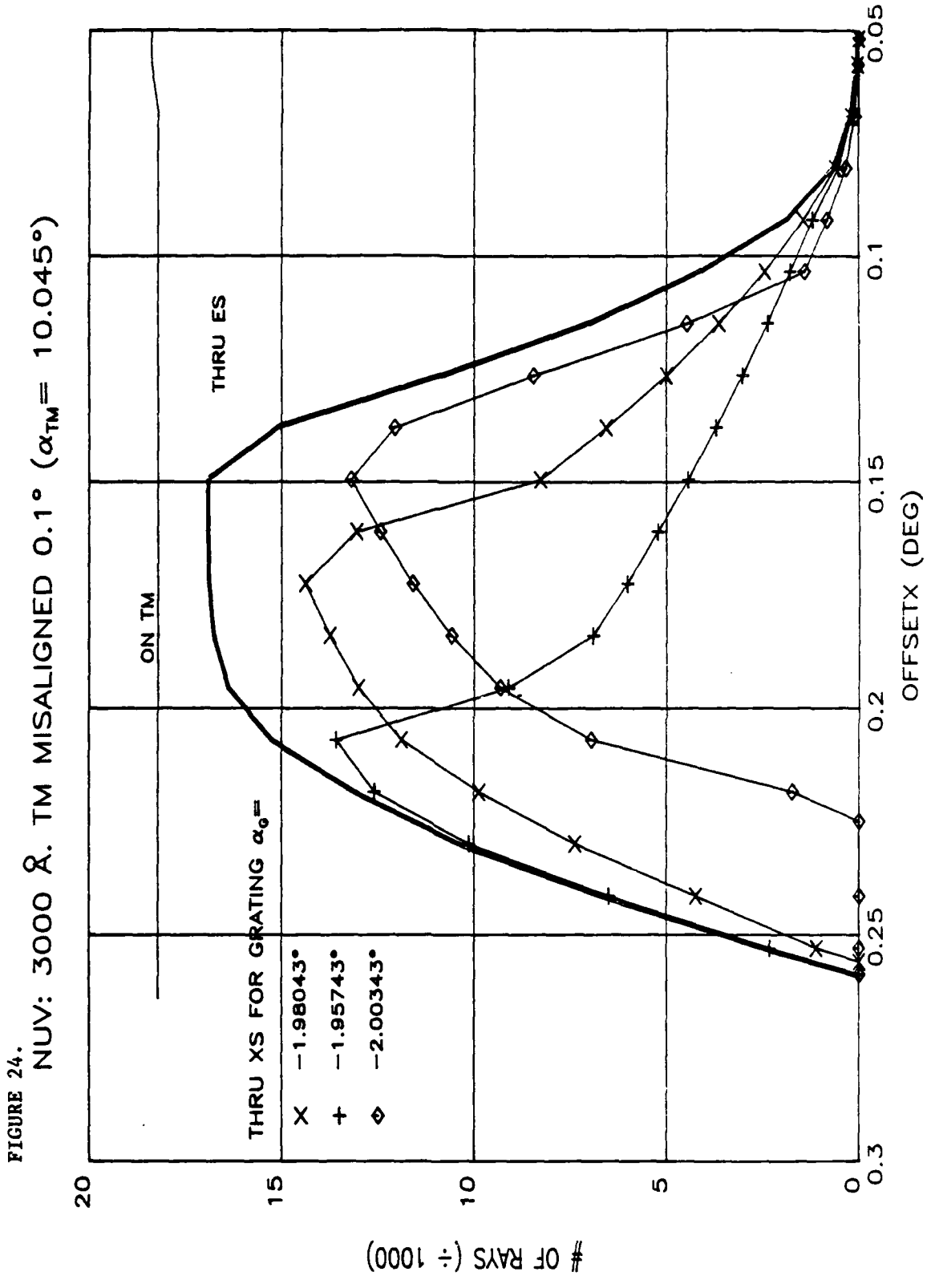
NUV: 3000 Å. TM MISALIGNED 0.1° (α_{TM}= 10.045°)
ON TM
THRU ES
THRU XS FOR GRATING α_G=
× −1.98043°
+ −1.95743°
◇ −2.00343°
OF RAYS (÷ 1000)
OFFSETX (DEG)
20
15
10
5
0
0.3
0.25
0.2
0.15
0.1
0.05

FIGURE 24.

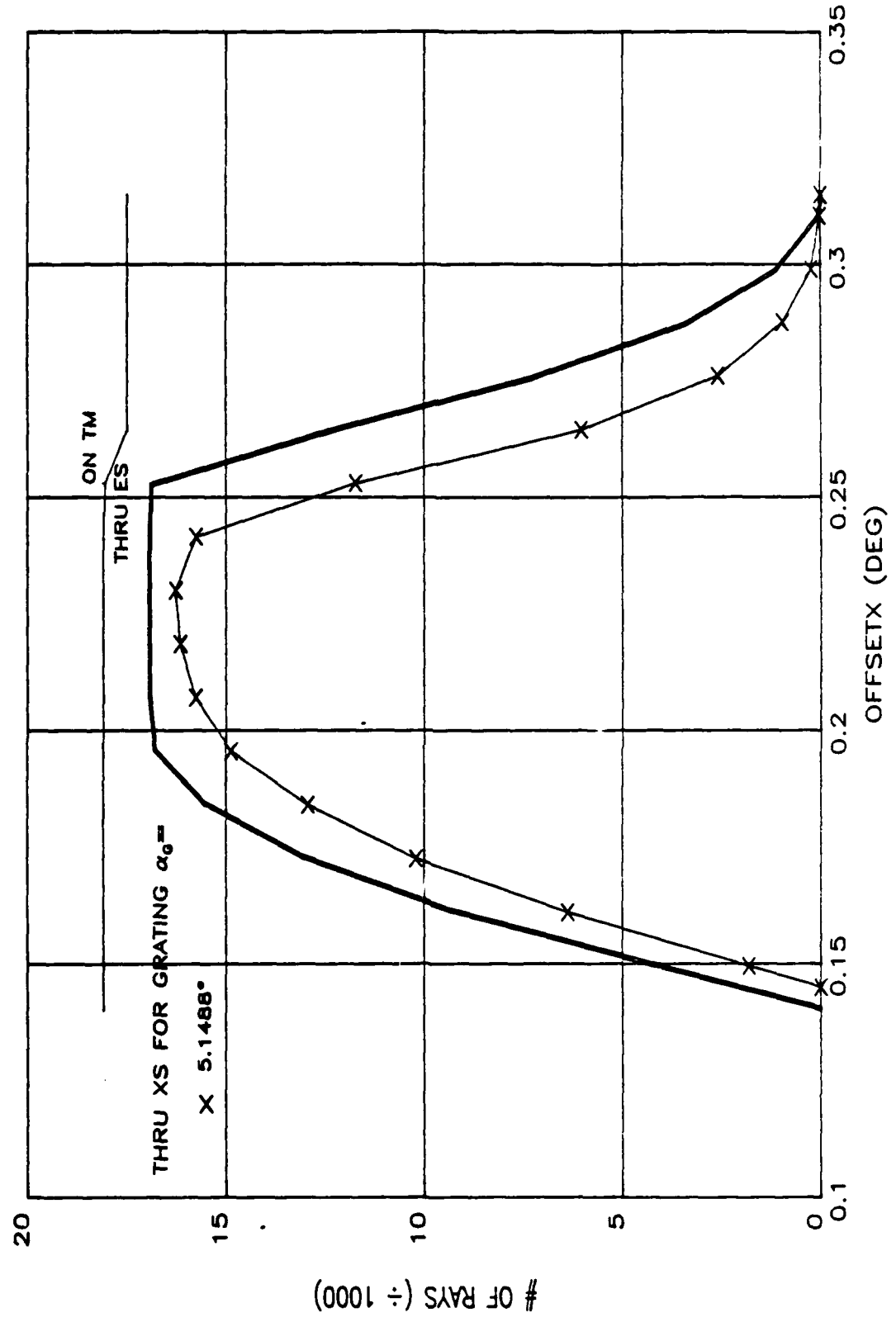
MUV: 1900 Å. TM MISALIGNED 0.1 DEG (α_{TM}= −8.1°)
ON TM
THRU ES
THRU XS FOR GRATING α_G=
× 5.1488°
OF RAYS (÷ 1000)
OFFSETX (DEG)
20
15
10
5
0
0.1
0.15
0.2
0.25
0.3
0.35

FIGURE 25.

FIGURE 26.

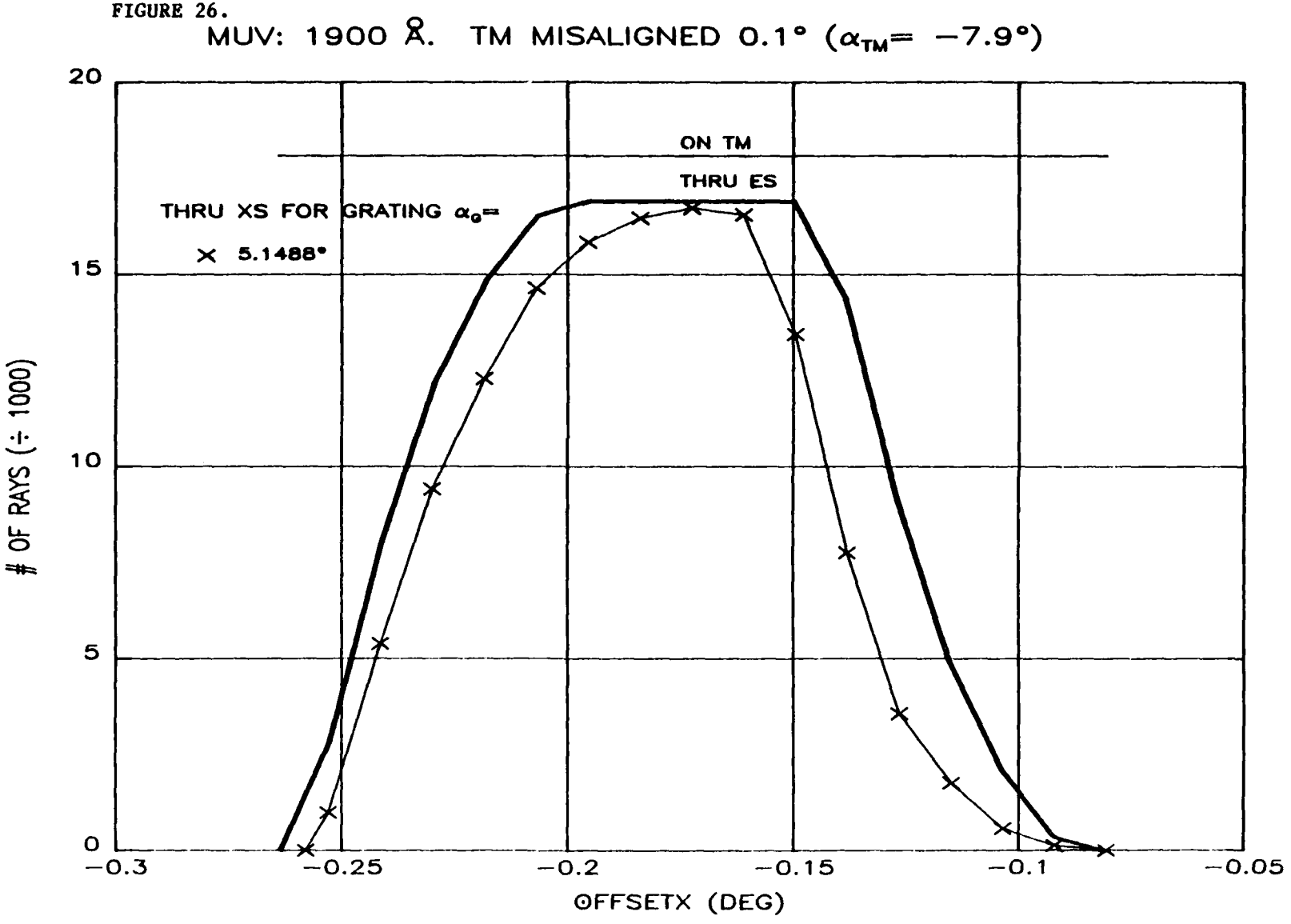
MUV: 1900 Å. TM MISALIGNED 0.1° (α_{TM}= −7.9°)
ON TM
THRU ES
THRU XS FOR GRATING α_0=
× 5.1488°
OF RAYS (÷ 1000)
20
15
10
5
0
−0.3
−0.25
−0.2
−0.15
−0.1
−0.05
OFFSETX (DEG)

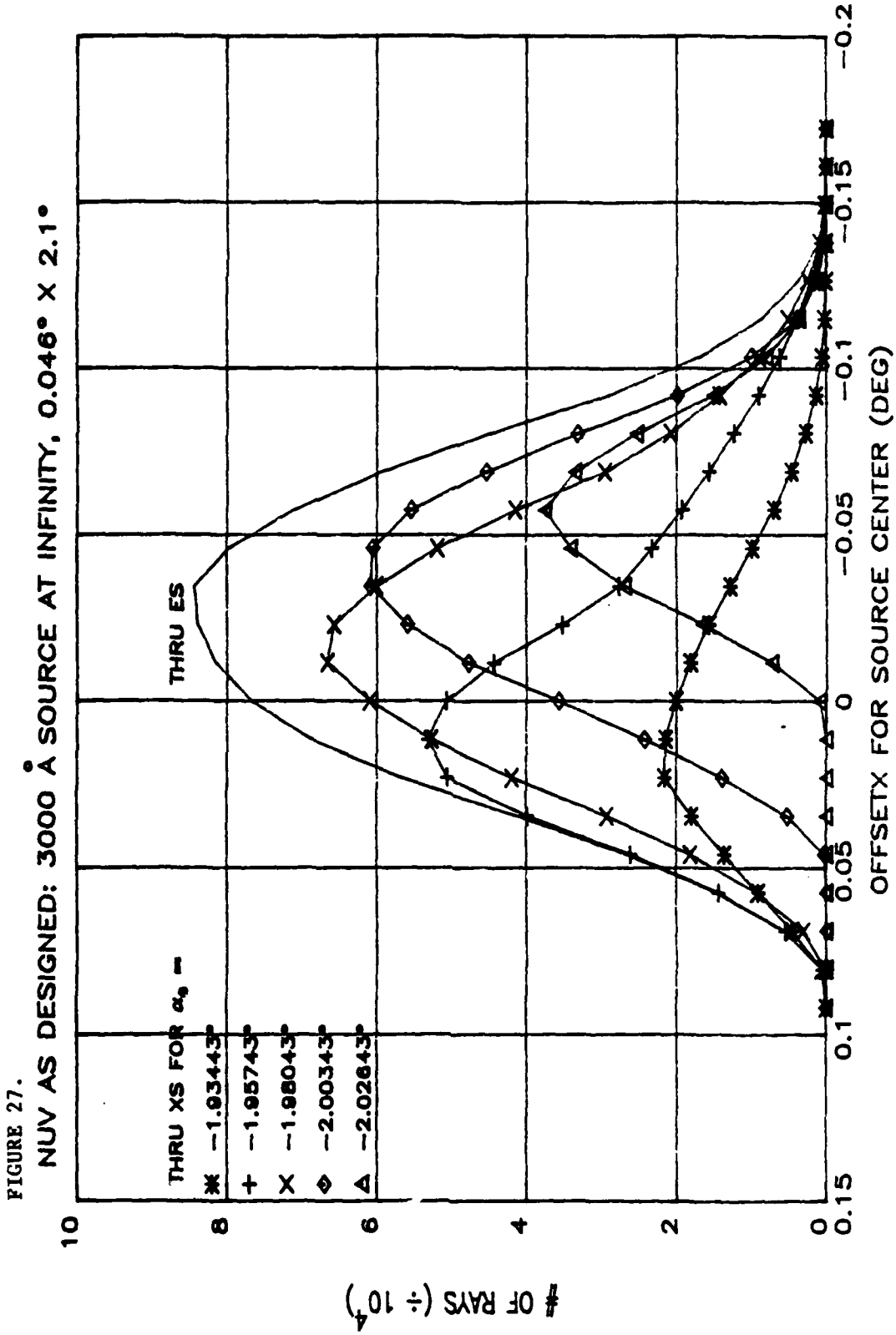
NUV AS DESIGNED: 3000 Å SOURCE AT INFINITY, 0.046° X 2.1°
THRU XS FOR α_s =
* −1.93443°
+ −1.95743°
X −1.98043°
◇ −2.00343°
△ −2.02643°
THRU ES
OF RAYS (÷ 10^4)
OFFSETX FOR SOURCE CENTER (DEG)
10
8
6
4
2
0
0.15
0.1
0.05
0
−0.05
−0.1
−0.15
−0.2

FIGURE 27.

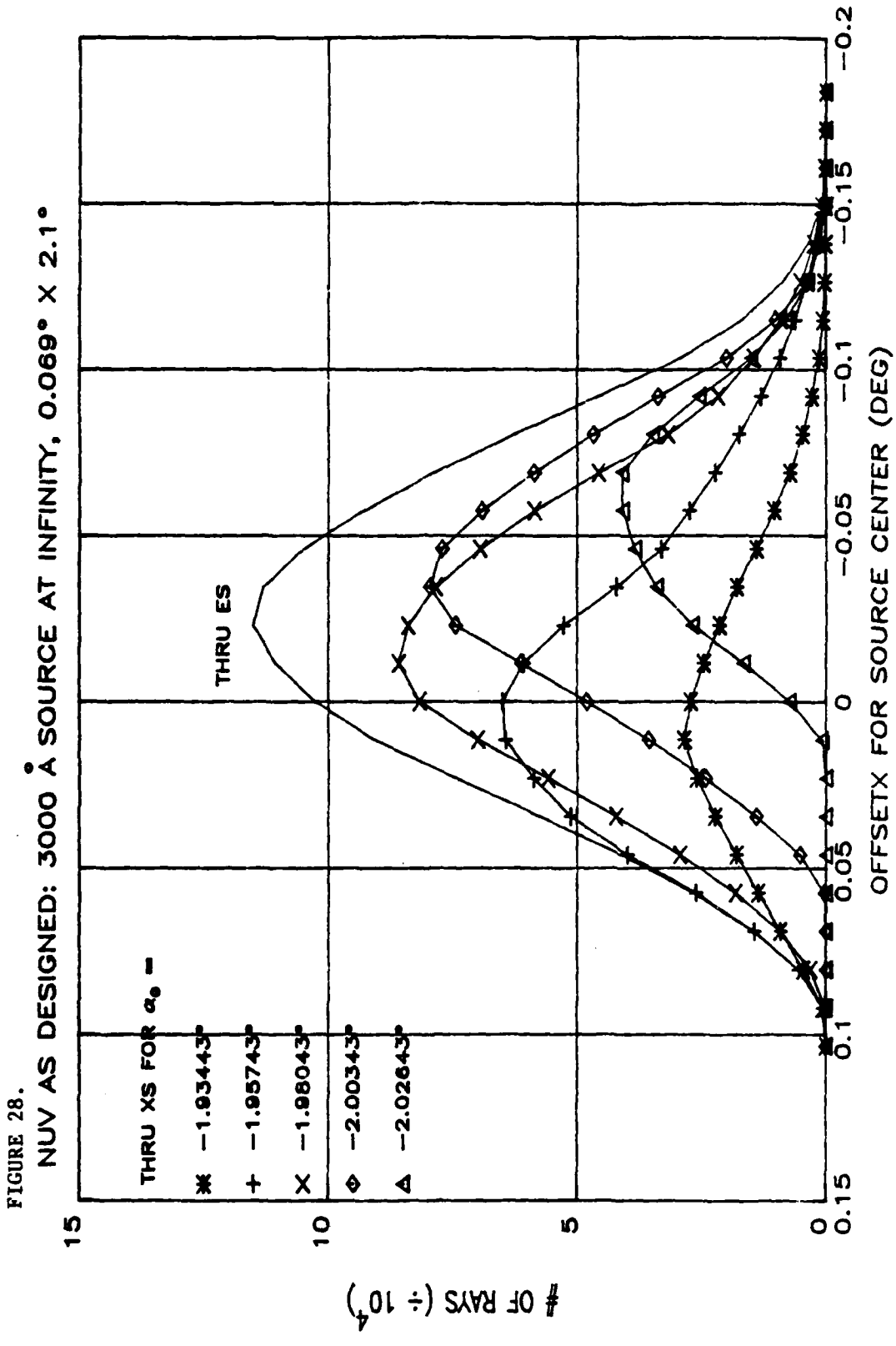
NUV AS DESIGNED: 3000 Å SOURCE AT INFINITY, 0.069° X 2.1°
THRU ES
THRU XS FOR α_0 =
−1.93443°
−1.95743°
−1.98043°
−2.00343°
−2.02643°
OF RAYS (÷ 10^4)
OFFSETX FOR SOURCE CENTER (DEG)
15
10
5
0
0.15
0.1
0.05
0
−0.05
−0.1
−0.15
−0.2

FIGURE 28.

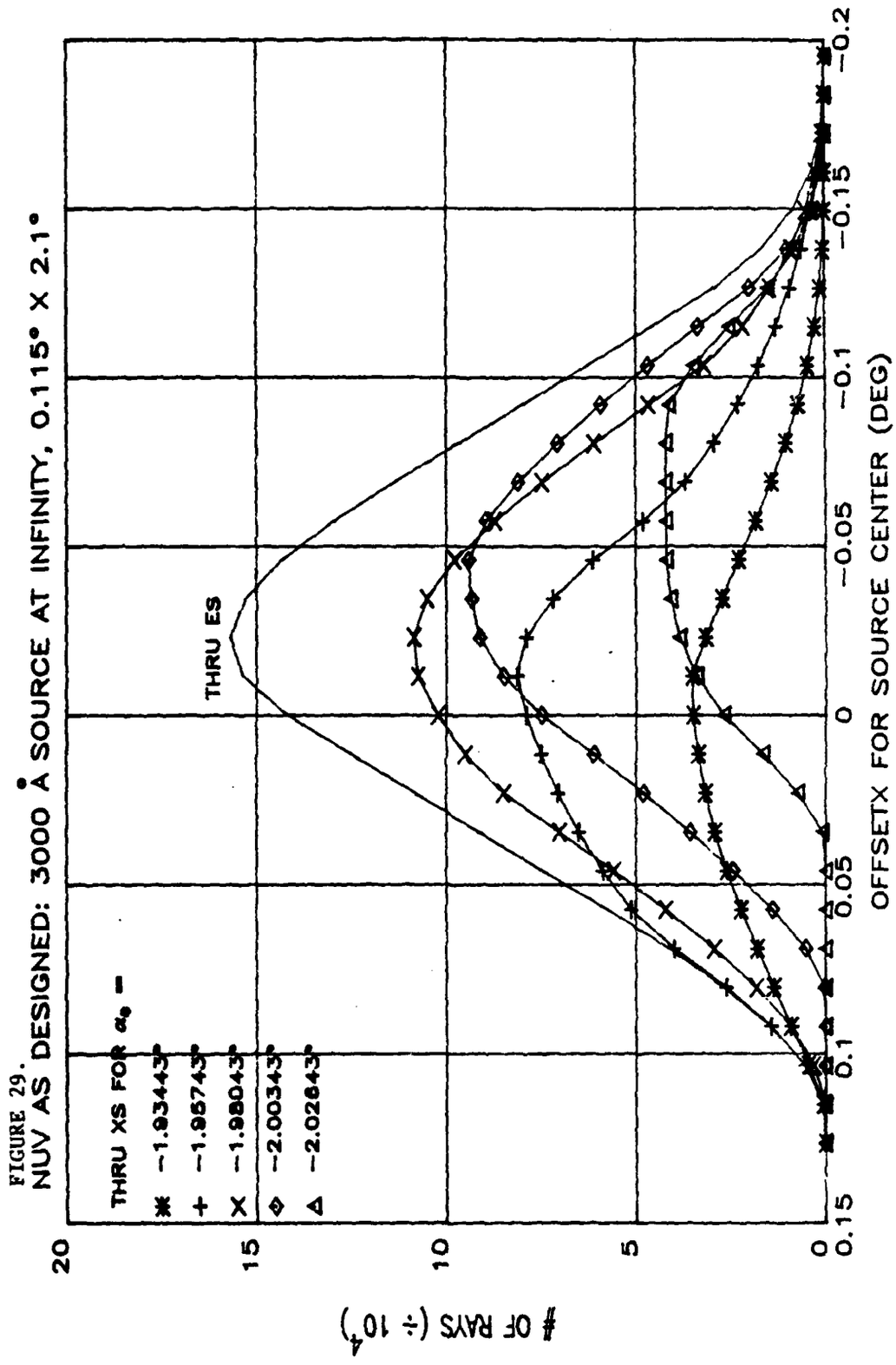
NUV AS DESIGNED: 3000 Å SOURCE AT INFINITY, 0.115° X 2.1°
THRU XS FOR α_0 =
-1.93443°
-1.95743°
-1.98043°
-2.00343°
-2.02643°
THRU ES
OF RAYS (÷ 10^4)
OFFSETX FOR SOURCE CENTER (DEG)
20
15
10
5
0
0.15
0.1
0.05
0
-0.05
-0.1
-0.15
-0.2

FIGURE 29.

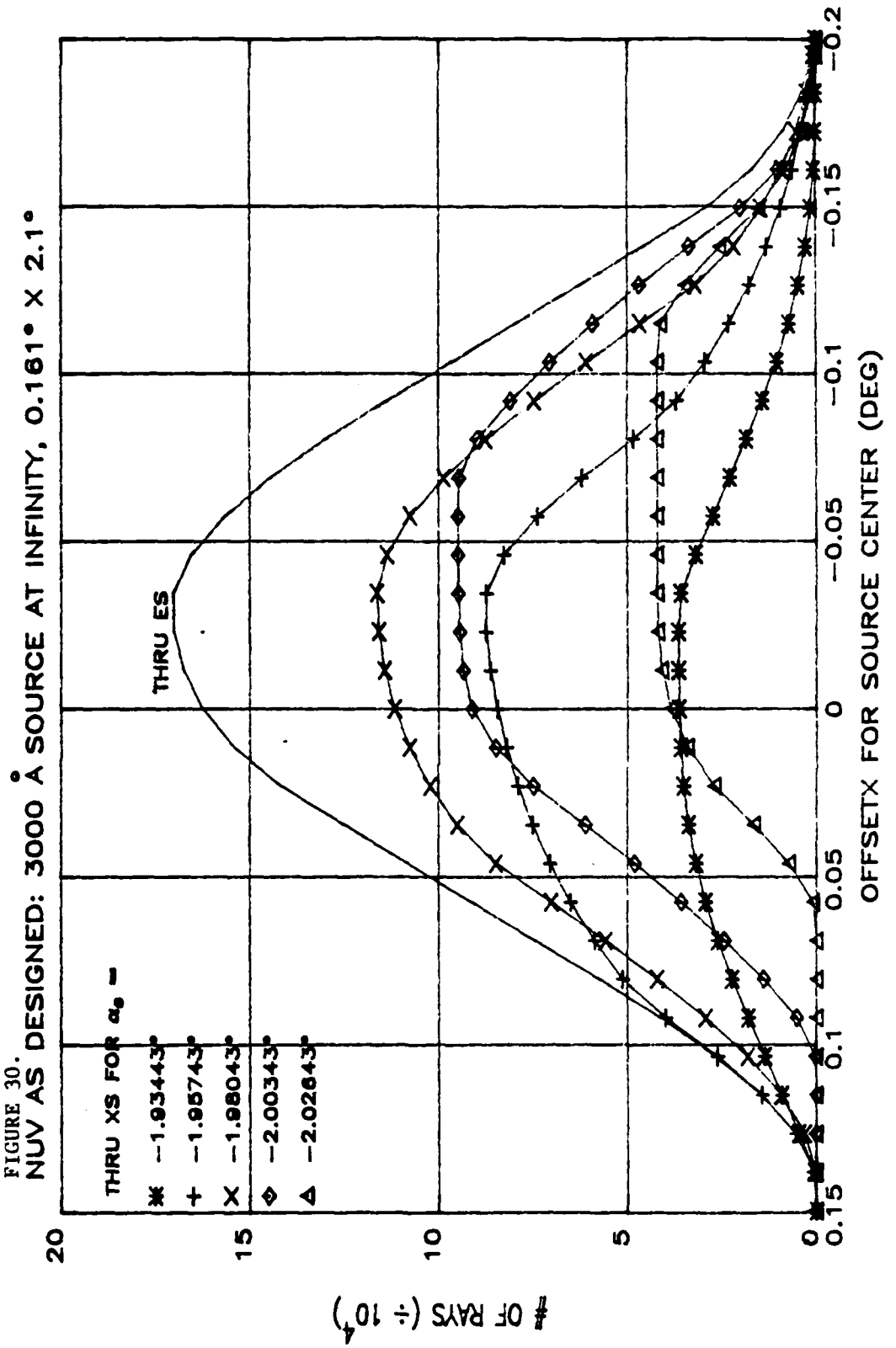
NUV AS DESIGNED: 3000 Å SOURCE AT INFINITY, 0.161° X 2.1°
THRU XS FOR α_0 =
-1.93443°
-1.95743°
-1.98043°
-2.00343°
-2.02643°
THRU ES
OF RAYS (÷ 10^4)
OFFSETX FOR SOURCE CENTER (DEG)
20
15
10
5
0
0.15
0.1
0.05
0
-0.05
-0.1
-0.15
-0.2

FIGURE 30.

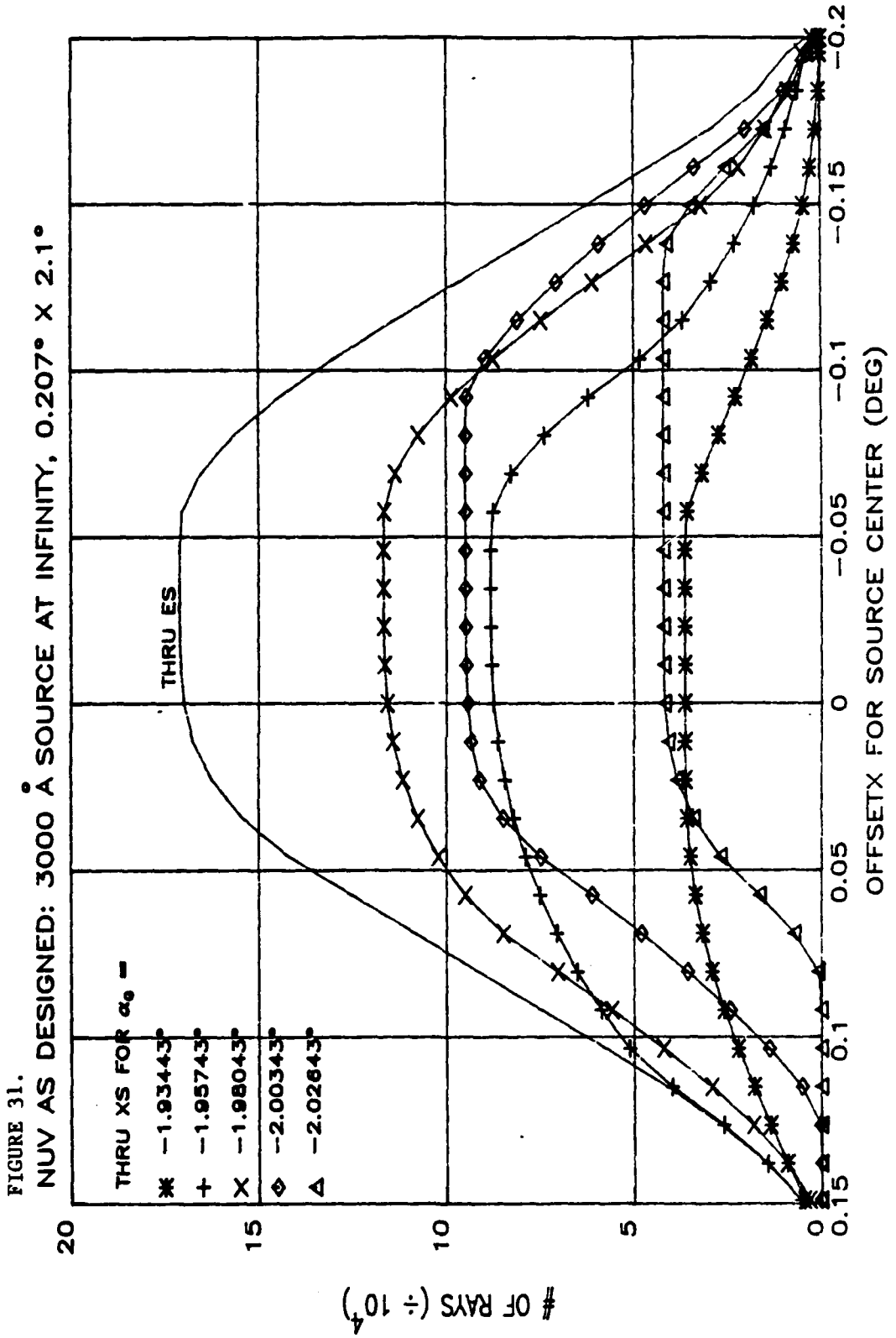
NUV AS DESIGNED: 3000 Å SOURCE AT INFINITY, 0.207° X 2.1°
THRU ES
THRU XS FOR α_0 =
-1.93443°
-1.95743°
-1.98043°
-2.00343°
-2.02643°
OF RAYS (÷ 10^4)
OFFSETX FOR SOURCE CENTER (DEG)
20
15
10
5
0
0.15
0.1
0.05
0
-0.05
-0.1
-0.15
-0.2

FIGURE 31.

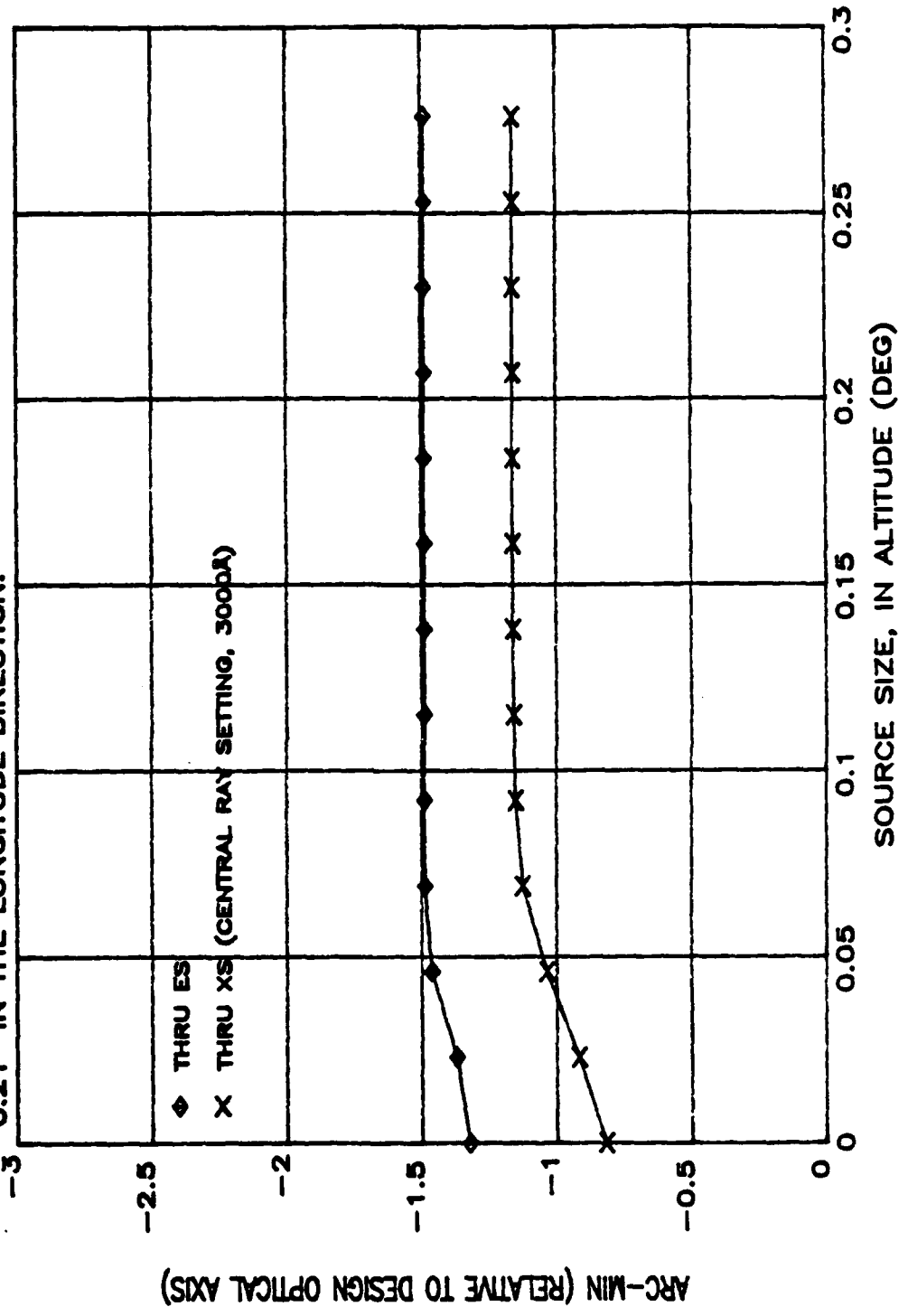
NUV AS DESIGNED. FWHM CENTER OF THE ALTITUDE COMPONENT OF THE FOV VERSUS SOURCE ALTITUDE SIZE. SOURCE AT INFINITY, 0.21° IN THE LONGITUDE DIRECTION.
◆ THRU ES
× THRU XS (CENTRAL RAY SETTING, 3000Å)
ARC-MIN (RELATIVE TO DESIGN OPTICAL AXIS)
SOURCE SIZE, IN ALTITUDE (DEG)
-3
-2.5
-2
-1.5
-1
-0.5
0
0.05
0.1
0.15
0.2
0.25
0.3

FIGURE 32.

FIGURE 33. NUV AS DESIGNED. PEAK OF THE ALTITUDE COMPONENT OF THE FOV VERSUS SOURCE ALTITUDE SIZE. SOURCE AT INFINITY, 0.21° IN THE LONGITUDE DIRECTION.

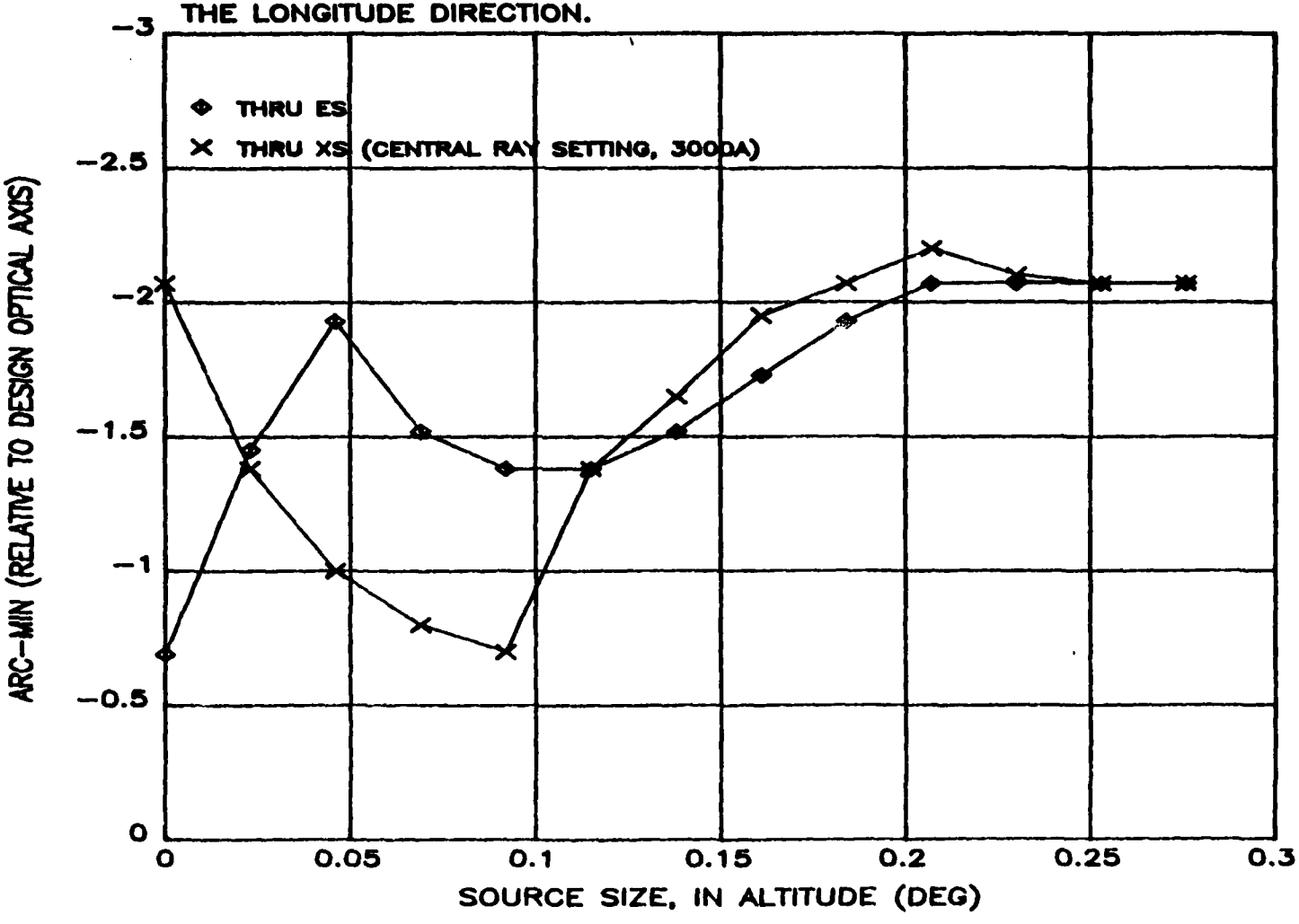

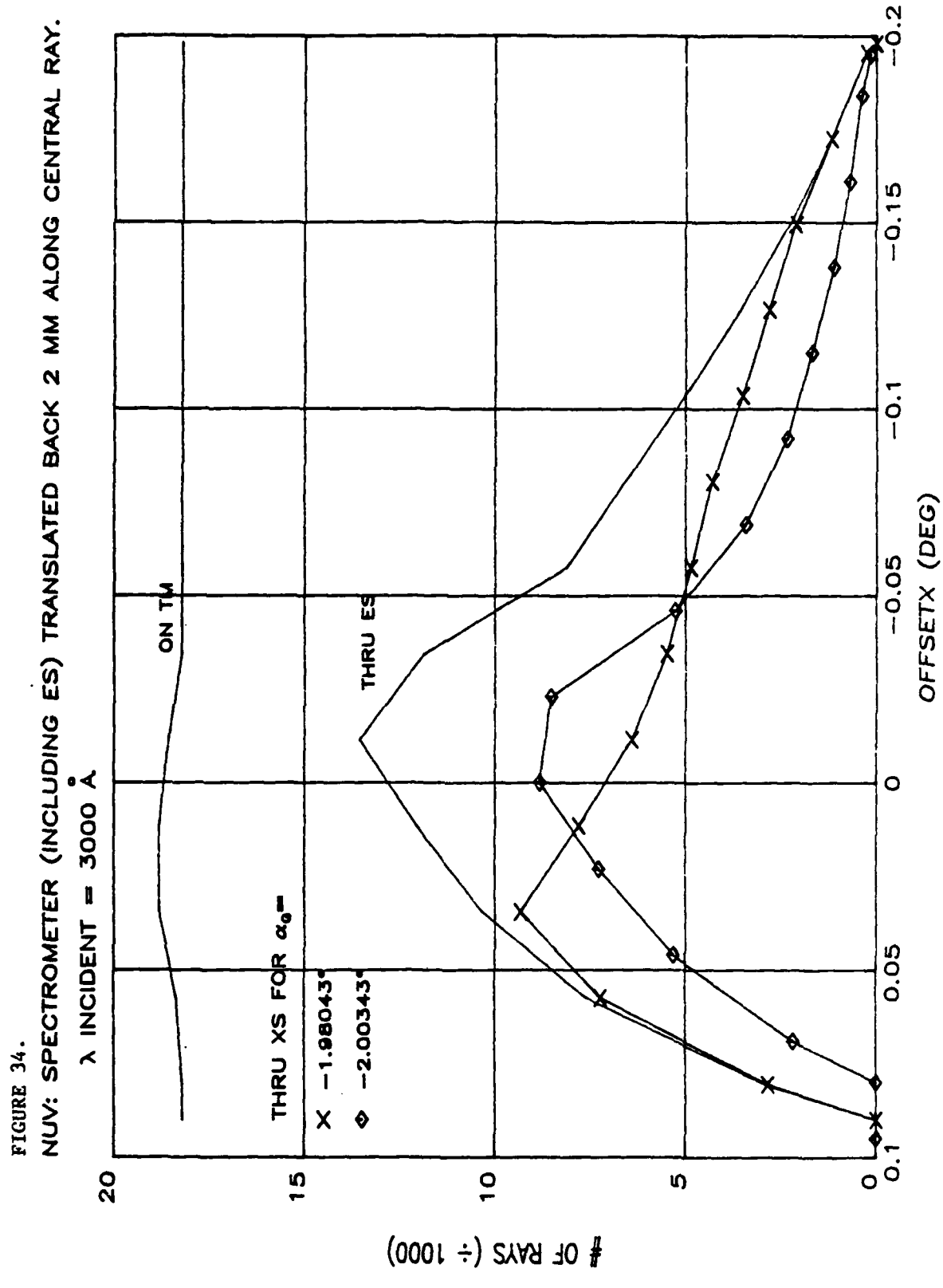
NUV: SPECTROMETER (INCLUDING ES) TRANSLATED BACK 2 MM ALONG CENTRAL RAY.
λ INCIDENT = 3000 Å
ON TM
THRU ES
THRU XS FOR α_0=
× −1.98043°
◇ −2.00343°
OF RAYS (÷ 1000)
OFFSETX (DEG)
20
15
10
5
0
0.1
0.05
0
−0.05
−0.1
−0.15
−0.2

FIGURE 34.

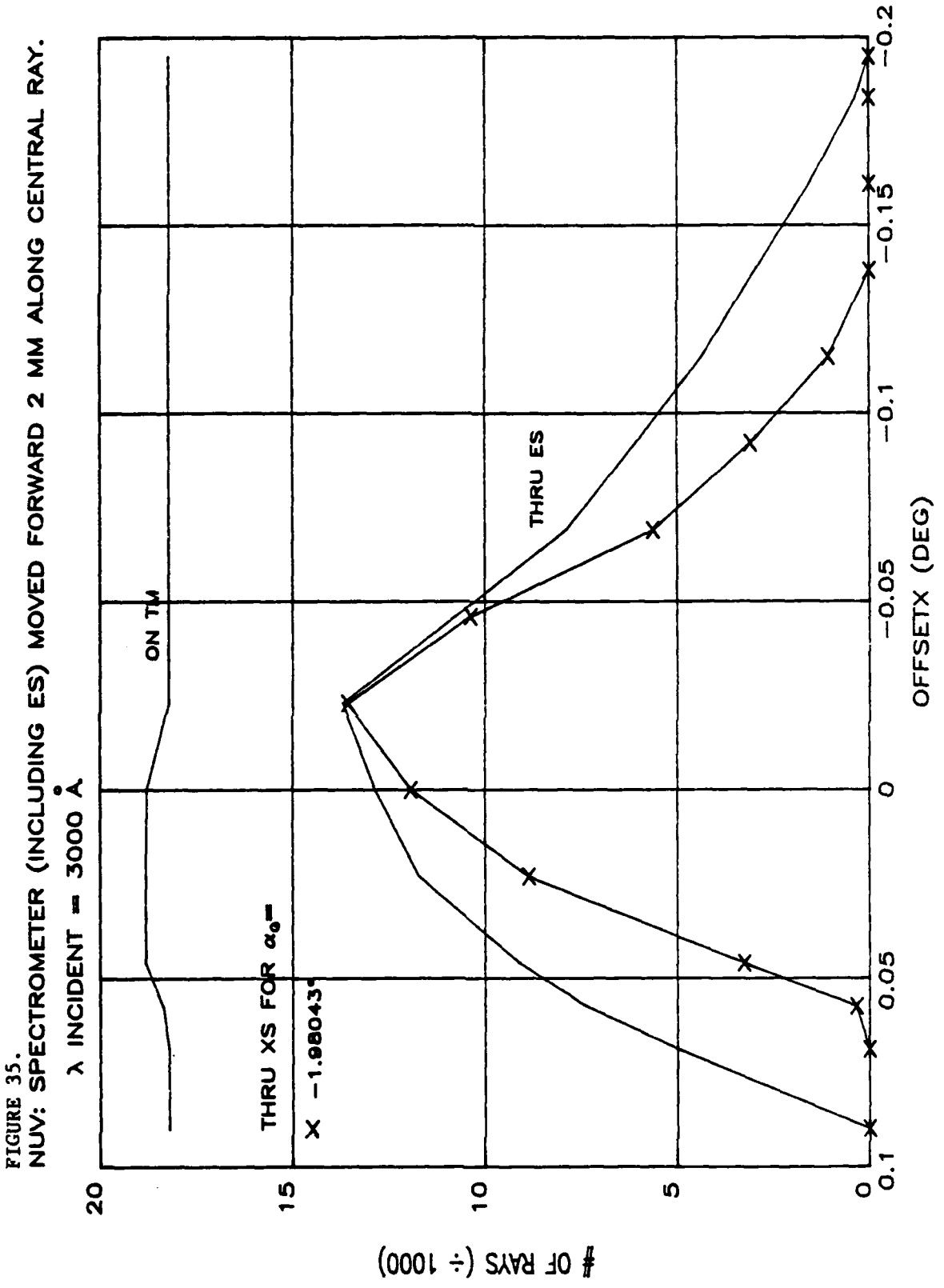

FIGURE 35.
NUV: SPECTROMETER (INCLUDING ES) MOVED FORWARD 2 MM ALONG CENTRAL RAY.

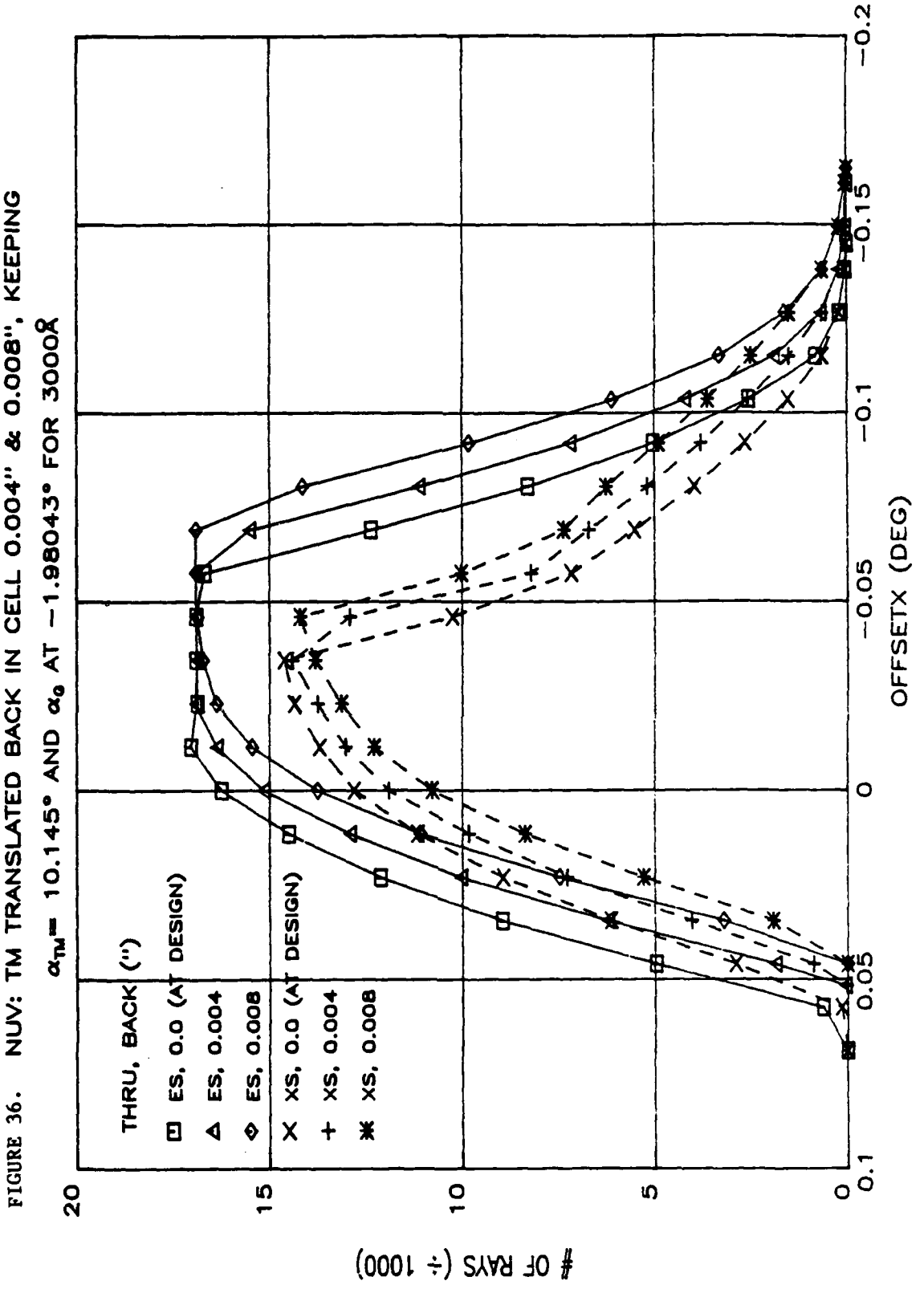

FIGURE 36. NUV: TM TRANSLATED BACK IN CELL 0.004" & 0.008", KEEPING α_{TM} = 10.145° AND α_0 AT −1.98043° FOR 3000Å

FIGURE 37. MAXIMUM DIVERGENCE OF A RAY REFLECTED FROM A PARABOLIC MIRROR OF FOCAL LENGTH F, RELATIVE TO THE RAY REFLECTED FROM MIRROR–CENTER (AT ANGLE A0 WITH RESPECT TO THE SYMMETRY (Z) AXIS), VERSUS THE RATIO OF THE OFF–AXIS DISTANCE, P, TO F, FOR A POINT SOURCE AT 6 OFF–AXIS POSITIONS (D) WITHIN A PLANE PERPENDICULAR TO THE Z AXIS AT A DISTANCE F FROM THE MIRROR. THE MAXIMUM DIVERGENCE OCCURS WHEN P IS 180° FROM D, MEASURED IN THE X–Y PLANE.

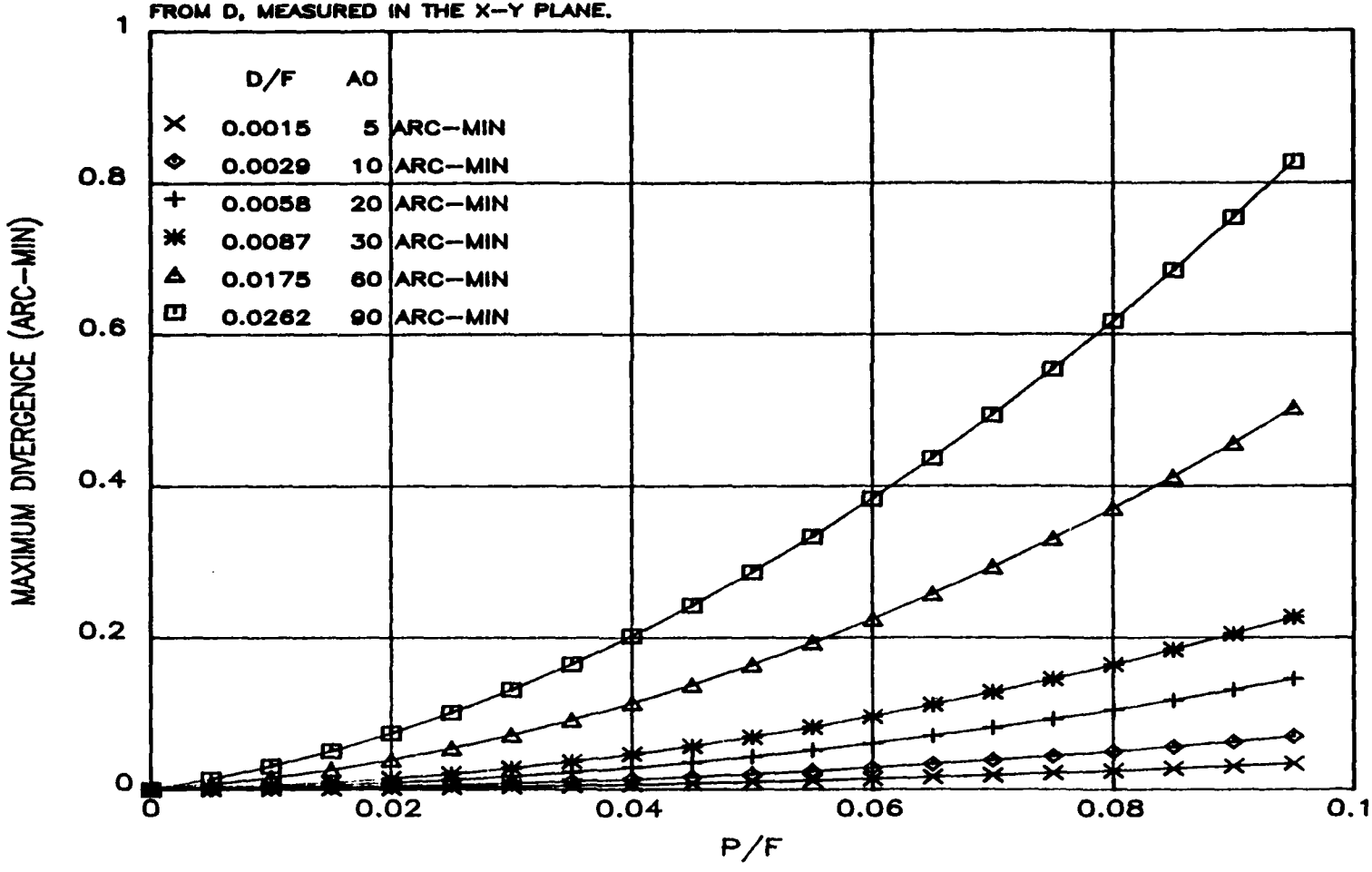

FIGURE 38. ANGULAR COMPONENTS OF A RAY REFLECTED FROM A SPHERICAL MIRROR OF RADIUS R VS THE RATIO OF THE OFF-AXIS DISTANCE P, TO R, FOR A POINT SOURCE ON THE SYMMETRY (Z) AXIS AT +R/2 FROM THE MIRROR. THE MIRROR SURFACE IS DEFINED BY $-X^2 -Y^2-Z^2 +2ZR =0$. P IS IN THE X-Y PLANE; P= X/COS(T)= Y/SIN(T). "C" IS THE COMPONENT RELATIVE TO THE +Z AXIS, AND DEPENDS ONLY ON THE MAGNITUDE OF P. "A-90" & "B-90" ARE THE COMPONENTS RELATIVE TO THE X & Y AXES, EACH MINUS 90°, AND ARE DEPENDENT ON THE ANGLE "T" OF P WITHIN THE X-Y PLANE.

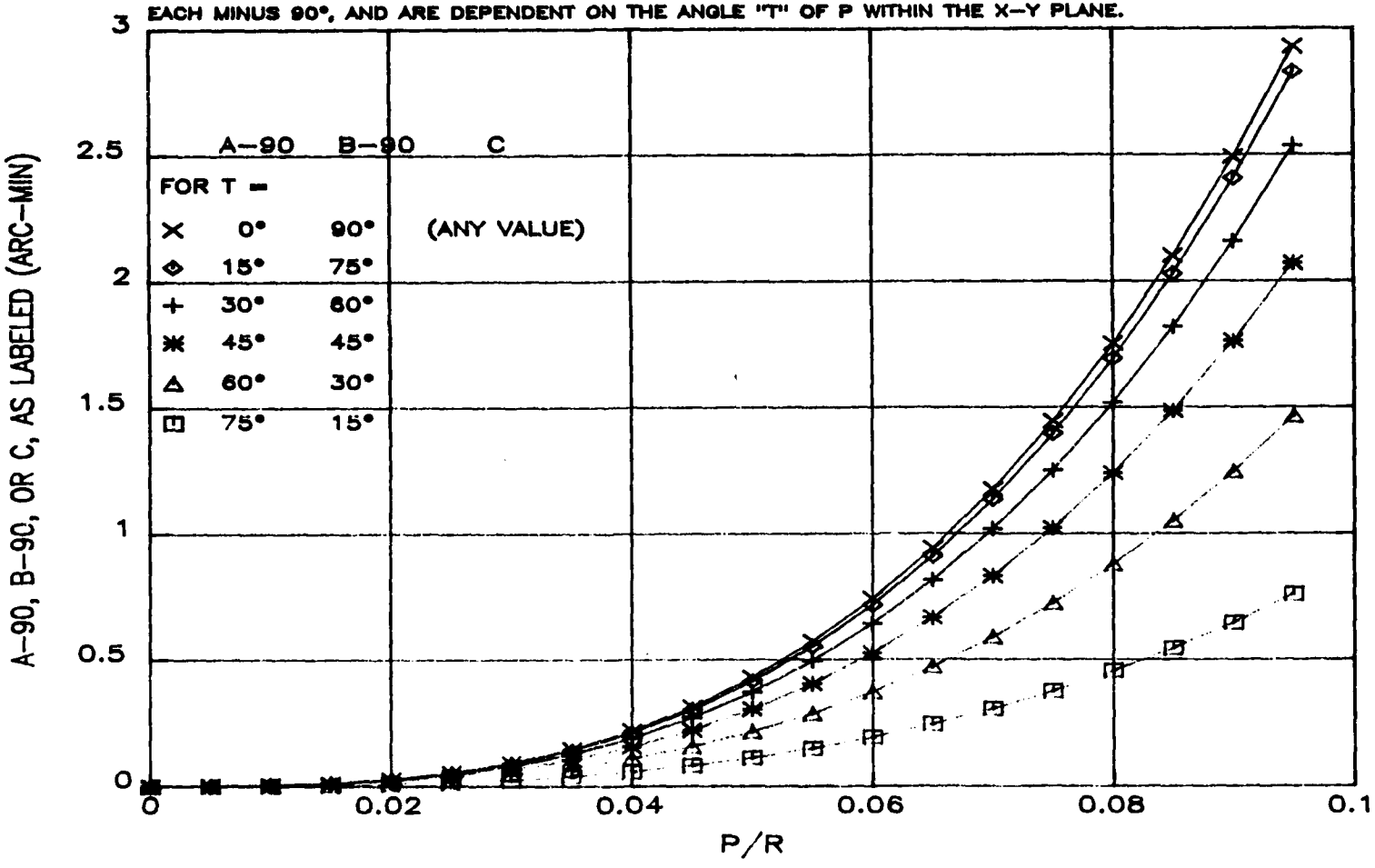

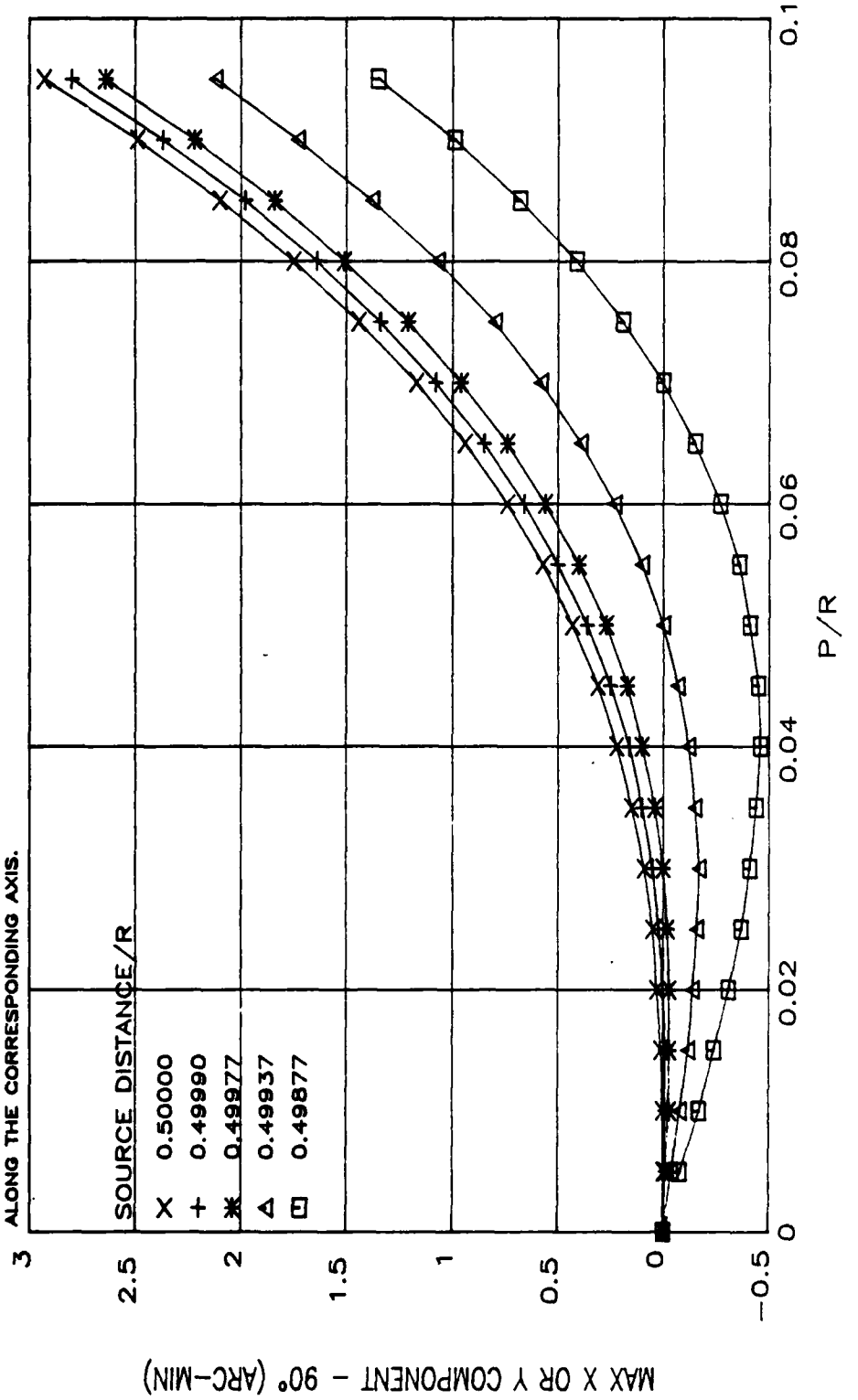

FIGURE 39. MAXIMUM VALUE OF THE X OR Y COMPONENT (−90°) OF A RAY REFLECTED FROM A SPHERICAL MIRROR OF RADIUS R, VERSUS THE RATIO OF OFF-AXIS DISTANCE, P, TO R, FOR A POINT SOURCE ON THE SYMMETRY (Z) AXIS AT 5 DIFFERENT DISTANCES FROM THE CENTER OF THE MIRROR. P IS IN THE X-Y PLANE, AND THE MAXIMUM VALUE OF THE X OR Y COMPONENT OCCURS WHEN P IS ALONG THE CORRESPONDING AXIS.

FIGURE 40. MUV & NUV, AS DESIGNED. POINT SOURCE 4 M FROM TELESCOPE MIRROR OF EACH. λ INCIDENT = 1900 Å (MUV) & 3000 Å (NUV).

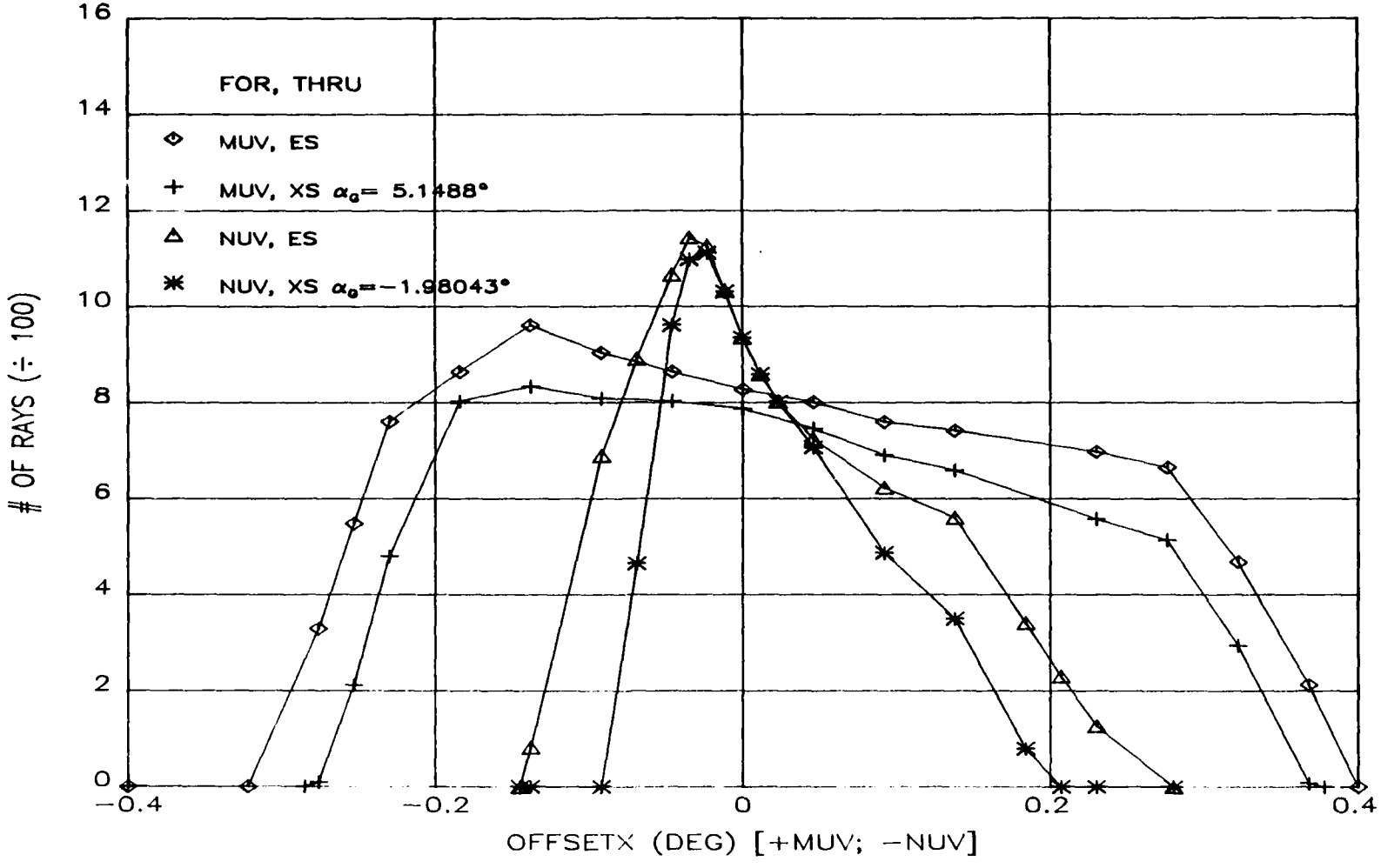

APPENDIX A. Instrument Design Parameters.

Table A2 lists the parameters that define the major optical elements in each instrument. These basically were obtained from RSI's design drawings. All linear measurements are in units of centimeters, and all angles are in units of degrees.

XCR, YCR, and ZCR define the location of the origin of the local coordinate system on each element in a reference coordinate system, defined as follows. The origin is located at the center of the Lyot-Stop, with +Z pointing outward, toward the incoming radiation; +X is to the right, if one is looking outward along +Z. (See Figure 1.) The orientation of the +Z axis of each local coordinate system is obtained by rotating the +Z axis of the reference CS through the Euler angle α, positive for clockwise rotations about the +Y axis of the reference coordinate system (The Euler angles β and γ are not needed since the origins are all in one plane.)

The exposed area of the elements are rectangles, with boundaries measured along the X and Y axes of the local CS. The four limits are given in the four columns under the heading of SIZE.

Table A1 interrelates the element to the acronyms used in subsequent tables and to the surface type used in the raytracing code.

TABLE A1. Element, acronym, and surface type used in raytracing.

ELEMENT	ACKRONYM	SURFACE TYPE
Front of Snout	SNOUT	BAFFLE
Lyot-Stop	LY-STP	BAFFLE (Reference Surface)
Telescope Mirror	TM	CONCAVE SPHERICAL MIRROR
Telescope Slit & Spectrometer Entrance Slit	ES	BAFFLE
Mask, 0.4 cm in front of SM	SM-MASK	BAFFLE
Spectrometer Mirror	SM	CONCAVE SPHERICAL MIRROR
Spectrometer Grating	G	PLANE REFLECTION GRATING
Spectrometer Exit Slit	XS	BAFFLE

In raytracing a spectrometer instrument, the SM surface was used twice, as required by a Ebert-Fastie spectrograph, since SM first renders the light from ES more-or-less parallel toward G, and then focuses the light diffracted from G toward XS. Similarly, the SM-MASK was used four times, because it could affect the ray path four times: between ES and SM, between SM and G, between G and SM, and between SM and XS.

TABLE A2. Parameters used in raytracings labeled "per design".

ELEMENT	XCR (cm)	YCR	ZCR (cm)	α (degrees)	SIZE (LIMIT ALONG LOCAL AXES) -X AXIS (cm)	+X AXIS (cm)	-Y AXIS (cm)	+Y AXIS (cm)	RADIUS OR GRATING CONST
MUV INSTRUMENT									
SNOUT	0.0	0.0	H 16.0*	0.0	4.00	4.00	4.70	4.70	
LY-STP	0.0	0.0	0.0	0.0	2.10	2.10	2.50	2.50	
TM	0.0	0.0	-35.00000	-8.0000	2.10	2.10	2.50	2.50	50.0 cm
ES	-6.80897	0.0	-11.25430	-14.1672	0.0250	0.0250	0.45	0.45	
SM-MASK	-11.74638	0.0	0.13362	165.8328	2.65	3.05	1.70	1.70	
SM	-11.80755	0.0	0.37602	165.8328	3.10	3.10	1.85	1.85	25.0 cm
G	-9.36002	0.0	-9.31984	H 5 to 20	1.05	1.05	1.25	1.25	36000.0 lines/cm
XS	-11.08792	0.0	-12.47264	-14.1672	0.0250	0.0250	0.45	0.45	
6300 Å & 7774 Å INSTRUMENTS									
SNOUT	0.0	0.0	H 16.0*	0.0	4.00	4.00	4.70	4.70	
LY-STP	0.0	0.0	0.0	0.0	2.10	2.10	2.50	2.50	
TM	0.0	0.0	-35.00000	-8.0000	2.10	2.10	2.50	2.50	50.0 cm
ES	-6.80897	0.0	-11.25430	-16.0000	0.0500	0.0500	0.45	0.45	
NUV INSTRUMENT									
SNOUT	0.0	0.0	H 36.0*	0.0	1.95	1.95	2.40	2.40	
LY-STP	0.0	0.0	0.0	0.0	1.05	1.05	1.25	1.25	
TM	0.0	0.0	-15.00000	10.145	1.05	1.05	1.25	1.25	25.0 cm
ES	4.26748	0.0	-3.45732	18.4572	0.0125	0.0125	0.225	0.225	
SM-MASK	9.99541	0.0	7.38707	-161.5428	3.05	2.65	1.7	1.7	
SM	10.12205	0.0	7.76649	-161.5428	3.17	3.17	1.85	1.85	25.0 cm
G	6.95609	0.0	-1.71911	H -2 to -10	1.05	1.05	1.25	1.25	24000.0 lines/cm
XS	8.443304	0.0	-4.99233	18.4572	0.0125	0.0125	0.225	0.225	
5890 Å INSTRUMENT									
SNOUT	0.0	0.0	H 36.0*	0.0	1.95	1.95	2.40	2.40	
LY-STP	0.0	0.0	0.0	0.0	1.05	1.05	1.25	1.25	
TM	0.0	0.0	-15.00000	10.145	1.05	1.05	1.25	1.25	25.0 cm
ES	4.26748	0.0	-3.45732	20.290	0.0125	0.0125	0.225	0.225	

APPENDIX B. Issues in Aligning an Off-Axis Spherical Mirror.

1. Insensitivity of the image quality to changes in the absolute FOV.

Suppose the MUV telescope initially was aligned exactly as designed, and was illuminated by an extended source of points of equal intensity at infinity. Suppose the widths and lengths of the images at the slit from specific source points within a 0.1° X 2.1° FOV were measured. Then, keeping the slit fixed, suppose the absolute FOV was shifted in the altitude (slit width) direction by, say, 0.2°, by rotating the telescope mirror 0.1°. If the dimensions of the images at comparable slit locations from the (new) source points were measured, raytracing predicts that the widths and lengths would differ from those previously measured by less than 7% for all source-points in the slit FOV. (This effect near the center of the slit is shown in Figures 4(A) and 4(B) for the MUV, and in Figures 5(A) and 5(B) for the NUV.) Thus, the quality of the image can't be used to establish an absolute angular reference, as can be done using an off-axis parabola. The only way the image can establish an absolute reference is if the source itself has some identifying feature that survives to the extent of being observable in the inherently degraded image.

2. Sensitivity of the image to illumination of the mirror.

Suppose the MUV telescope was aligned exactly as designed, and was illuminated with a perfectly parallel beam that filled the entrance aperture and had a direction parallel to the design optical axis. At the plane of the slit, such a beam would be imaged into an elongated arrowhead-like pattern, with the brightest part toward the "head". (See Figure 4(A).) More importantly, although the ray incident along the optical axis would pass thru the center of the slit, the image of a beam of such rays would not be centered with respect to the slit width. Instead, the "head" would be virtually at the center of the slit, and the "tails" would fan toward the side of the slit away from the incident beam. Thus, changing the angle of the mirror to center the image width-wise in the slit under this condition of illumination could lead to a considerable difference in absolute FOV's between this instrument and one aligned according to design, unless the boresight mirror alignment compensated for the angular difference.

Another effect of the illumination is that different parts of the image come from different areas of the mirror. Figure 6 illustrates this effect for the NUV telescope, aligned as designed. To the left is shown the image array diagram at the NUV telescope slit plane for an incident beam of light, parallel to the design optical axis, that fills the 2.05 cm by 2.45 cm entrance aperture at the Lyot-stop. The mesh size of the array is 25 microns in the X direction by 50 microns in the Y direction. The

array is positioned at the slit plane so that the element in the top right corner represents the number of rays falling within the slit-plane area with coordinates of 0≤ X <25 microns and -450≤ Y <-400 microns. (The slit center is close to the asterisk shown in the figure.) The array is the sum of 25 separate arrays obtained by sectioning the entrance aperture into 25 equal areas, as shown to the right in Figure 6. Each section was 0.41 cm wide (X) and 0.49 cm long (Y). 961 rays from 31 rows and 31 columns were sent toward the telescope mirror from each section. Since the incident beam is a grid of parallel lines, the rays from each section of the entrance aperture project onto a specific section of the mirror. Thus, the sectional drawing of the entrance aperture approximately illustrates the sectional illumination of the surface of the mirror. The entrance aperture drawing and image array in Figure 6 are oriented so that Figure 1 can be used to visualize the illumination and image within the instrument; the view direction for both the aperture and the image in Figure 6 is toward the mirror.

As is shown in Figure 6, the "tails" of the image come from the sides of the incident beam (and mirror), while the "head" comes from the center of the incident beam. The array elements with a value over 600 come mostly from the sections of the entrance aperture labeled 8, 13, and 18. Thus, if the full entrance aperture is not illuminated, the position of the image at the slit may not be indicated properly, which could lead to a misalignment of the telescope mirror.

The focal distance is also affected by the illumination. If the illuminated area of the mirror was reduced about its center to reduce some of the aberrations, by masking down the entrance aperture about its center, e.g. making it circular or elliptical would eliminate the "tails" of the arrowhead (which come mostly from the corners of the entrance aperture, particularly those on the side toward the slit, labeled "(D)" and "(H)" in Figure 6), it could lead to an erroneous conclusion regarding the focal distance because the tangential focal distance increases as the entrance aperture is masked down. Thus, changing the mirror-to-slit distance under this condition of illumination could cause the altitude resolution of the final image to be degraded in flight.

3. Summary of Traditional Telescope Alignment Techniques.

Traditional alignment techniques fall into four basic categories, depending on the number of times light strikes the telescope mirror, the location of the source, and the place the "image" is detected. These categories are: (1) single-pass, forward alignment, in which the source is in front of the telescope and the image is detected at the slit; (2) single-pass, backward alignment, in which the source is effectively at the slit and the image of it is detected by looking toward the mirror with an external telescope focused at infinity; (3) double-pass, backward alignment, in which the source is effectively at the slit, a flat mirror is

placed in front of the instrument to reflect the light back to the mirror, and the image is detected back at the slit; and (4) double-pass, forward alignment, in which the source is in front of the instrument, a flat mirror is placed behind the slit to reflect the light back to the mirror, and the image is detected back at the source.

Raytracing was done on the NUV and MUV telescopes for each of these categories. The results show that the image quality (size, shape, or spatial resolution) just is not sensitive enough, in any of them, for it to be used to optically establish a reference axis or direction with the required accuracy in the slit-width direction. The two "backward" alignment techniques, either of which permits very accurate determination of the optical axis when the mirror is an off-axis parabola and the source is at the focal point of the parabola, aren't very sensitive when the mirror is an off-axis sphere Another consideration in the "backward" techniques is whether the effective source is located where the flight slit would be.

The "double-pass" techniques both result in images with compounded aberrations because of the two reflections from the mirror, and thus require careful selection of the spatial character of the effective source if the image is to have the requisite spatial resolution. For example, in the backward, double-pass technique, an Air Force resolution target or grid mesh, etc. placed at the plane of the slit must have opaque rectangles between adjacent transparent rectangles at least as great as the limiting rectangle of the image from a point source in that region of the slit.

APPENDIX C. FIELDS OF VIEW

I. RAYTRACING INPUTS.

The Lyot-stop was used as the entrance aperture for each instrument. Parallel rays from a grid pattern within the Lyot-Stop simulated the incident beam from a distant point source, the angle of the rays relative to the the design optical axis determining the relative direction of the source. In the figures, OFFSETX indicates the component of this angle in the altitude or slit-width direction, and OFFSETY indicates the component in the perpendicular (longitude or slit-length) direction. The code requires that the sign of these components be positive when the general direction of the ray is toward the positive corresponding axis. (See Figure 1.)

The size of the entrance aperture was slightly reduced from the size of the Lyot-stop so that fewer rays from the aperture would miss the telescope mirror. The reduction was $\pm$0.025 cm in width and length in the 1/8th meter NUV instrument and $\pm$0.05 cm in width and length in the 1/4 meter MUV instrument, or about 4.3% in area in both instruments. With this reduction, the first column of rays on the side away from the slit sweeps off the mirror at an OFFSETX angle of about -0.018° in the NUV and about +0.038° in the MUV; the second column sweeps off that side of the mirror at OFFSETX values of about -0.154° in the NUV and +0.152° in the MUV. On the opposite side, the first column sweeps off the mirror at an OFFSETX angle of about +0.045° in the NUV and -0.058° in the MUV.

The cosine of the offset angle was not used to weight the number of rays at the entrance aperture, as would be required to accurately simulate illumination by an isotropic source. That is, the number of rays from the entrance aperture for each parallel beam was a constant for all offset angles. However, the offset angles over the FOV are small, the largest being about $\pm$1.25° in the longitude direction. The results probably are affected more by the density of rays at the entrance aperture than by the neglect of the cosine factor, since the spacing of the rays has an increasing effect as the beam sweeps off the mirror.

The simulation of the illumination at the plane of the entrance aperture as defined above, then, was approximately equivalent to illumination from a uniform, isotropically emitting source at infinity.

II. TERMINOLOGY

Certain terminology is used in the discussions below to simplify defining the angular size of the source and its position relative to the design optical axis. A "longitude line source" means that the source was equivalent to a line parallel to the longitude or slit-length direction, i.e. relative to the design optical axis, the component of the angle of the

parallel rays along the Y-axis of the reference coordinate system was varied (by ± some angle specified in the discussion), but the component along the X-axis was fixed (at a value denoted by the quantity OFFSETX). Similarly, an "altitude line source" means that the source was equivalent to a line parallel to the altitude or slit-width direction.

The number of rays that intersect a plane directly behind either the telescope slit or the exit slit of a spectrometer is called the "signal". A plot of the signal versus the angular motion of the center of the source (relative to the design optical axis) is called a "FOV curve".

III. TELESCOPES.

Figure 7 shows the number of rays passing through the telescope slit (ES) of the 1/8th meter NUV instrument from a source at infinity subtending a small rectangular solid angle at the instrument (0.0115° in the slit-width direction and 0.105° in the slit-length direction). The NUV telescope was assumed to be aligned as designed. This source was simulated as follows. The positional grid pattern of rays was 31 rows and 31 columns within a reduced Lyot-stop, 2.05 cm wide (X) by 2.45 cm long (Y); the angular grid pattern of rays from each positional grid point was 5 rays spanning the 0.0115° and 5 rays spanning the 0.105°. The angular center of the source was stepped in positive and negative increments of 0.105° in the longitude direction, keeping the center in the altitude direction fixed at one of six offset angles. In the figure, the angular components of the center of the source relative to the design optical axis are given by OFFSETX in the X (altitude) direction and OFFSETY in the Y (longitude) direction.

The curves for the six offsets illustrate the asymmetry that exists in the image for the component of the FOV in the altitude direction relative to the design optical axis, while the abscissa indicates the symmetry that exists in the image for the component of the FOV in the slit-length direction. That is, the figure shows that differential altitudes of the same magnitude on either side of the optical axis do not contribute equally to the signal, while differential longitudes of the same magnitude (at the same altitude) contribute exactly the same amount.

The longitude symmetry is also illustrated in Figure 8, which shows the number of rays through both the NUV telescope slit (labeled ES) and the NUV exit slit (labeled XS) for a grating setting corresponding to the central ray through the system for 3000Å light, when the distant source effectively was a uniform altitude line source, formed by a series of 19 equally spaced points spanning 0.207° in the altitude (X) direction (about equal to the full FOV in that direction).

The response of the telescope to longitude line sources, stepped in altitude, will be presented in the discussion of the complete instruments (Section V, below).

IV. ILLUMINATION AFTER THE TELESCOPE SLIT.

Asymmetry in the altitude direction is present not only in the signal, but also in the pattern of the illumination on optical components subsequent to the telescope slit. Figure 9 illustrates the effect for the NUV. The array diagrams show the illumination on the spectrometer mirror for a distant longitude line source at 4 different altitudes (OFFSETX values) within the FOV. This source was simulated as follows: the positional grid pattern within the slightly reduced Lyot-stop again was 31 rows and 31 columns; the angular grid pattern from each positional grid point was 21 rays spanning 2.1° in the Y (longitude) direction. The components of the angular center of the source relative to the design optical axis were zero in the Y direction, and one of the 4 values of OFFSETX in the X direction.

At the lower altitudes within the FOV, the illumination that passes through the slit comes from the "heads" of the composite of 21 images stacked along the length of the slit, each image being much like the array diagram shown in Figure 6. Since the more intense illumination near the head was shown to come from a composite of several sections centered in the incident beam (and, therefore, from comparable projected areas of the telescope mirror), the diverging illumination after the slit is filled.

As the altitude of the line source increases, more of X-component of each image passes through the slit, allowing contributions from more of the mirror. The illumination after the slit, thus grows in width, continuing to be filled in - until the altitude is reached for which the "head" of the image from each source point is located just beyond an edge of the slit (the side toward the incident beam). At that altitude (Figure 9 A) and above (Figure 9 B-D), the "heads" of each image are increasingly prevented from passing through the slit aperture. Since the "heads" come mostly from a central strip of the telescope mirror and the "tails" mostly from its sides, the illumination after the slit develops a hole approximately at its center that grows in size and eventually disappears, the last rays to leave coming from the two corners of the mirror on the side farthest from the slit. (Also see Figures 6 and 1.)

Diffraction from the slit has been neglected in this discussion; it will fill some of the depletions shown in Figure 9, more for the NIR than for the other instruments.

V. SPECTROMETER INSTRUMENTS.

To examine the FOV response of a complete spectrometer instrument, the same longitude line source that produced Figure 9 was used, i.e. 21 angles, spanning 2.1° and centered in the Y (longitude) direction, from each point within a grid pattern of 31 rows and 31 columns within the slightly reduced Lyot-stop (2.05cm X 2.45cm for the NUV, and 4.1cm X 4.9cm for the MUV).

The X-component of the angular center of the beam of rays from each positional grid point was stepped in positive and negative 0.0115° increments relative to the design optical axis in the X (altitude) direction (OFFSETX), until no rays passed through the exit slit of the spectrometer for a particular grating angle. The process then was repeated for several other grating angles. At each grating angle, the sum of the rays from all of the altitudes was equated to the signal from the full FOV. The plot of this signal versus grating angle then was interpreted to be the spectral line shape that would be obtained from a distant, uniform, isotropically emitting source that filled the full FOV.

A. 1/8TH METER NUV, ALIGNED AS DESIGNED.

Figure 10 shows the results for the NUV instrument, aligned as designed. The curve labeled "ON TM" in the plot to the right shows the number of rays that struck the telescope mirror as the longitude line source was stepped in altitude across the FOV. OFFSETX = 0 is the altitude direction parallel to the design optical axis; negative values of OFFSETX are toward higher altitudes. (Also see Figures 1 and 2.) The curve is included to show the statistics of the ray simulation of the illumination of the mirror. The two values of OFFSETX at the decreases from maximum are at the angles where the first column of rays from either side of the slightly reduced Lyot-stop misses the mirror.

The double-lined curve (enclosing the curves with symbols) is the number of rays that passed through the entrance slit (ES) of the NUV spectrometer as the longitude line source was moved in altitude across the FOV. The five curves with symbols are the number of rays of 3000Å radiation that passed through the exit slit (XS) of the spectrometer at five different grating angles for the same motion of the source.

The plot to the left shows the resulting line shape for the full FOV. Each symbol on the curve corresponds to the grating angle used for the curve with the same symbol on the right-hand plot. Wavelength increases toward the right, at the rate of ~129.3Å per degree. The grating angles labeled in the figure, thus are spaced ~3Å apart, and the FWHM of the spectral line is ~9.4Å.

Figure 10 shows that blue wing of a spectral line is weighted toward the lower altitudes within the FOV, while the red wing has no contributions from the lower altitudes within the FOV. The grating angle for a spectrometer, thus, is very important in determining the FOV of the complete instrument.

The grating angle labeled with an "X" is that angle for which the central ray of the telescope passes through the center of the exit slit. This ray will be called the central ray of the optical system, although it does not quite intersect the center of the grating. (The local X coordinate of the intersection is -66 microns.) Hereafter, the grating

angle satisfying this condition will be called the central ray grating setting. It should be noted that this angle is not quite the angle for the center of the FWHM of the line shape. The latter is at a slightly more negative value, i.e. at a slightly longer wavelength setting.

B. PHOTOMETER-SPECTROMETER COMPARISON: 1/8th METER.

Figure 10 can be used to compare the fields of view of a photometer and a spectrometer having like telescopes. It illustrates, as shown above, that the signal behind the telescope slit (the curve labeled "THRU ES") does not have symmetric contributions in altitude about the design optical axis. The center of the FWHM is shifted ~1.3 arc-minutes (0.022°) toward higher altitude. For the altitude contributions to the signal at the exit slit of the spectrometer, the center of the FWHM at the grating angle corresponding to the central ray for the optical system is shifted ~0.84 arc-minutes (0.014°) from the design optical axis, also toward higher altitude. The difference between the centers of the FWHM of the FOV of the telescope and the spectrometer at the central ray setting is then ~0.5 arc-minute. This difference should be reduced for the grating setting corresponding to the center of the FWHM of the line shape. For, if the curve for this grating angle had been included in the right-hand plot, the value of OFFSETX for the center of its FWHM would have been toward a slightly higher altitude than the center of the FWHM for the central ray setting, placing it closer to the center of the FWHM for the signal behind the telescope slit.

C. CO-ALIGNING THE 1/8TH METER INSTRUMENTS.

From the preceding discussion, it appears possible, in principle, to co-align a photometer and a spectrometer having like telescopes to within 0.5 arc-minute by defining the field-of-view axis for each as the center of the FWHM of the signal obtained by moving an angularly narrow source across the FOV, after the spectrometer has been set to the appropriate grating angle. The "appropriate" grating angle is the center of the FWHM of the line shape resulting from a source emitting the same wavelength that fills the full FOV.

Since the grating angle is not changeable in an analog fashion, but is changed in discrete steps (via a stepper-motor, gear arrangement, and cam device), we must consider how accurately the angle can be set. (Repeatability of angle with step number, which typically is within 1 or 2 steps in other Ebert-Fastie spectrometers made by RSI, is not an issue here because the signal itself can be used to indicate repeatability of the angle if the light source has a stable output.) Although the angular change for a grating step is not a constant for an instrument, for the

purposes here, we can consider it so. For the NUV instrument it is ~0.004°/step, so there should be about 4 or 5 other possible grating settings (steps) between any two of the curves on the right-hand plot. Since the centers of the FWHM of the FOV for the two curves at grating angles of -1.98043° and -2.00343° are spaced about 0.024° in altitude, assuming a linear relation holds for the change in the center with grating angle in this region of the FOV, it ought to be possible to set the grating angle close enough to the center of the FWHM of the line shape to identify the altitude component of the field-of-view axis for the NUV to within about 0.3 arc-minute.

This is not quite the final word on the co-aligning the field-of-view axes of the 1/8th m photometer and an 1/8th m spectrometer, since we have yet to compare the 1/8th m instruments with the 1/4 m MUV. Before doing that, we evaluate one other technique for determining the field-of-view axis of a spectrometer.

Since the finite size of a grating-angle step introduces a possible offset between the FOV of a spectrometer and the FOV of a photometer, another possible approach for determining the field-of-view axis of a spectrometer is to scan in wavelength at each offset angle of the line source. However, Figure 11 shows that establishing a criterion for a field-of-view axis from this procedure is less straightforward. It shows the line shapes that would be obtained for a 3000Å monochromatic longitude line source at 7 different altitude offset-angles within the FOV. Although it might be argued that the curve having its peak centered within the extremes of the grating angles (for signals above some small, but finite limit) does provide a selection criterion, in this case the repeatability of the grating-angle with step number does matter because the line shapes close to the center of the FOV are very similar.

Figure 11 shows that the peaks of the line shapes for OFFSETX values of 0.0° and -0.023° are separated by α_G values of ~0.012° for the NUV. Assuming that a linear relation holds between $\Delta\alpha_G$ and ΔOFFSETX for the peaks in this region of the FOV, i.e. that $\Delta\alpha_G/\Delta$OFFSETX = ~0.0087°/arc-minute, to distinguish two similarly-shaped curves with peaks separated by ΔOFFSETX = 0.5 arc-minute would require that a grating step be repeatable to within ~0.0044°. Since this is about equal to 1 grating step for the NUV, and since repeatability is 1 or 2 steps, determining a field-of-view axis this way could be both time-consuming and prone to error.

D. 1/4 METER MUV, ALIGNED AS DESIGNED.

Using the same longitude line source (0° by 2.1°), and the same number of rays (21 Y-angles from each point of a 31 by 31 positional grid pattern in the slightly reduced Lyot-stop), the same process that resulted in Figures 10 and 11 for the NUV was repeated for the MUV instrument for an incident wavelength of 1900Å, with the instrument aligned as designed.

The results are shown in Figures 12 and 13. The abscissae are plotted to correspond to those in Figures 10 and 11 for the NUV, e.g. in Figure 12, altitude increases to the right in the right-hand plot and wavelength increases to the right in the line-shape plot. The spacing of the grating angles selected for Figure 12, however, was 0.046° (twice that used for the NUV). Since the dispersion of the MUV is about 83.94Å per degree change of the grating angle, the wavelength separation then is ~3.86Å. The FWHM of the line shape from the full FOV is ~11.2Å.

As for the NUV, the grating angle corresponding to the central ray setting (labeled with the symbol "X") is not quite the angle corresponding to the center of the FWHM of the line shape. The latter, again, is toward a slightly longer wavelength setting. To investigate how accurately this angle can be set in this instrument, we again use an approximation for the change in grating angle with step size, and make use of the separation of the centers of the FWHM of adjacent curves in the FOV plot. For this instrument, the change in grating angle is about 0.009° per step. From the ~0.028° altitude separation of the two curves at grating angles of 5.1488° and 5.1948°, we conclude that the grating angle in the MUV can be set to identify the altitude component of a field-of-view axis to within about 0.35 arc-minute.

E. NUV-MUV COMPARISON.

That the design for the MUV is better optimized than the design for the NUV, and results in better altitude focusing, is shown by the fact that the FOV is more crisply terminated on the high altitude side, and by the fact that a larger percentage of the rays that pass through the telescope slit also pass through the exit slit. This is further illustrated in Figure 14, which shows the altitude FOV curves for the central ray grating setting in both instruments. With the same number of incident rays, the NUV signal had to be increased by about 15% to bring its peak to the peak of the MUV signal. However, the centers of the FWHM for the central ray grating setting in both instruments are almost exactly at the same altitude angle, about 0.85 arc-minute from the design optical axis in the direction of higher altitude.

Figure 14 also gives evidence that the full FOV of the MUV is slightly less than the full FOV of the NUV. This is better illustrated in Figure 15 which shows the signals through the telescope slits of the NUV and MUV instruments from Figures 10 and 12 plotted on the same graph. Although the NUV has a larger full FOV in the altitude direction (~0.207°, compared with ~0.184° for the MUV), the magnitude of the FWHM of both instruments is very nearly the same (~0.115°).

However, the center of the FWHM for the MUV telescope is about 0.3 arc-minute lower in altitude, i.e. relative to the design optical axis, about 1.0 arc-minute in the direction of higher altitude. Figure 16 shows these

results more clearly. For it, the NUV telescope signal was normalized to the MUV signal at the peak, and was shifted 0.3 arc-minutes toward lower altitude. (The justification for simply shifting the curve, rather than redoing the raytracing using an angle for the telescope mirror that differs from the design by 1/2 of the shift, is discussed in Appendix D.)

F. WAVELENGTH INDEPENDENCE OF THE FOV FEATURES.

Figures 17-22 illustrate the wavelength independence of the FOV features discussed above for the NUV and MUV instruments. Figure 17 is another version of the 1900Å FOV plot for the MUV as was shown in Figure 12, the difference being that the grating-angle spacing in Figure 17 is 0.023°, i.e. the same as was used for the NUV in Figure 10. This plot was included to also permit direct comparison with Figure 18, which is the MUV FOV response for the same source conditions, except that the wavelength of the incident radiation is 3200Å. The resulting line shapes for individual altitude positions of the source within the FOV are shown in Figure 19, which can be compared with Figure 13.

Figure 20 is a repeat of the FOV curve for the NUV shown in Figure 10, and was included so that a direct comparison could be made with Figure 21, which shows the NUV response for the same source conditions, except that the wavelength of the incident radiation is 4000Å.

The line shapes from the full FOV for the two wavelengths in the two instruments are shown in Figure 22. (The conversion factor to $\Delta\lambda$ from $\Delta\alpha_G$ is about 129.3Å per degree for the NUV and about 83.9Å per degree for the MUV.)

Examination of these figures shows that, while fewer rays from the entrance slit pass through the exit slit as the wavelength increases (being lost passed the grating because of its increased angle), the two important features used above to determine the field-of-view axis do not change: (1) the grating angle that centers the altitude FOV response of a spectrometer, and (2) the altitude-angle corresponding to the center of the FWHM of the FOV.

G. ANGULAR MISALIGNMENTS OF THE TELESCOPE MIRROR.

To extrapolate to the complete instruments, the conclusion of Appendix B regarding the insensitivity to angular misalignments of the telescope mirror, we include Figures 23-26, and draw attention to the values of the abscissae. Figures 23 and 24 show the results for the NUV when the telescope mirror is misaligned by $\pm 0.1°$. Figures 25 and 26 show similar results for the same angular misalignments of the telescope mirror in the MUV. These figures also should be compared with Figures 20 and 17.

Although we have not included many grating angles, nor shown the results obtained for other wavelengths, these would not have altered the conclusion that the signal, like the image at the plane of the telescope slit, does not change significantly with angular misalignments of the mirror that are equivalent to shifting the observed altitude regime by more than the magnitude of the FOV in that direction. Thus, the optical characteristics of an individual instrument can not be used to establish an absolute FOV. This conclusion emphasizes the importance of establishing the mechanical (or attachment) axis as an absolute reference direction before beginning alignment of the telescope.

VI. CONCLUSIONS.

From the preceding discussion, we conclude that, if we exactly co-align the field-of-view axes, as defined above, the following conditions should obtain for the common-sized fields-of-view in orbit. The signals for the NUV and MUV will have almost equal fractional contributions from altitudes within the lower one-half of the common field-of-view. Over the upper one-half, the NUV has first lower, then higher relative contributions, the cross-over occurring at an altitude about 3 arc-minutes from the coincident centers of the FWHM. If the 1/8th meter 5890Å photometer has the same-sized slit as the NUV telescope, its field-of-view will be shifted ~0.3 arc-minute toward lower altitudes, relative to the fields-of-view of the NUV and the MUV.

APPENDIX D. SIGNALS FOR SOURCES OF FINITE SIZE AND/OR AT FINITE DISTANCES FROM THE INSTRUMENT.

In Appendix C the altitude component of the field-of-view axis was determined, in principle, by moving an infinitely distant line source along the altitude direction of the field of view, the line being parallel to the longitude direction. Since the angular size and effective distance of this idealized source can not be exactly duplicated in the laboratory, we considered the effect on the previously identified features of the signal for more realistic laboratory sources.

I. SOURCES OF FINITE SIZE AT INFINITY

We first relaxed the most obviously unattainable feature of the idealized source - its line character - by increasing the angular size of the source in the altitude direction. The initial increase was to 0.046°, or slightly less than one-half of the the FWHM of the component of the FOV in this direction. Five angles were used to span the 0.046°, making the altitude angular spacing 0.0115° and the total number of rays from the source at the entrance aperture equal to 100905. The angular center of the source then was stepped in along the altitude direction, as had been done in obtaining Figures 10 and 12 for the idealized line source.

The results for the NUV at grating settings in the vicinity of 3000Å are shown in Figure 27. The resulting signal at any one altitude is equal to the convolution of the FOV curve for line sources in Figure 10 with a rectangular function of angular width in the altitude direction equal to the source width. This is a manifestation of the insensitivity of the optical system to angular offsets of the source of the order of $\pm 0.1°$, as was noted Appendices B and C.

Further increases of the angular size of the source in the altitude direction are shown in Figures 28, 29, 30, and 31. Comparison of these figures with Figure 10 shows that the grating angle that results in a FOV curve for the spectrometer that is nearly centered in the full FOV remains the angle corresponding to the center of the FWHM of the line shape for a source that fills the full FOV. However, as the angular size of source increases, the FOV curves for the NUV are not only broadened, but become more symmetric in shape (although the symmetry still is not about the design optical axis). As a result, the center of the FWHM is shifted toward slightly higher altitudes. This effect is quantitatively shown in Figure 32 for the FOV curves pertaining to the signal behind the telescope slit (labeled "THRU ES") and the signal behind the exit slit when the grating angle corresponded to the setting for the central ray condition.

Figure 32 shows that, although the center of the FWHM rapidly shifts toward a higher altitude as the source size increases, the shift remains less than ~0.3 arc-minute for both curves. This is in contrast to the behavior of the peak of the FOV curves, which is quantitatively shown in

Figure 33. The density of rays is partially responsible for the erratic behavior of the peak versus source-size, e.g. the angular spacing of rays was 0.69 arc-minute. Nevertheless, when Figures 27-31 are also considered, we conclude that there is more uncertainty in determining the offset angle for the peak than for the center of the FWHM. This was the reason for selecting the center of the FWHM as the defining feature for components of the field-of-view axis.

Although Figure 32 does not show sensitivity of the center of the FWHM to the source size above a value of ~0.06° (about one-half of the FWHM), this should not be interpreted to mean that none exists. As the source size increases, the span in its offset angles at the two positions corresponding to one-half the maximum signal increases. Other surfaces not considered in the raytracing, such as a pre-slit baffle, could begin to affect the signal, possibly asymmetrically. So, it is prudent to use a source that is as angularly narrow as possible in the direction for which the component of the field-of-view axis is to be determined.

II. COLLIMATING DEVICES.

The second feature of the idealized source not exactly attainable in the laboratory is the effective distance of infinity for all points within a finite-sized source. That is, to duplicate the idealized conditions requires a device that has three properties. (1) It creates a parallel beam of light from each point within the effective source; (2) the beam corresponding to <u>each</u> source point is large enough to fill the snout of the instrument; and (3) the beam from the required direction(s) <u>actually passes through the snout</u>. However, typical laboratory collimating devices, e.g. a lens, a parabolic mirror, or a spherical mirror, generally produce exact collimation only for a single source point.

As will be discussed in more detail below, properties (2) and (3) impose certain requirements on the laboratory setup. In particular, they require that the collimating device be larger than the snout aperture, and they require careful illumination of the collimating device, usually prohibiting direct use of an emitting source as the effective source for the collimator.

A. COLLIMATING LENSES.

A compound lens can be made to be nearly exactly collimating over a large source area, but only for one value of the index of refraction, i.e. for one wavelength. This wavelength dependence, and the cost of a lens having the diameter required to produce a beam that fills the snout (8 cm X ~9 cm) of a 1/4 meter instrument are factors that rule out the use of a lens for determining the fields-of-view, even for the instruments having a wavelength range within the transmission of lens materials.

B. PARABOLIC COLLIMATING MIRRORS.

The laboratory setup that most closely produces the idealized conditions by reflection is a secondary source at the focus of a mirror whose surface is a paraboloid of revolution. The secondary source, an aperture of dimensions that provide the required field of view, is illuminated by focused light from a primary (emitting) source oriented so that light reflected from the mirror is not vignetted by the holders of the aperture or the primary source on its transit to the front opening of the instrument. Provided that the figure of the mirror, indeed, is a paraboloid over the area illuminated, the light that passes through the point in the aperture exactly on the axis of revolution is rendered parallel upon reflection at the mirror surface (except near the edges, where diffraction spreads the beam), thus duplicating the idealized source for one point. However, light that passes through any other point of the aperture is not rendered exactly parallel. This is akin to, but not exactly equal to the inverse of the case when the mirror is used as a telescope, and aberrations in the image, mainly coma, are produced when the direction of the incident beam of parallel light is not parallel to the symmetry axis of the paraboloid; for, in the telescope, the same area of the mirror usually is involved for each (incident) direction, whereas, here, different areas of the mirror are involved for each (exiting) direction in order to fill the instrument aperture.

The divergence of the reflected beam can be examined through the direction cosines of the reflected rays. In a coordinate system with origin on the surface of the mirror and Z axis coincident with the axis of revolution of the mirror, with +Z pointing toward the source, the surface function, G, is defined by:

$$(1) \qquad G(X,Y,Z) = 0 = -X^2 - Y^2 + 4FZ \quad ,$$

where F is the focal length of the paraboloid. In this coordinate system, a ray originating from the source point X_0, Y_0, Z_0, and traveling a distance S to intersect the mirror surface at X,Y,Z, is reflected from the surface with direction cosines k',l',m', obtained by applying Snell's law of reflection at the local normal to the surface. (See "General Ray-Tracing Procedure", by G.H. Spencer and M.V.R.K. Murty, Journal of the Optical Society of America, 52, pp. 672-678, 1962.)

$$(2) \qquad k' = \frac{1}{S}\left\{ -X_0 + \frac{X}{2F(F+Z)}[XX_0 + YY_0 + 2F(F-Z_0)] \right\}$$

$$(3) \qquad l' = \frac{1}{S}\left\{ -Y_0 + \frac{Y}{2F(F+Z)}[XX_0 + YY_0 + 2F(F-Z_0)] \right\}$$

$$(4) \qquad m' = \frac{1}{S(F+Z)}\left\{ Z(3F - Z_0 + Z) + FZ_0 - XX_0 - YY_0 \right\} \quad ,$$

where

$$(5) \qquad S = \sqrt{(X-X_0)^2 + (Y-Y_0)^2 + (Z-Z_0)^2} \quad .$$

When $X_0=Y_0=0$ and $Z_0=F$, $k'=l'=0$ and $m'=+1$ regardless of the values of the intersection point (X,Y,Z) on the surface. (The m' result is obtained by using the equation of the surface to reduce S to F+Z in this case.) This proves the statement that the reflected beam of light originating from the source-point on the axis of revolution at a distance F from the center of the mirror is parallel (to the (Z) axis of revolution) regardless of where the light strikes the mirror.

When either X_0 or Y_0 is not zero, the direction cosines of reflected rays are not the same for all intersection points with the mirror, i.e. the reflected beam is not parallel. The divergence can be more easily demonstrated by expressing the direction cosines in terms of the off-axis distance of the source in the XY-plane, D, and the off-axis distance of the intersection of the ray with the mirror surface in the XY-plane, P. That is, if:

$$(6) \qquad X_0 = D\cos(\phi) \; ; \quad Y_0 = D\sin(\phi)$$

and

$$(7) \qquad X = P\cos(\theta) \; ; \quad Y = P\sin(\theta),$$

then the direction cosines of the reflected ray are given by:

$$(8) \qquad k' = \frac{1}{S}\left\{ -D\cos(\phi) + \frac{P\cos(\theta)}{F + P^2/4F}\left[\frac{PD\cos(\theta-\phi)}{2F} + F - Z_0\right]\right\}$$

$$(9) \qquad l' = \frac{1}{S}\left\{ -D\sin(\phi) + \frac{P\sin(\theta)}{F + P^2/4F}\left[\frac{PD\cos(\theta-\phi)}{2F} + F - Z_0\right]\right\}$$

$$(10) \qquad m' = \frac{1}{S(F + P^2/4F)}\left[\frac{P^2}{4F}(3F - Z_0 + P^2/4F) + FZ_0 - PD\cos(\theta-\phi)\right] \quad ,$$

where

$$(11) \qquad S = \sqrt{P^2 + D^2 - 2PD\cos(\theta-\phi) + \left[\frac{P^2}{4F} - Z_0\right]^2} \quad .$$

If the Z component of the source distance is equal to the focal length of the paraboloid, i.e. $Z_0 = F$, and if we let:

$$(12) \qquad S/F = s \; ; \quad D/F = d \; ; \quad P/F = p \quad ,$$

the above set of equations reduce to:

$$(13) \qquad k' = \frac{1}{s}\left\{ -d\cos(\phi) + \frac{p^2 d\cos(\theta)\cos(\theta-\phi)}{2(1 + p^2/4)}\right\}$$

$$(14) \qquad l' = \frac{1}{s}\left\{ -d\sin(\phi) + \frac{p^2 d\sin(\theta)\cos(\theta-\phi)}{2(1 + p^2/4)} \right\}$$

$$(15) \qquad m' = \frac{1}{s}\left\{ 1 + p^2/4 - \frac{pd\cos(\theta-\phi)}{(1 + p^2/4)} \right\} ,$$

where

$$(16) \qquad s = \sqrt{(1 + p^2/4)^2 + d^2 - 2pd\cos(\theta-\phi)} .$$

To illustrate the divergence of reflected rays that originate from the same off-axis source point, we consider two rays: one striking the center of the paraboloid and the other striking the mirror at the point P, at the angle θ in the XY plane. If γ is the angle between the two reflected rays, $\cos(\gamma)$ is equal to the dot-product of the two directional unit vectors, each of which has component direction cosines given by Equations (13)-(15), with appropriate values of the parameters. That is, if we let the subscript 1 refer to the ray reflected from the center of the mirror, and the subscript 2 refer to the ray reflected from the point P, then the cosine of the divergence angle γ between the two reflected rays is given by:

$$(17) \qquad \cos(g) = k'_1 k'_2 + l'_1 l'_2 + m'_1 m'_2 , \text{ or:}$$

$$(18) \qquad \cos(\gamma) = \frac{1}{s_1 s_2}\left\{ d^2 + A - \frac{pd\cos(\theta-\phi)}{A} - \frac{(pd\cos(\theta-\phi))^2}{2A} \right\} ,$$

where

$$(19) \qquad A = 1 + \frac{p^2}{4} ,$$

$$(20) \qquad s_1 = \sqrt{(1 + d^2} ,$$

and

$$(21) \qquad s_2 = \sqrt{(1 + p^2/4)^2 + d^2 - 2pd\cos(\theta-\phi)} .$$

For fixed values of d and p, the maximum angle between the two rays occurs when $\theta-\phi = 180°$. This maximum divergence is plotted versus p in Figure 37 for six values of d.

In practice, rays reflected from the center of a full parabolic mirror rarely are accessible because these usually are obscured by the physical extent of the primary and secondary sources. In fact, it is prudent to confine the illumination on the mirror to a section sufficiently off-axis so that the reflected beam passes the extremities of the setup undiffracted from any edge.

The previously developed equations can be used to obtain an exact expression for the angular divergence of the beam reflected from such an off-axis section, using the center of the section as the comparative point,

rather than the point P=0. (If the plane of the secondary source is maintained perpendicular to the symmetry axis, Equations (13)-(16) can be used; but, if the plane is rotated so as to be more or less perpendicular to the center of the illuminated section, Equations (2)-(5) must be used, since, then, all points of the source no longer are at Z_0=F.) Since the axis distance for any part of the section, then the approximate maximum expression involves two difference angles, it is less amenable to analytical analyses than was Equation (18). Rather than deriving the exact expression, we can use Figure 37 to estimate the results. If P_0 is the off-axis distance to the center of the section and P_2 is the largest off-divergence of a beam reflected from the section is the difference between the ordinate values corresponding to abscissa values of P_0/F and P_2/F in Figure 37. For example, suppose the projection of the boundary of the off-axis section in the XY plane was a square with center at (X,Y)= (0.05F, 0) and sides ($\pm\Delta X$, $\pm\Delta Y$) = ($\pm$0.02F, $\pm$0.02F), and the source was a disk of radius D/F= 0.0175 (60 arc-min). An exact calculation of the maximum divergence of the beam from such a section yields a value of 0.164 arc-min, while Figure 37 yields a value of about 0.14 arc-min between P_0/F = 0.05 and P_2/F = 0.07.

Figure 37 illustrates a further point for instruments having a rectangular or elliptical field of view; it shows that in order to minimize the divergence in the resulting beam, the longer axis of the secondary source should be parallel to that direction for which the section is less off-axis. In general, this will be the perpendicular to the off-axis direction of section of the mirror being used.

Of course, considerations of the size of an available mirror and the minimum distance that can be achieved between the mirror and the front of the instrument while still accommodating the primary and secondary sources, may dictate the orientation of the secondary source. That is, to provide illumination that approximates a $\pm\alpha°$ by $\pm\beta°$ source at infinity at the front of an instrument having an opening of dimensions W by H in the directions corresponding to α and β, respectively, using a collimating mirror located a distance L from the opening, would require a mirror of dimensions (2Ltan(α) + W) by (2Ltan(β) + H) in the direction corresponding to α and β, respectively. These dimensions, when compared with those of the available mirror, may dictate the orientation of the mirror, irrespective of the off-axis direction.

Implicit in the preceding discussion is the assumption that the secondary source is illuminated so as to provide the required illumination at the mirror, i.e. that the secondary source is fully illuminated and that the cone of light from each point in the secondary source has a direction and f-number to illuminate at least that area of the mirror required to subsequently fill the front opening of the instrument. These conditions, in turn, place requirements on the optics between the primary (emitting) source and the secondary source which are not addressed in this report.

In summary, although a parabolic mirror does not produce illumination that exactly duplicates that from an infinitely distant extended source,

with judicious choice of focal length and off-axis distances it can produce illumination that approximates such a source to within the required alignment tolerance, at least over a field-of-view sufficient to determine the field-of-view axis.

C. SPHERICAL COLLIMATING MIRRORS.

Since the co-investigators on the RAIDS program at Aerospace have a large spherical mirror, the diameter of which (~3-ft) would permit illuminating all of the apertures, the boresight mirrors, and the reference optical cube, we investigated whether such a mirror could be used at least for the co-alignment process, if not for determining the field-of-view axis of an individual instrument.

For co-alignment, the illumination produced by such a large collimating mirror potentially could be used in one of two ways. If the payload could be rotated with precision about two perpendicular axes, the mirror could be used to illuminate all of the apertures with light corresponding to a small field of view, and the signals themselves used to determine mutual alignment among the instruments. (Changing the emitting source to accommodate the wavelength coverage of individual instruments would be required, but this would not affect the illumination of an instrument if the secondary source was illuminated properly by each.)

However, the orientation of the field-of-view axis of at least one instrument relative to the optical cube on the payload baseplate still would have to be determined. In principle, this could be determined by viewing the image of the secondary aperture on the mirror-side of the aperture holder produced by the reflection of the beam from the optical cube back to the large mirror. The holder could be scribed with markings from which angles could be deduced.

Viewing similar images reflected from the boresight mirrors, rather than signals from the instruments, is, in fact, the second way to use the large collimating mirror for co-alignment. However, since the minimum angle between the approximate line of sight of an instrument and the payload reference axis of the optical cube is about 10° about the scan axis, if the instruments were approximately aligned to the collimating mirror, the angle between the incident and reflected beam from the cube would be 20°. Thus, the mirror would have to be very large in order to intercept the reflected beam unless the payload was very close to the mirror, and, even if the mirror were large enough, the displacement of the image relative to the source would be considerable.

An alternative approach would be to rotate the payload until the image of the secondary source reflected from the optical cube was appropriately positioned on the markings of the holder, and use the position of the image and the angle through which the payload had been rotated to deduce the relative orientation of instrument and optical cube. This approach also would require precise knowledge of the rotation angle of the payload - to

better than 0.5 arc-min.

However, all of these considerations are irrelevant if the illumination of all of the instruments (be it of the flight apertures or of the boresight mirrors) from the same source-point is not parallel to within an overall angle less than 0.5 arc-min. Given that the apertures span distances of up to ~24 inches (~30 inches if all eight instruments are considered; see Figure 3), we proceed to examine the requirement on the radius of the sphere in order to satisfy the 0.5 arc-min parallelism.

We first consider that the source is a point located on that normal to the surface of the mirror which is centered between the extremities of the mirror that would need to be illuminated in order that the reflected beam illuminate two or more apertures or boresight mirrors. We let this normal define the Z axis of a coordinate system whose origin is on the surface of the sphere, with +Z pointing toward the source. In this coordinate system the equation representing the surface function, G, is:

$$(22) \quad G(X,Y,Z) = 0 = -X^2 - Y^2 - Z^2 + 2ZR,$$

where R is the radius of the sphere. Applying Snell's law of reflection at the local normal, the direction cosines (k',l',m') of a ray reflected at the point (X,Y,Z) after traveling a distance S from the source point $(0,0,Z_0)$, are given by:

$$(23) \quad k' = \frac{X}{S}\left[1 - \frac{2Z}{R} - \frac{2Z_0}{R} + \frac{2Z_0 Z}{R^2}\right]$$

$$(24) \quad l' = \frac{Y}{S}\left[1 - \frac{2Z}{R} - \frac{2Z_0}{R} + \frac{2Z_0 Z}{R^2}\right]$$

$$(25) \quad m' = \frac{Z_0}{S}\left[1 + \frac{3Z}{Z_0} - \frac{4Z}{R} - \frac{2Z^2}{Z_0 R} + \frac{2Z^2}{R^2}\right] ,$$

where

$$(26) \quad S = \sqrt{X^2 + Y^2 + (Z - Z_0)^2} = \sqrt{2Z(R-Z_0) + Z_0^2}$$

For the reflected ray to be parallel to the Z axis, m' must equal +1 or, equivalently, k' and l' must equal 0. For the ray that strikes the center of the mirror (X=Y=Z=0), this condition obtains for any value of the source distance, Z_0. For rays striking the mirror elsewhere, examination of Equations (23)-(26) shows that the condition is approximately obtained when Z_0=R/2, provided Z<<R/2. In Figure 38 the exact angular components of rays reflected from the point (X,Y,Z) when the source is a point at (0,0,+R/2) are plotted versus the ratio of the off-axis distance in the XY plane, P, to R. That is, P is defined, as before, as:

$$(27)\quad P = \sqrt{X^2 + Y^2}\ .$$

In Figure 38, "A", "B", and "C" are the arc-cosines of k', l', and m', respectively, i.e. if the reflected ray were parallel to the Z-axis, "A"-90°, "B"-90°, and "C", each, would be 0°.

Figure 38 also illustrates the complementary angular relation between k' and l' given in Equations (23) and (24). That is, if "T" is the angle of the intersection point measured in the XY-plane relative to the X-axis, then X = Pcos(T) and Y=Psin(T), and thus, k'(T) = l'(90°-T).

Figure 38 shows that R must be greater than P/0.0525 (≅19P) to have the reflected beam be parallel to the Z-axis to within 0.5 arc-min for a point source at (0,0,+R/2). If P is 15 inches (one-half of the maximum span of the apertures of all 8 instruments), then R must be at least 23.8 feet. Since the large spherical mirror at Aerospace has a radius of only about 16 feet, it would appear that this mirror could not be used to co-align the instruments.

However, before dismissing this prospect, a further examination of Equations (23)-(25) is in order. k' and l', both, can be made equal to zero if the common quantity in brackets is zero, i.e. if $2Z/R + 2Z_0/R - 2ZZ_0/R^2 = 1$. Solving this equation for Z_0 yields:

$$(28)\quad Z_0 = \frac{R/2 - Z}{1 - Z/R} = R\left[1 - \frac{0.5}{\sqrt{1 - (P/R)^2}}\right]$$

In other words, if the source is moved toward the mirror along the central normal so that it is closer to the center of the mirror than R/2, the rays reflected from the circle of the surface having the value of Z that satisfies Equation (28) will be parallel to the Z-axis. This is illustrated in Figure 39.

Thus, if the secondary source (kept small in angular extent) could be translated with the required precision for each aperture to be illuminated, and if the required area of the mirror adjacent to the circle did not spread the beam beyond the alignment tolerances, using the large sphere for co-alignment might be feasible.

III. SOURCES AT A FINITE DISTANCE.

A common alternative to use of a collimating mirror is positioning of the source at a large, but finite, distance from the instrument, it being assumed that this approximates a source at infinity if the distance is large compared with the focal length of the optics used in the instrument. To investigate the use of this technique for determining the components of the FOV axes for the NUV and MUV instruments, raytracing was done for a point source located 4 meters from the telescope mirror in each instrument,

a distance typical of that attainable within a laboratory room. Many of the results can be predicted from considerations of elementary geometrical optics, and we proceed to do this because the simple equations that result are useful in establishing constraints on the laboratory source without elaborate raytracing.

If we consider the spherical telescope mirror of radius "R" to be illuminated by a point source of light at a distance "S" from the center of the mirror and at an angle "ϕ" with respect to the normal at the mirror center, by elementary geometrical optics the tangential focal distance from the center of the mirror, S'_T, is given by:

$$(29) \quad S'_T = f_T/(1 - f_T/S),$$

where $$(30) \quad f_T = R \cos(\phi)/2.$$

Since the telescope slit is approximately at the distance f_T from the mirror, Equation (29) shows that the tangential focus of a source at a finite distance is further from the mirror than f_T, the approximate distance of the slit. The width of the illumination at the slit plane, X, from a point source that illuminates the full width of the mirror, W, is thus given very approximately by:

$$(31) \quad X = W(S'_T - f_T)/S'_T = Wf_T/S.$$

Since W and f_T for the MUV telescope are both twice as great as their NUV counterparts (see Appendix A), if a point source is placed on the design optical axis at the same distance from either telescope mirror and illuminates the full width of the mirror, the width of the illumination at the plane of the slit for the MUV (or any of the 1/4 m telescopes) will be about four times the width for the NUV (or any of the 1/8 m telescopes).

As the source is offset about the design optical axis in the slit-width direction, X shifts across the slit, remaining about the same magnitude if the source continues to illuminate the full width of the mirror and if the offset angles are small. If we assume that X is greater than the slit-width, w_{sl}, i.e. that $S < Wf_T/w_{sl}$, and that X is of uniform intensity, we can predict certain features of the signal behind the telescope slit. The signal should be constant over an angular offset about the design optical axis given by θ_C, where:

$$(32) \quad \theta_C = \tan^{-1}[(X - w_{sl})/f_T] = \tan^{-1}[W/S - w_{sl}/f_T].$$

The component of the full FOV in the slit-width direction, θ_F, should be given by:

$$(33) \quad \theta_F = \tan^{-1}[(X + w_{sl})/f_T] = \tan^{-1}[W/S + w_{sl}/f_T],$$

and the FWHM of this component, θ_H, should be given by:

(34) $\theta_H = \tan^{-1}[(X/f_T] = \tan^{-1}[W/S]$.

For a point source 4 meters from the telescope mirror, elementary optics thus predicts that the signal behind the telescope slit should have the features given in Table D1 (below) for the MUV, for which W = 4.2 cm; w_{sl} = 0.05 cm; f_T = 24.703 cm, and the NUV, for which W = 2.1 cm; w_{sl} = 0.025 cm; f_T = 12.306 cm.

TABLE D1. Predictions from elementary geometrical optics of features of the signal behind the telescope slit for a point source 4 meters from the telescope mirror of the MUV and NUV instruments.

	~CONSTANT θ_C	FWHM θ_H	FULL FOV θ_F
	deg (arc-min)	deg (arc-min)	deg (arc-min)
MUV	0.49 (29)	0.60 (36)	0.72 (43)
NUV	0.18 (11)	0.30 (18)	0.42 (25)

The raytracing results for the same source conditions are given in Figure 40, the curves labeled "ES" being the signal directly behind the telescope slits. These curves show values close to those given in Table D1 for θ_H and θ_F. There is less agreement with the predictions from elementary optics for θ_C because the assumption that X is uniform across the slit plane is not borne out in raytracing. And, elementary optics does not correctly predict the offset angle corresponding to the center of the FWHM because it neglects aberrations. Nevertheless, estimating the distance an uncollimated source must be from the telescope Equations (33) and (34) are useful in mirror in order to have the shape of the resulting signal be more closely related to flight conditions.

Table D2 shows the approximate source distances required if we demand that the FWHM be 0.115°, or that the full FOV be 0.21° for the signal behind the telescope slit of either instrument.

TABLE D2. Predictions from elementary geometrical optics for the distance that a point source must be from the telescope mirror in the MUV and NUV spectrometers in order that: (a) the FWHM be 0.115° or (b) the full FOV be 0.21° for the signals in the slit-width (altitude) direction..

	DISTANCE (meters)	FWHM (deg)	FULL FOV (deg)	X (cm)
MUV	20.92	0.115	0.23	0.0500
NUV	10.46	0.115	0.23	0.0250
MUV	25.60	0.094	0.21	0.0400
NUV	12.85	0.094	0.21	0.0200

Also listed in Table D2 is the approximate illuminated width at the slit plane, X, for each source distance. That X is approximately the same width as the slit width should not be unexpected. In determining the FOV, the important source parameters are those that determine the size and distribution of the illumination at the plane of the slit. For a source at a finite distance from the telescope mirror, the most important parameter is the distance, S, if the source emits into a solid angle that always fills the mirror; the size of the source or, equivalently, the angular subtense of the source from the mirror matters only if magnification, S'/S, substantially adds to the illuminated width at the slit. That is, for a source of finite width, d, the illuminated width at the slit plane would be:

$$(35) \quad X = f_T[\, W/S \; + \; d/(S-f_T)\,].$$

This value of X then should be used in Equations (32), (33), and (34) to re-evaluate θ_C, θ_H, and θ_P.

In summary, simple equations derived from elementary optics can be used to obtain the minimum distance that a source must be from an instrument in order to (approximately) measure certain parameters for the field-of-view response of the instrument that will obtain during flight. But, detailed features of the response function that will obtain during flight, including the direction corresponding to the center of the FWHM, are not necessarily accurately determined by this method. Thus, it is recommended that this method not be used to determine the field-of-view response of an instrument.